CIVIL ENGINEERING STUDIES
STRUCTURAL RESEARCH SERIES NO. 193

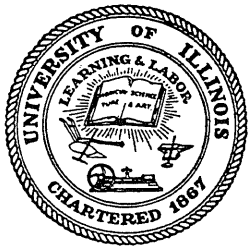

PRIVATE COMMUNICATION
NOT FOR PUBLICATION

BEHAVIOR AND DESIGN OF DEEP STRUCTURAL MEMBERS

PART 2

TESTS OF REINFORCED CONCRETE DEEP BEAMS WITH WEB AND COMPRESSION REINFORCEMENT

By
J. R. Winemiller
and
W. J. Austin

Approved by
C. P. Siess

Report to
RESEARCH DIRECTORATE
AIR FORCE SPECIAL WEAPONS CENTER
Air Research and Development Command
Kirtland Air Force Base, New Mexico
Contract AF 29(601)-468
Project 1080

UNIVERSITY OF ILLINOIS
URBANA, ILLINOIS
AUGUST 1960

R N Wright

AFSWC-TR-59-72
Part 2

BEHAVIOR AND DESIGN OF DEEP STRUCTURAL MEMBERS

Part 2

TESTS OF REINFORCED CONCRETE DEEP BEAMS WITH WEB AND COMPRESSION REINFORCEMENT

by

J. R. Winemiller and W. J. Austin

Approved by C. P. Siess

University of Illinois
Department of Civil Engineering

August 1960

Research Directorate
AIR FORCE SPECIAL WEAPONS CENTER
Air Research and Development Command
Kirtland Air Force Base
New Mexico

Approved:

ERIC H. WANG
Chief
Structures Division

LEONARD A. EDDY
Colonel USAF
Director, Research Directorate

Project No. 1080
Contract No. AF 29(601)-468

ABSTRACT

The results of tests of seven reinforced concrete deep beams with tensile and web reinforcement and two beams with tensile and compressive reinforcement are described in this report. Several patterns of web reinforcement were used. The beams with web reinforcement had a span-depth ratio of about 3.0 and the beams with compressive reinforcement had a span-depth ratio of 2.32. All beams were tested under uniform, slowly-applied loading. The general behavior of the test specimens is described and explanations of the observed phenomena are given.

PUBLICATION REVIEW

This report has been reviewed and is approved.

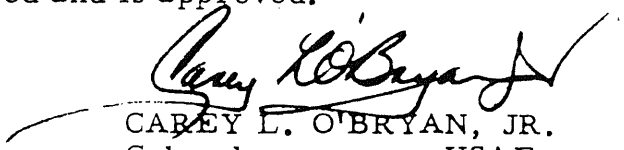

CAREY L. O'BRYAN, JR.
Colonel USAF
Deputy Commander

TABLE OF CONTENTS

TABLE OF CONTENTS (Continued)

LIST OF TABLES

LIST OF FIGURES

LIST OF FIGURES (Continued)

LIST OF FIGURES (Continued)

I. INTRODUCTION

1.1 Object and Scope

The studies described in this report were performed as a part of a comprehensive investigation of the strength and behavior of reinforced concrete deep beams. The object of the investigation reported herein was to gain information concerning the strength and behavior of concrete deep beams reinforced in both tension and compression and of reinforced concrete deep beams with web reinforcement. Several patterns of web reinforcement were tested in order to obtain some indication of the most efficient means of reinforcing the web.

Two rectangular concrete beams reinforced in both tension and compression with a span/depth ratio of 2.32 were tested under uniform load on a simple span of 36 in. The beams had the same cross-sectional properties, with the exception of the compression reinforcement, as a beam of a previous test series reinforced in tension only.

Seven rectangular concrete beams, designated as C-series specimens, were also tested under uniform loading on a simple span of 36 in. Two of the seven beams had only tensile reinforcement. They were reinforced with 1.15 and 1.99 percent intermediate grade steel bars. The depth to the lower layer of the longitudinal reinforcement was 12 in. Then two variations of each of the two beams containing either vertical stirrups or inclined bars were tested. The seventh C-series specimen tested had no web reinforcement, but instead, had the longitudinal reinforcement distributed along its depth.

1.2 Acknowledgment

This investigation was carried out in the Structural Research Laboratory of the Engineering Experiment Station at the University of Illinois as part of a cooperative project between the University and the Air Force Special Weapons Center, Department of the Air Force. General direction of the

project was furnished by N. M. Newmark, Professor and Head, Department of Civil Engineering, and Dr. C. P. Siess, Professor of Civil Engineering. The project was under the immediate direction of Dr. W. J. Austin, Associate Professor of Civil Engineering. Mr. R. E. Untrauer, Research Associate in Civil Engineering, provided the direct supervision. The studies described in this report also served as the basis for an M.S. dissertation by Mr. Winemiller.

1.3 Notation

The following notation has been used:

A_s = total area of tension reinforcement

A'_s = total area of compression reinforcement

A_v = area of web reinforcement

a = depth of stress block in concrete at maximum load-carrying capacity

b = width of member

C_1 = total compressive force in the concrete

C_2 = total compressive force in the compression reinforcement

d = effective depth, distance from the top compressive fiber to the centroid of the tension reinforcement

d' = distance from the centroid of the compression reinforcement to the centroid of the tension reinforcement.

E_c = modulus of elasticity of concrete

E_s = modulus of elasticity of reinforcing steel

f_c = stress in the concrete

f'_c = compressive strength of concrete determined from tests of 6- by 12-in. cylinders.

f_s = stress in the tension reinforcement

f'_s = stress in the compression reinforcement

f_v = stress in the web reinforcement

f_y = yield-point stress of the tension and web reinforcement

f'_y = yield-point stress of the compression reinforcement

$f^* = f'_y - 0.85\, f'_c$

j = ratio of lever arm of internal resisting moment to effective depth, d, for concrete, for elastic section

k = ratio of depth of compression zone to effective depth, d, for fully-cracked elastic section, see Fig. 53

k_1 = ratio of area of concrete stress block to area of enclosing rectangle at maximum load, see Fig. 54

k_2 = fraction of depth of compressive zone which determines the position of the compressive force in the concrete at maximum load, see Fig. 54

k_3 = ratio of maximum compressive stress in concrete beam to cylinder strength

L = span of simply-supported beam, distance between centers of supports

M = bending moment

M_f = computed ultimate flexural moment ($\epsilon_u = 0.004$)

M'_f = computed ultimate flexural moment ($\epsilon_u = 0.008$)

M_u = measured moment at maximum load

M_y = measured moment at flexural yielding

$p = A_s/bd$

$p' = A'_s/bd$

q = reinforcing index $= \dfrac{pf_y}{f'_c}$

q_o = lower critical value of q corresponding to $\epsilon_s = \epsilon_o$; $= \dfrac{k_1 k_3 \epsilon_u}{\epsilon_u + \epsilon_o}$

T = total tensile force in the tension reinforcement

W = total uniform load

W_u = total uniform load at maximum load

W_y = total uniform load at flexural yielding

Δ_u = measured midspan deflection at maximum load

Δ_y = measured midspan deflection at flexural yielding

ϵ_c = strain in the concrete

ϵ_o = strain in the tension and web reinforcement at beginning of work-hardening region

ϵ'_o = strain in the compression reinforcement at beginning of work-hardening region

ϵ_s = strain in the tension reinforcement

ϵ'_s = strain in the compression reinforcement

ϵ_u = crushing strain of concrete

ϵ_y = yield-point strain of the tension and web reinforcement

ϵ'_y = yield-point strain of the compression reinforcement

beam C-6, the top layer of the tension steel was bent up at 45 deg. beyond the point where it was no longer needed to develop the flexural capacity of the beam. Since the depth to the bottom layer of steel remained constant at 12 in. throughout this series of tests, the effective depth measured to the centroid of the tensile steel area of these three beams is slightly less than that for the first group due to the addition of the two top bars. The effective depth is 11.39 in., and consequently, the span-depth ratio is 3.16.

Beam C-7 had the same total steel area as beam C-4, but instead of placing the two No. 4 bars in a horizontal plane they were placed one above the other as shown in Fig. 5. By distributing the longitudinal tension steel along the depth of the beam in this manner, it was believed that the reinforcement might more effectively retard the development of the inclined cracks than if it were concentrated near the bottom edge of the specimen. Because of the steel arrangement, the effective depth is decreased to 10.82 in., increasing the span-depth ratio to 3.32.

As mentioned previously, the two top longitudinal bars of beam C-6 were bent up beyond the point where they were no longer necessary to provide flexural resistance. Once this point was established, the diagonal web steel of beam C-3 was placed in exactly the same position. The top bars of beam C-6 were bent up at 7 1/2 in. on both sides of midspan. In beam C-3 the diagonal bars intersected the longitudinal steel at 6 in. on both sides of midspan.

The vertical stirrups were spaced so as to intersect effectively the inclined cracks observed from the tests of beams without web reinforcement. Both the stirrups in beams C-2 and C-5 and the inclined bars of beam C-3 were welded to the longitudinal tension steel.

II. DESCRIPTION OF TEST SPECIMENS

2.1 Description of Beams

A-series: The two beams of this series were designed to give information which would supplement the studies made during the previous year (1). They have the same properties as beam A-3-2 of the previously mentioned reference except for the addition of compression reinforcement. Their properties are given in Table 1, and drawings of the two beams are shown in Fig. 1. For beam A-3-4, $p' = 1/2\ p$, and for beam A-3-5, $p' = p$. Since beam A-3-4 failed by bearing, 6- by 12- by 1-in. steel plates were clamped to the sides of beam A-3-5 above the supports to laterally confine the concrete and thereby increase the bearing strength.

C-series: Two basic rectangular beams without web reinforcement were first designed, and then variations of these basic beams were made by adding web reinforcement in several different arrangements. The basic beams had a width of 4 1/2 in., an over-all length of 42 in., and a depth to the bottom layer of steel of 12 in. The nominal area of the tension reinforcement was chosen as 0.62 sq. in. for the one basic beam and 1.02 sq. in. for the other.

Drawings of the specimens are shown in Figs. 2 through 5, and the properties of the beams are listed in Table 2. Beams C-1, C-2, and C-3 constitute one group. They have the same cross-sectional dimensions and tension reinforcement. The only difference between them is the manner of reinforcing the web. Beam C-1 had no web reinforcement while vertical stirrups and inclined bars were provided to reinforce the webs of beams C-2 and C-3, respectively. The effective depth, d, of the three beams is 12 in., resulting in a span-depth ratio of 3.

Similarly, beams C-4, C-5, and C-6 constitute a group. The cross sections of the three beams are the same at midspan. Vertical stirrups were added to reinforce the web of beam C-5. To provide web reinforcement for

For the C-series beams the mix was designed for a 14-day strength of 3000 psi; the actual strength varied from 2970 to 3690 psi. Because of expected bearing difficulties, the mix for the two beams with compression steel was designed for a 14-day strength of 5000 psi. The actual concrete strengths were 4860 psi for beam A-3-4 and 5550 psi for beam A-3-5. Properties of the concrete mixes are given in Table 4. Compressive strengths are the average values obtained from tests of five standard 6- by 12-in. cylinders loaded at a rate of 45,000 lb/min, and the moduli of rupture values are those obtained from bending tests of two 6- by 6- by 20-in. control beams loaded at the third-points of an 18-in. span. Moisture determinations for the sand and gravel were made at the time of mixing.

Fabrication and Curing: All the beams were cast horizontally in a wooden form. Before casting, the steel was prepared for the future application of electric SR-4 strain gages. Usually this preparation consisted of grinding the bar smooth at the gage locations and then attaching 1 1/2-in. diameter corks with wire to the bar over the smoothed area to provide access for mounting the gages by removing the corks after casting.

The SR-4 gages on the stirrups of beam C-5 and on the top two horizontal bars of beam C-7 were attached before casting to avoid cork holes in the concrete close to or within the compression zone. This necessitated waterproofing the gages to prevent them from coming in contact with the moist concrete. Waterproofing was accomplished by pouring hot Petro-elastic over the gages. The performance of the waterproofing was then checked by submerging each bar in water for several hours before placing it in the specimen.

The concrete was mixed from 3 to 6 minutes in a 6-cu. ft. capacity non-tilting drum type mixer and placed in the previously oiled form with the aid of a high frequency internal vibrator. Two 6- by 6- by 20-in. flexural control beams and five 6- by 12-in. control cylinders were cast at the same time.

2.2 Materials and Fabrication

Cement: Marquette Type III Portland Cement was used in the concrete mixes for all specimens. The high-early-strength cement was purchased in paper bags from a local dealer and stored under proper conditions.

Aggregates: The aggregates employed in the mixes were Wabash River sand and pea gravel obtained from an outwash of the Wisconsin glaciation. The gravel is composed mainly of limestone and dolomite with minor quantities of quartz, granite, and gneiss, while the sand consists mostly of quartz. Both aggregates have been used in the laboratory for previous investigations and have passed the usual specification tests. The maximum size of the pea gravel was 3/8 in., and the absorption of both the sand and gravel was approximately 1 percent by weight of the surface dry aggregate.

Reinforcing Steel: Intermediate grade deformed bars were used in all of the beams. One coupon 2 ft. long was cut from each bar and tested in a 120,000-lb Baldwin-Southwark-Tate-Emery hydraulic testing machine at a straining rate of 0.005 in./in./min. up to yield. Strains into the work-hardening region were measured with an 8-in. extensometer employing a Baldwin "microformer" coil and recorded by an automatic recording device. The extensometer was removed from the coupon shortly after entering the strain hardening region, and the strains beyond this point up to ultimate were determined by measuring the elongation of an 8-in. gage length with dividers. In each beam the bars were matched as closely as possible according to their yield points, using bars cut from the same piece of steel to assure identical properties whenever possible. Table 3 lists the properties of the reinforcing steel, and a typical stress-strain curve is shown in Fig. 6.

Concrete Mixes: The mix design was based on experience obtained in other investigations conducted in the laboratory using the same aggregates.

III. TEST EQUIPMENT AND PROCEDURE

3.1 Instrumentation

Deflections: Dial indicators with a smallest division of 0.001 in. were used to determine the vertical deflections of each specimen at various positions along the span. Locations of the dial indicators are shown in Fig. 2. The indicators were mounted to vertical 1/4-in. round steel rods which in turn were attached to heavy base plates resting on the bed of the testing machine.

Steel Strains: Strains in the reinforcing steel were measured with Type A-7 SR-4 electric strain gages. The gage locations are given in Figs. 2 through 5. The gages on the web steel were attached at the point where the inclined crack was expected to cross the reinforcement.

Duco cement was used to mount the electric gages to the reinforcement. The drying period was not hastened by the application of heat, for it was thought that it might influence the concrete strength. Therefore, the gages were applied at least two days before the test to allow sufficient drying time.

Strains were read to the nearest 5 micro-in/in. with a Baldwin portable strain indicator. A temperature compensation gage and a check gage were mounted on an unstressed steel block and connected into the circuit.

Strains in the bottom layer of the longitudinal tension reinforcement were also measured over continuous 6-in. gage lengths using a mechanical gage employing an Ames dial with a smallest division of 0.001 in. The purpose of these measurements was to obtain some indication of the magnitude of the steel strains if the capacity of the electric gages was exceeded. While the SR-4 gages were functioning, only the strains over the two center 6-in. gage lengths were measured. After the electric gage readings became irregular, the strains

Several hours after casting, the top surface of the beam was trowelled smooth, and the cylinders were capped with neat cement paste. The beam and control specimens were removed from their forms the next day and wrapped in wet burlap for an additional day. They were then stored in the laboratory until tested.

plugs. No measurements of elongation of tensile reinforcement were made for the two beams with compression reinforcement. It is assumed that the displacements of the tensile reinforcement are equal to the displacements of the surrounding concrete at the point of measurement.

3.2 Loading Apparatus

A typical test set-up is shown in Fig. 7. Uniform load was simulated by means of 20-ton capacity Blackhawk hydraulic jacks mounted to a 10 WF 39 beam which in turn was bolted to the moving head of a 300,000 -lb Olsen mechanical universal testing machine. The jacks were joined by high pressure hoses to a common brass manifold connected to a Blackhawk hydraulic pump. Eight jacks spaced at 4 in. comprised the uniform load for all the beams except A-3-4, the first beam tested. For the test of this beam, ten jacks at 4 in. were used. However, the first beam failed by crushing of the concrete above the supports. To reduce the possibility of a bearing failure in the following tests, the end jacks were eliminated, making the midspan moment more critical for a given load. The two center jacks were rigidly attached to the WF beam, but the other jacks bore against rollers allowing them to rotate as the specimen deformed.

Load was transmitted from the jacks to the beam through 1-in. diameter chrome steel balls placed in depressions at the center of 4- by 3 7/8- by 2-in. steel loading blocks. The blocks rested on 1/4-in. thick leather pads which helped to distribute the load uniformly.

Each beam was supported by two 6- by 6- by 2-in. steel bearing blocks which rested on the bed of the testing machine. The top of the blocks accommodated a 2-in. diameter roller which bore against a 6- by 6- by 2-in. plate seated in Hydrocal against the bottom of the beam. The distance between the vertical center lines of the rollers was 36 in.

were determined mechanically over all the 6-in. gage lengths. The strain readings were taken twice. If they did not agree within 0.0002 in./in., additional readings were taken until two readings agreed within the prescribed limit.

Concrete Strains: Concrete strains along the depth of each beam at midspan were measured by means of a 2-in. Whittemore strain gage. Steel plugs with gage holes at their centers were cemented to the concrete to establish the gage lines as shown in Fig. 2.

The strain readings were taken twice. If they did not agree within 0.0001 in., additional readings were taken until agreement was reached.

Concrete strains were also measured at various positions along the span with A-1 SR-4 electric strain gages. Locations of the gages are shown in Fig. 2. The method of application of these gages was the same as for the steel gages. However, since the moisture entrained in the concrete could be detrimental to the behavior of the gages, they were mounted only within 48 to 24 hours before the test. Strains were measured to the nearest 5 micro-in./in. with a Baldwin portable strain indicator.

Elongation of Tensile Reinforcement: In order to determine the relationship between deflection and total elongation of the tensile reinforcement, the elongation was measured. Two plugs were cemented to each specimen at the point where the level of the bottom layer of the tensile reinforcement intersected the centerlines of the supports. In beam C-1 the separation of these plugs was measured directly with a mechanical gage which employed a dial indicator with a least reading of 0.001 in. At each recording the gage was read twice or more until the readings agreed within 0.001 in. For the other six specimens of the C-series, the elongation of the tensile reinforcement was measured by means of two dial deflection gages mounted horizontally, as shown in Fig. 2. These gages measured the horizontal displacements of the

IV. BEHAVIOR OF BEAMS WITH WEB REINFORCEMENT

4.1 Test Results and Modes of Failure

Test results for the seven beams of this series are given in Table 5. The most significant properties of the specimens are also listed for convenient reference. Values of the load at yield and final collapse include live load only, the dead load never being more than about 0.5 percent of the total vertical load. In the last column of the table is given the mode of failure for each beam.

As can be observed from the table, all the beams failed in flexure. All beams failed by first yielding of the longitudinal reinforcement followed by crushing of the concrete in the compression zone at midspan.

Although all of the specimens failed in flexure, the cracking patterns developed were somewhat different. Evidence of this can be seen in the photographs of the beams shown in Figs. 8 through 10. The numbers marked on the specimens are the total load in kips and indicate the observed progress of the cracks at that load. Three distinct cracking patterns are recognizable, and the photographs are grouped according to these patterns. The manner of cracking seems to depend upon the type of web reinforcement.

Beams Without Web Reinforcement: Well developed inclined cracks formed, extending from the inside face of the support to top midspan, as shown in Fig. 8. This particular pattern is much more noticeable for beam C-1 than beam C-4. The two inclined cracks practically meet at midspan, giving the appearance of an arch to the beam and, as shown in detail later, causing the specimen to act as a tied arch, the longitudinal steel serving as a tie between the supports. For beam C-7 the cracking pattern is similar to that of beams C-1 and C-4, the arrangement of the top two horizontal bars exerting little, if any, influence on the cracking pattern.

3.3 Testing Procedure

Load was applied in 10 to 17 increments to failure. After a load increment, all deflection and strain readings were taken, and the cracks observed through a low power illuminated magnifying glass and marked with ink. A certain amount of drop-off in load and change in deflection occurred while the readings were being taken. These changes were recorded before the next increment of load was applied.

The beams were loaded until they ruptured completely or reached a condition of unstable equilibrium, i.e., increasing deflection with decreasing load. In the vicinity of the expected yield load, the load was applied by increments of steel strain (usually a hundred micro-in./in.) and the load and midspan deflection read until first yielding was evident from observation of the steel strains. After yielding, the load was applied by increments of deflection. Between increments several load and deflection readings were taken simultaneously.

Photographs of the test specimens were taken at important stages during the test and after failure. The control beams and cylinders were tested the same day.

forcement. In Fig. 16 the curve for beam C-4 is replotted for comparative purposes. The curves are for the deflection measured at the top midspan. Drop-off of load occurring while the readings were being taken is not shown.

All the curves are characteristic of members failing in flexure. An elastic range is recognizable up to yield, beyond which considerable deflection of the beam takes place. The curves of Fig. 14 show a definite change of slope at yield. However, this sharp break is not present for the beams with multiple layers of steel; the change in slope in the vicinity of yield is more gradual due to successive yielding of the layers of longitudinal steel. Yield load and deflection were chosen for this report as the load and corresponding deflection at the intersection of the initial and secondary slopes of the curves. These values are listed in Table 5.

Ultimate deflection is listed in Table 5 as that occurring at ultimate load, except for beam C-6. Examination of the curve for this specimen shows that the maximum measured load occurred at a deflection of 0.343 in. Beyond this point the load decreased but slightly until a deflection of 0.728 in. was reached then dropped off rapidly. Therefore, it was thought justifiable to list 0.728 in. as the ultimate deflection for this beam.

As would be expected, the smaller the steel percentage the more ductile was the member. This can be seen by comparing the load-deflection curves for the three beams without web reinforcement. For the specimens having steel ratios of 0.0115, 0.0199, and 0.0209, the midspan deflections at failure were 0.875, 0.412, and 0.352 in., respectively. The decrease in ductility with increase in longitudinal steel ratio can also be observed by comparing beams with similar web reinforcement patterns and different percentages of longitudinal steel.

Observation of the elastic portion of the load-deflection curves shows that the presence of web reinforcement had little effect upon the

stiffness of the beams. A small difference in stiffness for the beams with a longitudinal steel ratio of 0.0199 is noticeable. However, the difference can probably be attributed mostly to the variation in concrete strengths.

The web reinforcement also had little effect upon the ultimate deflection. Figure 14 shows that beams C-2 and C-3 with vertical stirrups and inclined bars, respectively, deflected slightly less than beam C-1 without web reinforcement. However, because of instrumentation difficulties the deflection of beam C-1 near ultimate was extrapolated from measurements of the deflection of the bottom at midspan. The difference in ultimate deflections could possibly be due to this extrapolation. The curves for beams C-4, C-5, and C-7 indicate that the ultimate deflection was increased slightly by the addition of stirrups and decreased by distributing the longitudinal reinforcement along the depth of the beam. The only beam in which a pronounced change in ultimate deflection occurred was beam C-6 which had inclined web reinforcement. The ultimate deflection for this beam was much greater than the deflections for the companion beams C-4 and C-5 and was almost as large as the ultimate deflections obtained for beams C-1, C-2, and C-3 which had less tension reinforcement. The greatly increased ductility of beam C-6 is believed to be due to the fact that the top layer of the longitudinal steel was bent up to form the web reinforcement, leaving a reduced amount of tension reinforcement in the outer parts of the span and at the anchorage. The strains in the outer sections were, therefore, much greater than in beams C-4 and C-5 in which both layers of longitudinal steel ran the full length of the beam, and the increased strain produced increased deflection and increased energy-absorbing capacity in beam C-6.

The deflected shapes of the specimens are given in Figs. 17 through 20. As can be seen from the figures, the deflected shape of the top surface

of the beams can be approximated by two straight lines. This would seem to indicate that the concrete at top midspan is acting as a hinge, resulting in large strain concentrations at midspan. It can also be noted from the figures that there is a small deflection occurring at the centerline of the supports. H. A. R. dePaiva, Research Assistant in Civil Engineering, performed compression tests on the support systems used for this series of tests and obtained the curve shown in Fig. 21. For loads of the magnitude occurring in the tests of the C-series beams, the supports would be expected to compress as much as 0.009 in. Practically the entire deflection shown at the supports appears, therefore, to be due to the compression of the support system.

4.3 Steel Strains

Load-steel strain curves for the bottom row of longitudinal reinforcement are given in Figs. 22 through 28. The top figure represents the full measured range, while the elastic region plotted to a larger scale is presented in the bottom figure. The locations of the gages are shown in the partial sketch of the beam in Fig. 22. Since gages S1 and S5 and gages S2 and S4 are symmetrical about midspan, the strains measured at the two corresponding gage locations were nearly identical. Therefore, in order to make the top figure more easily read, only the strains measured at each of the three different sections along the span are presented. In cases where the strains were different for symmetrical sections, the greater measured strain is shown.

For the three beams reinforced with 1.15 percent longitudinal steel, the strains were well into the work-hardening region at failure. The ultimate steel strain at midspan was estimated either by extrapolation of the steel strain-deflection curve or from the results of the strains measured on 6-in. gage lengths. For the two beams with web reinforcement, the estimated steel strain at failure was much greater than that for the companion specimen without web reinforcement.

The longitudinal steel strains also reached the work-hardening region for the beams with 1.99 percent or more tension steel, except for beam C-4. However, the maximum strains were not very far into the work-hardening region. Again the measured maximum steel strains were greater for the beams with reinforcement than for the beam without.

The web reinforcement affected to a considerable extent the distributions of stress and strain along the tension reinforcement and reduced the force in the tension reinforcement near the anchorage. The distribution of stress along the length of the longitudinal reinforcement indicates to some extent how the beam is internally acting to resist the applied load. Of particular interest are the conditions in the outer gages S1 and S5. A plot of the total tensile force vs. load is given in Fig. 29 for the three beams with 1.15 percent steel and in Fig. 30 for the other four C-series beams. The total tensile force was plotted in these figures instead of stress in order to take into account the various moduli of elasticity of the reinforcement and the variation in steel area in the case of beam C-6 which had longitudinal steel areas of 1.02 sq. in. at midspan but only 0.62 sq. in. at the sections of gages S1 and S5. The total tensile force was computed by first averaging the measured strains at the two sections and then using the experimentally determined tensile force-strain curve of the reinforcement to convert the strain to force. For beams with multiple layers of steel, the strain measured in each layer was used in determining the total tensile force at the section. Also shown in Figs. 29 and 30 are curves designated as theoretical beam and arch behavior. The curve for theoretical beam behavior was obtained by dividing the moment at the gage section by the effective internal lever arm of an assumed fully cracked section, jd, and the curve labelled theoretical arch behavior, which represents the theoretical tensile force, equal for all sections between supports, was obtained by dividing

the moment at midspan by the same lever arm. Since the lever arm depends upon the concrete strength, it did vary slightly, but not enough to warrant different theoretical curves for each specimen.

As can be observed from the two figures, the curves for the beams without web reinforcement follow more closely the theoretical curve for arch behavior than the theoretical curve for beam behavior. Close to yield the measured tensile force agrees very well with the theoretical force for arch behavior. The vertical stirrups decreased the force in the tensile reinforcement near the anchorage, and the inclined bars were even more effective in reducing the longitudinal tensile force near the anchorage. For beam C-6, the measured tensile force agrees very well with the theoretical curve for beam behavior.

The above-noted effect of the web reinforcement on the longitudinal tension force can be explained qualitatively by considering free-body diagrams of the specimens. In Fig. 31 are shown free body diagrams of the portions of beams C-1, C-2, and C-3 to the left of the measured inclined crack at a load of 50 kips and include the internal forces which are believed to act across the crack and cut sections. From statics it is known that the force in the longitudinal steel must be equal to the external moment divided by the effective internal lever arm, jd. The external moment causing the tensile force in the steel at the location of gages S1 and S5 is equal to the moment at the head of the crack passing through the gage section. As the crack extends more toward midspan, the external moment resisted by the longitudinal steel becomes greater, resulting in a larger tensile force. The presence of the web reinforcement hindered the development of the crack passing through the gage section for beams C-2 and C-3 so that it did not extend as far toward midspan as for beam C-1. Hence, it is easily seen why the tensile force at the gage section for beam C-1 was greater than that for beams C-2 and C-3.

Besides retarding the development of the crack, the stresses in the web reinforcement introduce an additional internal resisting moment that tends to reduce the force in the longitudinal steel. For a given amount of web reinforcement, this moment will depend upon how far the crack extends beyond the web reinforcement, for this furnishes the lever arm when taking moments about the point where the compressive force acts at the head of the crack. In the case of the beams with vertical stirrups, the crack, as can be seen in Fig. 31, did not extend much beyond the stirrup. Hence, the lever arm developed was small and the additional resisting moment provided by the web reinforcement could not be expected to influence greatly the tensile force in the longitudinal steel. Because of the particular location of the inclined web reinforcement, the lever arm provided by cracking was greater than that for the vertical stirrups. Thus, the reduction of the longitudinal steel force was greater.

The above discussion is concerned with the effect of the web reinforcement upon the longitudinal tensile force near the anchorage. In order to determine the effect of the web reinforcement upon the distribution of tensile force along the span, the longitudinal steel force at each gage location was computed from the measured strains in the same manner as for the sections at gages S1 and S5 discussed above, and is shown in Fig. 32 for the beams with 1.15 percent steel at a load of 50 kips and in Fig. 33 for the three beams with 1.99 percent steel at a load of 80 kips. The distribution is not shown for beam C-7 because instrumentation difficulties were encountered during the test, and several of the strains recorded for the two top layers of longitudinal steel are believed to be erroneous. The effect of the web reinforcement upon the distribution of tensile force along the span is more noticeable in Fig. 33 than Fig. 32. The tensile force for beam C-4 is nearly constant along the span, whereas the distribution of force

in the longitudinal steel for the beams with web reinforcement is similar to that of the external moment diagram. The figures indicate, then, that the addition of web reinforcement does produce to some extent the desired effect of maintaining beam behavior.

Strains in the Web Reinforcement: Figure 34 shows measured strains in the web reinforcement vs. applied load. Locations of the gages are given in the partial sketch of the beams. The inclined bars of beam C-3 were at yield when the specimen failed, and the bars of beam C-6 which followed the same straining pattern had, of course, yielded before collapse of the beam. The strains measured in the vertical stirrups of beam C-5 were, however, not near the yield strain at failure. Strains in the stirrups of beam C-2 were not measured, but it would seem logical to assume that they would be very similar to those measured for beam C-5.

4.4 Concrete Strains

Strains in the concrete were measured both along the depth of the beam at midspan using a 2-in. Whittemore mechanical gage and along the span at the top edge of the specimen with SR-4 electric gages. The locations of the gages are shown in Fig. 2.

Results of the strain measurements along the depth of the beam are given in Figs. 35 and 36. Although there were five gage lines, at higher loads cracks usually formed between the plugs of the lower gage lines invalidating the measured strain. This accounts for readings not being shown in some instances on the lower gage lines of the beams reinforced with 1.15 percent longitudinal steel. At loads near ultimate the concrete at midspan began crushing, causing the steel plugs cemented to the beam to become loose and eliminating further measurements. The ultimate concrete strain was therefore obtained by extrapolation of the concrete strain-deflection curve for each beam. As can be seen in Fig. 2, an electric gage was located between the two plugs forming

the top gage line. When estimating the ultimate strain, both the strain measured with the Whittemore gage and that measured with the electric gage were extrapolated, and the value thought to be more reliable was chosen.

Although much cannot be said regarding the distribution of concrete strain along the depth at midspan from a study of Fig. 35, since only a few gage lines are shown, Fig. 36 does show that the distribution is in good agreement with the linear strain distribution ordinarily assumed.

It is interesting to note the large values of the estimated ultimate concrete strain. Usually it is assumed that concrete crushes at a limiting strain of 0.004, yet all the estimated ultimate strains are greater than this value. The lowest strain is 0.005 estimated for beam C-5. Estimated ultimate strains for the other specimens are approximately twice that assumed for ultimate flexure theory, the values ranging from 0.007 to 0.010. Since the top gage line was located 0.5 in. from the top edge of the beam, the strains at the extreme fiber can be expected to be even greater than those presented here. A possible explanation of the large strains is that the loading blocks which covered practically the entire span confined the concrete vertically and this confinement increased the crushing strain.

Figures 37 through 39 show the distribution of concrete strains along the span. Since the specimens had a width of 4 1/2 in., whereas the loading blocks were only 4 in. wide, the outer 1/4-in. layer of concrete that was not confined vertically by the loading block on both sides of the beam tended to spall off at loads near ultimate. This spalling-off, of course, prevented the measuring in some instances of the concrete strain near midspan with the electric gages. Therefore, several of the strain readings presented in the three figures are estimated values obtained in the same manner as previously mentioned. The figures are not intended to give quantitative values of the

strains, but instead to show more or less qualitatively the distribution along the span. The estimated values are believed to be sufficiently accurate for this purpose.

As would be expected of beams failing by flexure, there is a concentration of strain near midspan. Because of the limited number of specimens, no definite conclusion can be formed concerning the effect of web reinforcement. It appears from the figures, however, that there is a tendency for the addition of web reinforcement to distribute the concentration of strain at midspan over a larger area, thus reducing the peak strain at midspan. This is especially noticeable if beams C-4, C-5, and C-6 are compared. It would seem logical that web reinforcement should affect the strains in this manner, for it retarded the development of the inclined cracks, and prevented the cracks from joining or almost joining at midspan.

4.5 Total Elongation of Tensile Reinforcement

In order to obtain information on the internal behavior of deep beams and the relationship between internal strains and deflections, the total elongation of the tensile reinforcement was measured. The total elongation of the tensile reinforcement is given as a function of the load in Figs. 40 and 41. The top graph in the figures shows the full measured range of values, and the lower graph is a plot to a larger scale of the values in the elastic region. The elongation is equal to the sum of the strains in the longitudinal reinforcement. This fact is verified experimentally in Figs. 42 and 43 in which the sum of the measured strains in the longitudinal reinforcement is plotted against the measured total elongation up to yield. The sum of the steel strains was obtained by computing the area under the curve of measured distribution of strain along the span, assuming linear distribution between adjacent gage sections and zero strain at the centerline of the supports. The dashed line in the figures represents the theoretical condition that the measured

elongation is equal to the sum of the strains in the longitudinal reinforcement. It can be seen that for the majority of the specimens the experimental curve is in good agreement with the theoretical dashed curve, which indicates that both the strains and the total elongations were accurately measured and that the distribution of strains between gage points is smooth as assumed. These measurements indicate that an accurate prediction of total elongation can be made if the strains at a number of points along the length can be predicted accurately.

To determine the relationships between the midspan deflections and the total elongations of the tensile reinforcement, the midspan deflections are plotted versus the total elongations for beams C-1, C-2, C-3, C-4, C-5, and C-6 in Figs. 44 and 45. In each figure the lower graph shows the full measured range of values and the upper graph is a plot to a larger scale of the behavior before yielding. In the upper graph the curve which best fits the post yield range is reproduced for direct comparison.

In Fig. 44 the plots for beams C-1, C-2, and C-3 are given. It may be noted that the midspan deflections are proportional to the total elongations of the tensile reinforcement for both the elastic and post yield ranges. There is a slight departure in the elastic range, possibly caused by the gradual cracking phenomenon, etc., but at yield the points are close to the post yield curve. Note that the slopes of all three curves are about equal, indicating no effect on the deflection--elongation relationship due to web reinforcement.

It may be noted that neither the deflection versus load nor elongation versus load curves are linear (see Figs. 14, 15, 40, and 41), but both have very pronounced yield points. If the midspan deflections were due to any extent to shearing or compressive strains in the concrete, or to other effects which are proportional to load, then the deflection versus elongation curves would have an abrupt change of slope at the yield point. Since these

measured curves appear to be linear with a constant slope over the entire elastic and post yield ranges, it appears that the midspan deflection for beams C-1, C-2, and C-3 is due practically entirely to the elongation of the tensile reinforcement.

In Fig. 45 are given the curves of midspan deflection versus elongation of the tensile reinforcement for beams C-4, C-5, and C-6. For these beams there is a definite break in the slope of the curves at the yield point. In each beam the graph for both the elastic and post yield regions is linear, but the two segments have different slopes; after yielding the deflections increase less rapidly with respect to the increase of elongations. The ratios of the slope in the post yield range to the slope in the elastic range are about 0.62 for beams C-4 and C-5 and 0.84 for beam C-6. It may be noticed for each beam that the projection of the curve for the post yield range does not pass through the origin; the projections intersect the vertical axis at 0.03 in. for beams C-4 and C-5 and 0.015 for beam C-6. This behavior is possibly due to the effect of compressive and shearing strains in the concrete and to compression of the roller supports. The only explanation which can be offered for the difference in behavior between beams C-1, C-2, C-3 and C-4, C-5, C-6 is that the concrete strains and roller deformations were more significant in the latter group, beams C-4, C-5, and C-6, because the yield load is about 50 percent greater than for the first group which have a smaller steel percentage.

From these measurements it can be concluded that the maximum deflections can be considered to be due entirely to elongation of the tensile reinforcement. The yield deflection may be partly due to shearing and compressive strains in the concrete but the major part is also due to the elongation of the tensile reinforcement. Web reinforcement appears to have little effect on the deflection-elongation relationship.

V. BEHAVIOR OF BEAMS WITH COMPRESSION REINFORCEMENT

5.1 Test Results and Modes of Failure

Test results and the most significant properties of the two beams reinforced in both tension and compression are given in Table 6. Also listed are the test results and properties of beam A-3-2 tested during the previous year. Since beams A-3-4 and A-3-5 were tested under different loading conditions, it seems best to present the data, for comparative purposes, in terms of midspan moment instead of total load. The uniform load used in the test of beam A-3-4 was simulated by 10 jacks at 4 in., while the load for the test of beam A-3-5 was comprised of 8 jacks at 4 in. Thus, for a given load, the moment at midspan for the systems of 10 and 8 jacks is 4W and 5W, respectively, where W = total load. When computing yield and ultimate moments only live load was considered.

Beam A-3-4 definitely failed by crushing of the concrete above the support at a bearing stress of 0.80 f'_c. The manner of failure of beam A-3-5 is not definitely known. At a load of 179.2 kips the specimen suddenly dropped at midspan. Computations show that the average bond stress at the anchorage at ultimate load was equal to 0.5 f'_c, and since no special anchorage was provided for the longitudinal tension steel, it is very likely that the failure of the specimen occurred at the anchorage. In both cases the beams failed before their full flexural capacities were developed, as is evident from the photographs shown in Fig. 46. The concrete at top midspan had begun to crush, but the crushing was not so pronounced as to cause failure of the beams by compression.

Well developed inclined cracks extending from the inside face of the supports to the top at midspan formed in both beams. At loads near ultimate, the inclined cracks had progressed as high as the level of the compression steel, thus greatly reducing the effective concrete area.

5.2 Deflections

In Fig. 47 are shown the moment-deflection curves for the two beams. The data are presented in terms of moment since, as mentioned before, the number of jacks used in the tests of the two beams were different. The curves are for the deflection measured at top midspan. Drop-offs in load which occurred while readings were being taken are not shown. Also shown for comparative purposes is the moment-deflection curve for beam A-3-2 of the previous A-series tests. Although both beam A-3-4 and beam A-3-5 failed prematurely they deflected more than beam A-3-2 which failed by flexure.

5.3 Steel Strains

Measured strains in the longitudinal tension steel are shown in Figs. 48 and 49. The full measured range is given in the top figure, while the elastic region is shown to a larger scale in the lower figure. Only the steel strains at three gage sections are presented in the top figure. When selecting the three sections the same procedure was used as discussed in the preceding chapter. Locations of the strain gages are shown in the partial sketch of the beam accompanying Fig. 48.

The strains in the longitudinal tension steel were well into the work-hardening region at failure. The estimated ultimate midspan strains noted in the figures were obtained by extrapolation of the steel strain-deflection curve for each beam. However, the electric gages on the longitudinal reinforcement of beam A-3-5 were destroyed long before the ultimate deflection was reached. Therefore, the results of the strains measured on 6-in. gage lengths were plotted against the deflections and extrapolated to obtain the strain at failure. Since the strain measured over a 6-in. gage length is an average value, the value of the ultimate steel strain listed for beam A-3-5 is perhaps somewhat less than the actual strain occurring at midspan.

From observation of the elastic region of the load-steel strain curves it can be noted that the curves for all the gage sections fall within a narrow envelope and progress nearly parallel to each other as the load increases. This indicates that the strains in the longitudinal tension steel were nearly constant along the span. Consequently, it may be said that the specimens behaved as tied arches rather than beams, the longitudinal reinforcement serving as the tie.

Shown in the lower figure is a theoretical curve for the steel strain at midspan. The curve was obtained by dividing the moment at midspan by the effective internal lever arm of an assumed fully cracked section, jd, and converting the resulting tension force to strain. It can be seen that the measured strains at midspan agree fairly well with the computed values. The deviation of the strains from the theoretical curves at low loads is due to the specimen not being fully cracked as assumed when computing the effective internal lever arm.

5.4 Concrete Strains

The concrete strains at midspan varied linearly along the depth of the beam as shown in Fig. 50. It was not possible to present the strain distributions at high loads, for cracking had extended as high as the second gage line eliminating further measurements.

The value of the concrete strain over the top gage line at failure was estimated by extrapolation of the concrete strain-deflection curves. For beams A-3-4 and A-3-5 the estimated concrete strains at failure were of the order of 0.009 and 0.007, respectively. The strains at the extreme fiber could be expected, then, to be even greater, since the top gage line was located 0.5 in. from the top edge of the specimens. Because the two beams failed prematurely, the value of the concrete strain at midspan at failure

of the beams by flexure is not known, although the strain would be much greater than the value of 0.004 normally assumed for shallow beams failing by compression.

The variation of the concrete strains along the top edge of the specimens is shown in Fig. 51. As can be seen from the distribution of strains for beam A-3-4, there is a great concentration of strain at midspan. The distribution of concrete strains for beam A-3-5 is similar to that of beam A-3-4 up to a load of 130 kips. Upon applying another load increment, the gage at midspan was destroyed. Unfortunately, it was impossible to estimate the strain beyond this load. However, it seems logical that the strain distribution at higher loads would be similar to the distributions at lower loads and to that of beam A-3-4.

VI. STUDIES OF THE FLEXURAL STRENGTH AND BEHAVIOR OF DEEP BEAMS WITH WEB REINFORCEMENT AND WITH COMPRESSION REINFORCEMENT

6.1 Effect of Web Reinforcement Upon External Behavior

Yield Moment: Listed in Table 7, Column (4), are the yield moments computed from the test yield loads, and in Column (5) are listed the ratios of the yield moments of the beams with web reinforcement to the yield moment of their companion specimen without web steel, M_{yw}/M_{ywo}. Beam C-1 is the companion specimen of beams C-2 and C-3, and beam C-4 is the companion specimen of beams C-5 and C-6. The maximum deviation in yield moments is only 7 percent, and therefore it can be concluded that the addition of web reinforcement had no effect upon the yield strength of the specimens.

Ultimate Moment: The effect of web reinforcement upon ultimate moment can be studied in the same manner as for the moment at yielding of the beam. Ultimate moments computed from the ultimate test loads are given in Column (6), and the ratios of the ultimate moments of the beams with web reinforcement to the ultimate moment of their companion specimen are listed in Column (7) of Table 7. The ultimate moment was increased by reinforcing the web, the greatest increase in load-carrying capacity occurring for beams C-2 and C-3.

It has been noted previously that the addition of web reinforcement retarded the development of the inclined cracks. Since the inclined cracks cause concentrated concrete strains at midspan, any retardation of the cracks allows the steel strains to reach a higher value before the limiting concrete strain is attained. If the steel strain is in the work-hardening region, any increase in strain will produce a greater tensile force resulting in a greater resisting moment.

In Fig. 52 are shown the strain distributions along the entire depth of the beam near midspan at loads near ultimate for beam C-4, which had no web reinforcement, and for beam C-6, which had inclined web reinforcement. The strain distribution for beam C-4 is non-linear. A non-linear strain distribution at midspan is always obtained for deep beams without web reinforcement, for loads greater than the transition cracking load, for the following reason. In such beams extensive diagonal cracks develop and run from the bottom edge near each support almost to the top edge near midspan. Because of these cracks the strains in the tensile reinforcement are roughly constant from support to support. This typical behavior has been likened to that of a tied arch or a beam with reinforcement which is not bonded to the concrete between supports. The strain in the reinforcement at every cross section is roughly equal to the separation of the supports divided by the distance between supports. It is meaningless to compute curvature at a section from the tensile reinforcement strains because the extensive cracking has invalidated the assumption of continuity of member upon which such a computation would be based. In contrast, the compressive concrete strains are highly concentrated at midspan. The distribution of compressive concrete strains through the depth to the neutral axis is roughly linear. The curvature at a section can be computed from the distribution of concrete strains. However, because of the concentrated nature of the concrete strains at midspan and the distributed nature of the steel strains, for any given deflection the curvature indicated by the distribution of concrete strains will always exceed the "apparent curvature" computed by dividing the steel strain by the distance to the neutral axis. In other words, the strain distribution through the depth is non-linear, as shown.

The strain distribution through the depth is linear for beam C-6. This linear distribution, which is typical of true flexural behavior, was obtained in this beam because of the web reinforcement, as discussed fully in Section 4.3.

The type of strain distribution, non-linear as in beam C-4 or linear as in beam C-6, may affect the ultimate moment, because when the limiting concrete strain is reached the steel strain for deep beams with linear distributions will be greater than for similar deep beams with typical non-linear distributions. Due to instrumentation difficulties at loads near ultimate, it was impossible to obtain strain distributions along the entire depth of the beam for other C-series specimens. However, it seems that the addition of web reinforcement would affect the strain distributions of the other beams in the same manner as noted in Fig. 52.

Since the steel strain at midspan for beam C-1 which had no web reinforcement was within the work-hardening region at failure, the increased strain in beams C-2 and C-3 caused by the inclusion of web reinforcement increased the longitudinal tensile force and resulted in greater load-carrying capacities for these beams. The longitudinal steel of beam C-4 was not strain-hardened at failure, although the ultimate steel strain was close to the work-hardening region. The ultimate strengths of beams C-5 and C-6 were not appreciably greater than their companion specimen, beam C-4, because the increased steel strains did not result in increased steel stresses.

Ductility and Energy-Absorbing Capacity: Ductility is an important property of beams subjected to blast loads. It is defined as the ratio of ultimate deflection to yield deflection and is shown in Column (8) of Table 7. The values range from 4.2 to 17.1. Beam C-7 which had the longitudinal tension steel distributed along the depth was the least ductile, while the three beams having a longitudinal steel percentage of 1.15 exhibited the greatest ductility. In all cases, web reinforcement increased the ductility of the members. Web reinforcement in the form of inclined bars increased the ductility considerably more than vertical stirrups.

Listed in Column (9) of Table 7 are values of the energy-absorbing capacity. The values were determined by approximating the load-deflection curves by two straight lines, one from the origin to yield load and deflection, and the other from yield load and deflection to ultimate load and deflection, and then computing the area under the approximated curve multiplied by a factor depending upon the loading condition. Beam C-6 which had inclined web reinforcement exhibited the greatest energy-absorbing capacity, while beam C-7 exhibited the least. The addition of web reinforcement increased the energy-absorbing capacity of the beam in every case, although the increase was very small for the specimens with 1.15 percent longitudinal steel.

6.2 Effect of Compression Reinforcement Upon External Behavior

In order to determine the effect of compression reinforcement upon the external behavior of the beams, the test data of beam A-3-2 obtained from the previous series of tests (1) are presented along with the data for beams A-3-4 and A-3-5.

Yield Moment: Values of the ratios of the yield moments of the beams with compression reinforcement to the yield moment of the companion specimen without compression steel are presented in Column (5) of Table 7. It can be seen that there is a marked increase in the yield moments of beams A-3-4 and A-3-5. The increase is believed to be due mostly to the variation in the yield stress of the tension reinforcement. The yield stresses of the steel used in beams A-3-4 and A-3-5 were 9 and 13 percent, respectively, greater than the yield stress of the tension steel of beam A-3-2. It appears, therefore, that compression reinforcement had little, if any, effect upon the yield moment.

Ultimate Moment: A comparison of moments at failure for the three beams is of only limited value since beams A-3-2, A-3-4, and A-3-5 failed by

flexure, bearing, and anchorage, respectively. However, the ratios of ultimate moments of the two beams with compression reinforcement to the ultimate moment of beam A-3-2, listed in Column (7) of Table 7, are of some interest in that they show that even though the two beams reinforced in both tension and compression failed prematurely, the moments at failure were greater than that causing the flexure failure of beam A-3-2. It seems, therefore, that the flexural strength of beams with a L/d ratio of 2.32 may be increased considerably by the addition of compression steel if they are proportioned so as to prevent them from failing by other modes before their full flexural capacities are developed.

Ductility and Energy-Absorbing Capacity: Because of the different modes of failure of the three beams, no direct comparisons can be made to determine the effect of compression reinforcement upon ductility and energy-absorbing capacity. Nevertheless, the values of ductility are listed in Column (8) of Table 7. It can be seen that the ductilities of the two specimens reinforced in both tension and compression are almost as great as that for beam A-3-2 which was reinforced in tension only and failed by flexure. The deflections at yield of beams A-3-4 and A-3-5 were somewhat greater than the yield deflection of beam A-3-2, causing the lower values of ductility.

The energy-absorbing capacities of the three beams are listed in Column (9) of Table 7. It can be seen that even though beams A-3-4 and A-3-5 failed prematurely, the energy-absorbing capacities of these two specimens were greater than that for beam A-3-2.

6.3 Prediction of External Behavior

Moment at Yielding: In Table 8 are listed the values of computed moments at first yielding of the tension reinforcement. The moments for the seven C-series beams were computed by the conventional straight-line theory. The strain and stress distributions are assumed to be as shown in Fig. 53(a).

For the two beams reinforced in both tension and compression, the moment at first yielding was computed by consideration of the strain and stress relationships shown in Fig. 53(b). A summary of the theoretical expressions for the moment at yielding is given in Appendix A of Part 3 of this final report.

Shown in Table 8 are the yield moments determined from the test loads at yielding of the specimens in Column (2), the computed yield moments in Column (3), and the ratios of the test yield moments to the computed yield moments in Column (4). The ratios are all greater than 1.00, ranging from 1.04 to 1.14. It should be remembered that the test yield loads were determined by the intersection of the primary and secondary slopes of the load-deflection curves. In general, this method of determining the yield load over-estimates slightly the actual load at which the longitudinal reinforcement yields. Although the ratios of the test yield moments to the computed yield moments are all greater than one, the computed moments at first yielding are in good agreement with the actual moments at flexural yielding of the specimens.

Ultimate Moment: It is known that the ultimate moment of shallow reinforced concrete beams failing by compression at midspan after yielding of the longitudinal tension reinforcement can be predicted with reasonable accuracy by consideration of the strain and stress distributions shown in Fig. 54(a) for beams reinforced in tension only and in Fig. 54(b) for beams reinforced in both tension and compression. A summary of the theoretical expressions for ultimate moment is given in Appendix A of Part 3 of this final report.

In view of the fact that at the present time there is no available theory to predict the ultimate strength of deep reinforced concrete members, the procedure for beams of normal proportions was applied in an attempt to predict the ultimate moments of the test specimens. The theoretical ultimate moments, M_f, the ultimate test moments computed from the test loads, and the ratios of the test moments at failure to the theoretical moments are listed in

Table 8. It can be seen that the actual moments were greater in every case, the ratios ranging from 1.07 to 1.39. It is interesting to note that although the two beams reinforced in both tension and compression failed prematurely, the flexural moments at failure were greater than the predicted values.

It appears that the ultimate strength theory for shallow beams underestimates the strength of the test specimens, and especially the ultimate strength of the beams with web reinforcement in which the longitudinal tension steel had strain-hardened prior to failure. However, when computing the theoretical moments, the strain at which the concrete crushes, ϵ_u, was assumed to be 0.004 in./in. As was pointed out in Chapter IV, the estimated concrete strains at failure of the C-series specimens were of the order of 0.007 to 0.010 in./in. If an average value of 0.008 is assumed for the limiting concrete strain, and the ultimate flexural moments of the C-series beams are computed using this value, the moments, M_f', listed in Column (8) of Table 8 are obtained. In Column (9) are given the ratios of the actual moments at failure to the theoretical moments. The ratios range between 0.98 and 1.20, indicating that the theoretical moments computed by assuming $\epsilon_u = 0.008$ are in much better agreement with the test results than the theoretical moments obtained under the assumption that $\epsilon_u = 0.004$.

The assumption that the concrete crushes at a limiting strain of 0.008 in./in. affects, of course, the critical value of the reinforcing index, q_o, corresponding to $\epsilon_s = \epsilon_o$, used to determine whether the steel strain at failure will be in the yield or work-hardening region. By assuming $\epsilon_u = 0.004$ when computing q_o, only the q values for the beams reinforced with 1.15 percent longitudinal steel indicated that the steel would be strain-hardened at failure, as can be seen in Table 9. However, the load-steel strain curves presented in Chapter IV show that the longitudinal steel strains at midspan reached the work-hardening region prior to failure in all the specimens except beam C-4. For this beam the steel strain was very close to the work-hardening region

when the specimen failed. The comparison in Table 9 between q and the value of q_o obtained by assuming $\epsilon_u = 0.008$ indicates that the strain at midspan in the longitudinal reinforcement of all the specimens should enter the work-hardening region. This appears to agree more closely with the test results.

Due to the limited number of specimens, no definite conclusions can be drawn regarding the value of the limiting strain at which the concrete crushes. The value of 0.004 usually assumed for the ultimate strength theory of shallow beams does not, however, agree with test results. Possibly a larger limiting concrete strain should be assumed, as above, for beams tested under uniform loads that confine the top surface of the beam.

Deflections: There are insufficient data from this series of tests to develop formulas for the prediction of the yield and ultimate deflections. A comprehensive study of the calculation of deflections is given in Part 3 of this final report. However, the following qualitative inferences can be drawn.

(1) Web reinforcement does not affect appreciably the yield deflection.

(2) Web reinforcement has two somewhat counterbalancing effects on the deflection at maximum load, as follows:

   (a) Web reinforcement, by reducing the concentration of concrete strain at midspan, increases the steel strain at midspan at failure; this effect tends to increase the deflection at maximum load.

   (b) Web reinforcement changes the distribution of internal stresses and strains in the beam and tends to restore beam action and to reduce arch action. A deep beam without web reinforcement behaves at ultimate as if the steel is anchored only at the ends and is unbonded between ends. A deep beam with web reinforcement acts more like a normal bonded beam. This partial restoration of beam behavior tends to decrease the ultimate deflections.

The net result of these two effects in the case of beams C-1, C-2, and C-3, with p = 1.15 percent, was to produce essentially

no change in the deflections at maximum load, while in the case of beams C-4 and C-5, with p = 1.99 percent, the deflection at maximum load was increased by web reinforcement. The ultimate deflection of beam C-6 was greatly increased owing to another effect discussed previously.

VII. SUMMARY AND CONCLUSIONS

7.1 Summary

Nine rectangular reinforced concrete deep beams were tested under uniform load on a simple span of 36 in. Two of the beams (A-series specimens) were reinforced in both tension and compression and had a span-depth ratio of 2.32. The other seven beams (C-series specimens) were tested to investigate the effect of web reinforcement. Two of the seven beams had different percentages of longitudinal tension steel and no web reinforcement. Then two variations of each of the two beams were made by adding vertical stirrups and inclined bars. The last beam had the longitudinal reinforcement distributed along the depth. Since the depth to the centroid of the bottom layer of the longitudinal steel was kept constant at 12 in. for the seven C-series specimens, the span-depth ratios ranged from 3.00 to 3.32.

The deflections at top and bottom at midspan, the strains in the longitudinal tension steel, and the concrete strains along the depth of the beam at midspan and along the top edge of the beam were measured for all nine specimens. For beams that were reinforced with multiple layers of longitudinal tension steel, the strains were measured in one bar of each layer. In addition, the deflections at various positions along the span and the total elongation of the tensile reinforcement were determined. Strains in the web reinforcement of three of the C-series specimens were also measured.

The two beams reinforced in both tension and compression failed before their maximum flexural capacities were developed. One beam failed in bearing, and the other one failed at the anchorage. In both beams, inclined cracks extending from the inside face of the supports to midspan at the level of the compression reinforcement formed, greatly reducing the effective concrete area and causing the beams to behave as tied arches.

All the C-series specimens failed in flexure by first yielding of the longitudinal reinforcement followed by crushing of the concrete at midspan. In the two beams without web reinforcement and the beam with the longitudinal steel distributed along the depth, inclined cracks developed and extended very near to the top edge of the specimens at midspan. The presence of vertical stirrups retarded the development of the inclined cracks and forced them to progress more vertically. Inclined web reinforcement confined the major cracks to within the middle portion of the span. The inclined web reinforcement seemed to be most effective in reducing the extent of the diagonal cracking and the influence of this cracking on the distribution of strains in the tension reinforcement.

The concrete strains along the depth of the beam at midspan varied linearly in all nine beams. A great concentration of concrete strain occurred at midspan in the beams reinforced in both tension and compression and in the beams without web reinforcement. The addition of web reinforcement appeared to distribute the concrete strains more uniformly over a larger area near midspan. The average estimated midspan concrete strain at failure was 0.008 in./in., twice that usually assumed for the strain at which concrete crushes. This larger value of the strain is believed to be due to the vertical confinement of the top surface of the specimen by the uniform load.

7.2 Conclusions

The following conclusions may be drawn from the results of the tests described herein. These conclusions are of course limited by the fact that only a very small range of each variable was investigated. In particular, only one span/depth ratio, 2.32, was considered for beams reinforced in both tension and compression. The span/depth ratio for the C-series specimens varied only between 3.00 and 3.32.

1. Neither the compression nor the web reinforcement had any effect upon the yield strength or corresponding yield deflection of the member.
2. Compression reinforcement appeared to increase the ultimate flexural strength of deep beams, although how much so cannot be determined because the two beams tested failed prematurely.
3. Web reinforcement had two major effects on the internal strain distributions at failure in the deep beams tested. First, the concentration of compressive strain in the concrete at midspan was reduced; for this reason the strains in the tensile reinforcement at midspan at failure were increased. Secondly, normal flexural action was partially restored and the typical arch action of deep beams without web reinforcement was reduced. In deep beams without web reinforcement the strain distributions in the beams at failure are like those which would exist if the tensile reinforcement were anchored at the ends and unbonded between ends. With sufficient web reinforcement the strain distributions are more like those of a normal beam.
4. Web reinforcement, by increasing the strain in the tensile reinforcement at midspan at failure, increased the ultimate strength of the beams which failed when the strain in the tensile reinforcement was in the strain-hardening range, but it did not affect the ultimate strength of the beams which failed when the strain in the tensile reinforcement was in the yield range.
5. The deflections at maximum load of beams C-2 and C-3, with 1.15 percent tensile reinforcement, were not appreciably affected by the web reinforcement. The two effects of web reinforcement on the internal strains at maximum load approximately counterbalanced

each other insofar as the deflections of these beams were concerned. However, the midspan deflection at maximum load for beam C-5, with 1.99 percent reinforcement, was substantially greater than for the companion beam without web reinforcement.

6. The midspan deflection of beam C-6, which had inclined web reinforcement formed by bending up the top layer of tensile reinforcement bars, had a greatly increased maximum value over that of beam C-4 due primarily to the very large strains developed in the tensile reinforcement in the region between the ends and the bend-up point. This design appears to be very advantageous for blast-resistant construction as it gives both high strength and great ductility and energy-absorbing capacity.

7. Ductility and energy-absorbing capacity of the beams were increased by the addition of web reinforcement and decreased by distributing the longitudinal reinforcement along the depth. The increase in ductility and energy-absorbing capacity was very small for the beams reinforced with 1.15 percent longitudinal tension steel but was considerable for the beams reinforced with 1.99 percent longitudinal steel.

8. The moment at flexural yielding can be predicted with reasonable accuracy by the usual straight-line theory for beams reinforced in both tension and compression and for beams with web reinforcement.

9. The ultimate strength theory for shallow beams under-estimates the maximum flexural capacity of the members when the value of 0.004 in./in. is assumed for the crushing strain of the concrete. When the average test value of 0.008 in./in. is used for the limiting concrete strain, along with the ultimate strength theory

for beams of normal proportions, the predicted values of ultimate flexural capacity agree very well with the test results of the C-series specimens except for the two beams with web reinforcement whose longitudinal tension steel was greatly strain-hardened prior to failure. Because of the premature failure of the two A-series specimens, no conclusion can be formed regarding the agreement between predicted and test values of the ultimate flexural capacity of beams reinforced in both tension and compression.

VIII. BIBLIOGRAPHY

1. Austin, W. J., Untrauer, R. E., Egger, W., and Winemiller, J. R., "An Investigation of the Behavior of Deep Members of Reinforced Concrete and Steel", Technical Report to Air Force Special Weapons Center, AFSWC-TR-59-18, 1960

2. Sozen, M. A., "Strength in Shear of Prestressed Concrete Beams Without Web Reinforcement", Ph. D. Thesis, University of Illinois, August 1957. Issued as a part of the Sixth Progress Report of the Investigation of Prestressed Concrete for Highway Bridges, Civil Engineering Studies, Structural Research Series No. 139, August 1957.

3. Gaston, J. R., Siess, C. P., and Newmark, N. M., "An Investigation of the Load-Deformation Characteristics of Reinforced Concrete Beams up to the Point of Failure", Civil Engineering Studies, Structural Research Series No. 40, University of Illinois, December 1952.

4. Laupa, A., Siess, C. P., and Newmark, N. M., "Strength in Shear of Reinforced Concrete Beams", University of Illinois Engineering Experiment Station Bulletin No. 428, March 1955.

TABLE 1 PROPERTIES OF A-SERIES SPECIMENS

b = 4 in.; L = 36 in.

Beam Mark	d in.	d' in.	L/d	f'_c psi	Tension Reinforcement			Compression Reinforcement		
					No. & Size	p	f_y ksi	No. & Size	p'	f'_y
A-3-4	15.5	14.125	2.32	4860	2-#5	0.0100	56.13	1-#5	0.0050	56.13
A-3-5	15.5	14.125	2.32	5550	2-#5	0.0100	58.06	2-#5	0.0100	58.06

TABLE 2 PROPERTIES OF C-SERIES SPECIMENS

b = 4 1/2 in.; L = 36 in.

Beam Mark	d in.	L/d	f'_c psi	Tension Reinforcement			Web Reinforcement		
				No. & Size	p	f_y ksi	Type	No. & Size	f_y
C-1	12.00	3.00	2970	2 - #5	0.0115	43.55	None	--	--
C-2	12.00	3.00	3250	2 - #5	0.0115	43.55	Vertical Stirrups	6 - #3	54.54
C-3	12.00	3.00	3520	2 - #5	0.0115	43.55	Inclined Bars	4 - #4	46.50
C-4	11.39	3.16	3690	2 - #4 2 - #5	0.0199	48.00 43.87	None	--	--
C-5	11.39	3.16	3060	2 - #4 2 - #5	0.0199	48.00 43.87	Vertical Stirrups	6 - #3	54.54
C-6	11.39	3.16	3530	2 - #4 2 - #5	0.0199	46.50 43.87	Inclined Bars	4 - #4	46.50
C-7	10.82	3.32	3140	2 - #4 2 - #5	0.0209	48.00 45.16	None	--	--

TABLE 3 PROPERTIES OF THE REINFORCING STEEL

Beam Mark	Tension Reinforcement			Compression Reinforcement		
	f_y ksi	ϵ_y in./in.	ϵ_o in./in.	f'_y ksi	ϵ'_y in./in.	ϵ'_o in./in.
A-Series Specimens						
A-3-4	56.13	0.0018	0.0108	56.13	0.0018	0.0108
A-3-5	58.06	0.0022	0.0071	58.06	0.0022	0.0071

Beam Mark	Tension Reinforcement			Web Reinforcement		
	f_y ksi	ϵ_y in./in.	ϵ_o in./in.	f_y ksi	ϵ_y in./in.	ϵ_o in./in.
C-Series Specimens						
C-1	43.55	0.0015	0.0152	---	---	---
C-2	43.55	0.0015	0.0152	54.54	0.0018	0.0166
C-3	43.55	0.0015	0.0152	46.50	0.0016	0.0169
C-4	(#4)48.00 (#5)43.87	0.0015 0.0017	0.0137 0.0143	---	---	---
C-5	(#4)48.00 (#5)43.87	0.0015 0.0017	0.0137 0.0143	54.54	0.0018	0.0165
C-6	(#4)46.50 (#5)43.87	0.0016 0.0017	0.0169 0.0143	46.50	0.0016	0.0169
C-7	(#4)48.00 (#5)45.16	0.0015 0.0014	0.0137 0.0130	---	---	---

TABLE 4 PROPERTIES OF THE CONCRETE MIXES

Beam Mark	Gravel:Cement:Sand by Weight	W/C Ratio by Weight	Slump in.	Comp. Str. psi	Mod. of Rupt. psi	Age at Test days
			A-Series Specimens			
A-3-4	3.53:1.00:3.26	0.68	1/2	4860	465	12
A-3-5	3.56:1.00:3.29	0.62	1/4	5550	570	12
			C-Series Specimens			
C-1	4.52:1.00:4.22	0.81	1/2	2970	430	21
C-2	4.51:1.00:4.22	0.82	1/2	3250	470	11
C-3	4.51:1.00:4.22	0.84	3/4	3520	365	15
C-4	4.52:1.00:4.13	0.85	3/4	3690	415	17
C-5	4.50:1.00:4.20	0.86	1	3060	330	11
C-6	4.57:1.00:4.16	0.84	1/2	3530	390	22
C-7	4.50:1.00:4.18	0.89	1	3140	410	15

TABLE 5 TEST RESULTS OF C-SERIES SPECIMENS

Beam Mark	f'_c psi	f_y ksi	p %	Web Reinforcement	Yield Load W_y kips	Ultimate Load W_u kips	Yield Deflection Δ_y in.	Ultimate Deflection Δ_u in.	Mode of Failure
C-1	2970	43.6	1.15	None	64.5	76.2	0.060	0.875	Flexure
C-2	3250	43.6	1.15	Vertical Stirrups	61.0	89.5	0.056	0.828	Flexure
C-3	3520	43.6	1.15	Diagonal Bars	60.0	94.5	0.048	0.823	Flexure
C-4	3690	46.0	1.99	None	99.5	102.0	0.087	0.412	Flexure
C-5	3060	46.0	1.99	Vertical Stirrups	93.8	106.0	0.091	0.512	Flexure
C-6	3530	45.2	1.99	Diagonal Bars	98.2	102.6	0.078	0.728	Flexure
C-7	3140	46.6	2.09	None	90.6	95.9	0.084	0.352	Flexure

TABLE 6 TEST RESULTS OF A-SERIES SPECIMENS

Beam Mark	f'_c psi	f_y ksi	p %	f'_y ksi	p' %	Yield Moment M_y in.-kips	Ultimate Moment M_u in.-kips	Yield Deflection Δ_y in.	Ultimate Deflection Δ_u in.	Mode of Failure
A-3-4	4860	56.1	1.00	56.1	0.50	552	745	0.080	0.608	Bearing
A-3-5	5550	58.1	1.00	58.1	1.00	565	896	0.095	0.840	Anchorage
A-3-2*	5610	51.4	1.00	--	0	480	659	0.064	0.570	Flexure

* Data obtained from previous A-series tests.

TABLE 7 COMPARATIVE TEST RESULTS

(1) Beam Mark	(2) f'_c psi	(3) f_y ksi	(4) M_y in.-kips	(5) $\frac{M_{yw}}{M_{ywo}}$	(6) M_u in.-kips	(7) $\frac{M_{uw}}{M_{uwo}}$	(8) Ductility Δ_u/Δ_y	(9) Energy-Absorbing Capacity in.-kips
				C-Series Specimens				
C-1	2970	43.6	322	--	381	--	14.6	32.9
C-2	3250	43.6	305	0.95	448	1.17	14.8	33.2
C-3	3520	43.6	300	0.93	472	1.24	17.1	34.0
C-4	3690	46.0	498	--	510	--	4.7	20.6
C-5	3060	46.0	469	0.94	530	1.04	5.6	25.7
C-6	3530	45.2	491	0.98	513	1.01	9.3	37.9
C-7	3140	46.6	453	--	480	--	4.2	16.0
				A-Series Specimens				
A-3-4	4860	56.1	552	1.15	745	1.13	7.6	45.5
A-3-5	5550	58.1	565	1.10	896	1.36	8.8	63.5
A-3-2*	5610	51.4	480	--	659	--	8.9	37.9

* Data obtained from previous A-series tests.

TABLE 8 COMPARISON OF MEASURED AND COMPUTED MOMENTS

(1) Beam Mark	(2) Test M_y in.-kips	(3)* Comp. M_y in.-kips	(4) Test M_y / Comp. M_y	(5) Test M_u in.-kips	(6)* M_f (ϵ_u=0.004) in.-kips	(7) Test M_u / M_f	(8)* M'_f (ϵ_u=0.008) in.-kips	(9) Test M_u / M'_f
				C-Series Specimens				
C-1	322	284	1.13	381	328	1.16	381	1.00
C-2	305	285	1.07	448	332	1.35	387	1.16
C-3	300	286	1.05	472	339	1.39	394	1.20
C-4	498	451	1.10	510	472	1.08	521	0.98
C-5	469	450	1.04	530	465	1.14	497	1.06
C-6	491	445	1.10	513	465	1.10	504	1.02
C-7	453	434	1.04	480	447	1.07	483	0.99
				A-Series Specimens				
A-3-4	552	486	1.14	745	600	1.24	---	---
A-3-5	565	508	1.11	896	831	1.08	---	---

* A summary of the theoretical expressions for the computation of the values of M_y, M_f, and M'_f is given in Appendix A of Part 3 of this final report.

TABLE 9 PREDICTION OF STEEL STRAINS AT FAILURE

Beam Mark	q	q_o (ϵ_u=0.004)	Expected Strain Range	q_o (ϵ_u=0.008)	Expected Strain Range	Measured Strain Range
C-1	0.169	0.220	W.H.*	0.364	W.H.	W.H.
C-2	0.154	0.210	W.H.	0.348	W.H.	W.H.
C-3	0.142	0.205	W.H.	0.339	W.H.	W.H.
C-4	0.246	0.217	Yield	0.354	W.H.	Yield
C-5	0.296	0.233	Yield	0.380	W.H.	W.H.
C-6	0.253	0.215	Yield	0.353	W.H.	W.H.
C-7	0.309	0.243	Yield	0.393	W.H.	W.H.

* W.H. indicates work-hardening region.

$$q = \frac{pf_y}{f'_c}$$

$$q_o = \frac{k_1 k_3 \epsilon_u}{\epsilon_u + \epsilon_o}$$

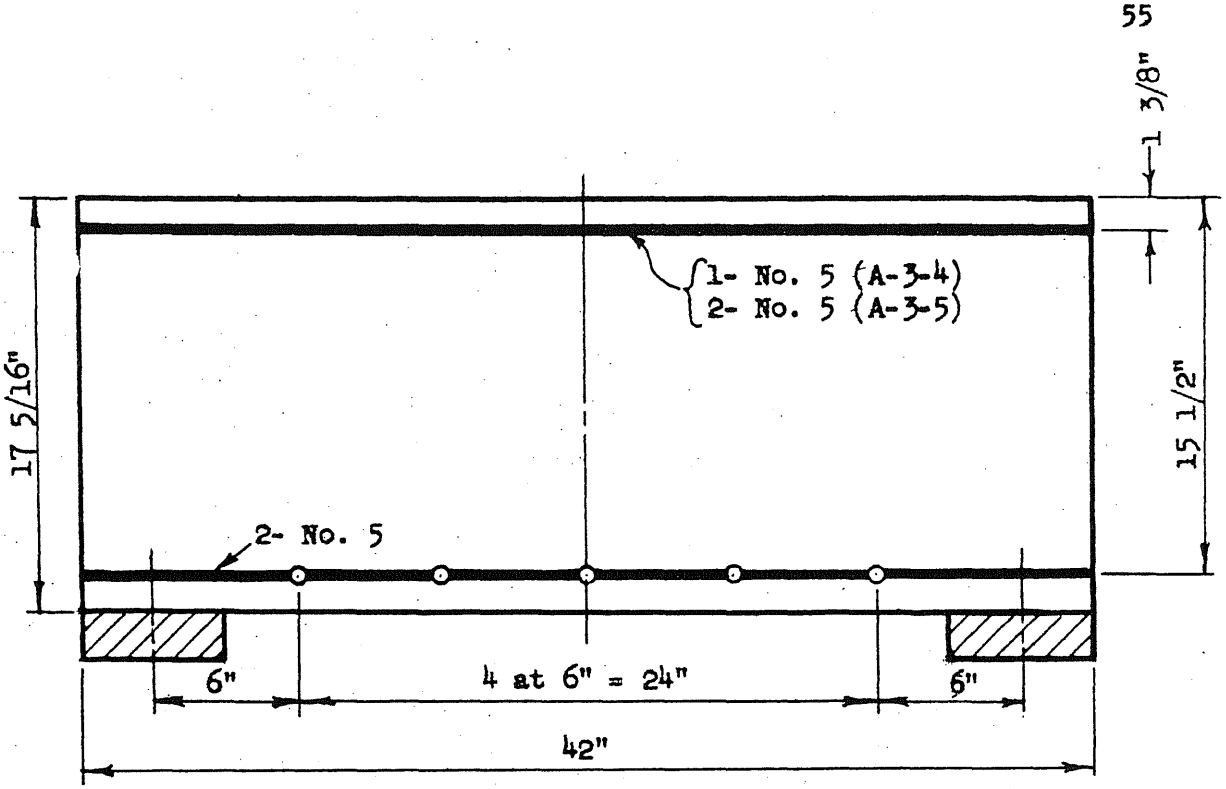

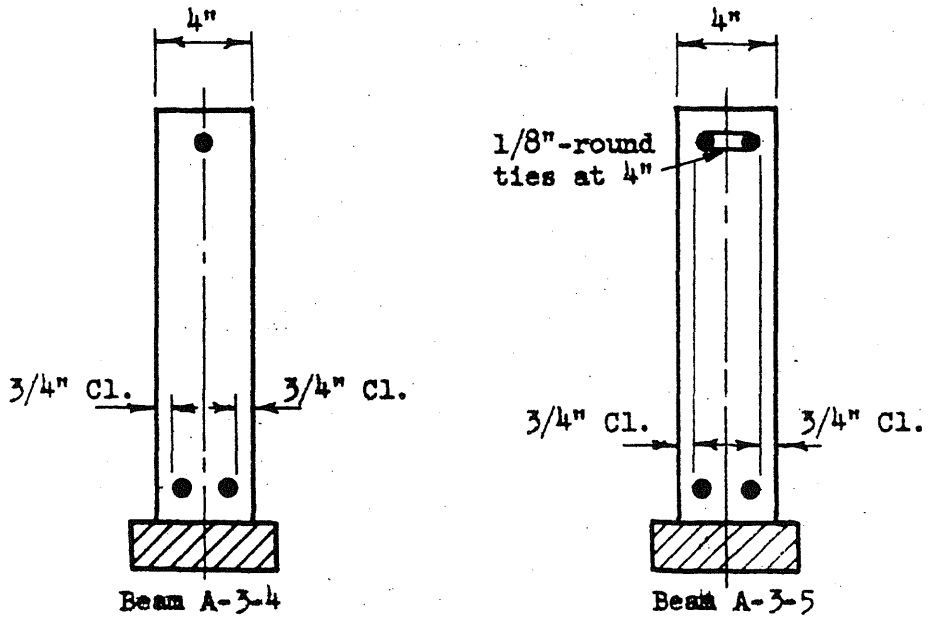

FIG. 1 A-SERIES TEST SPECIMENS

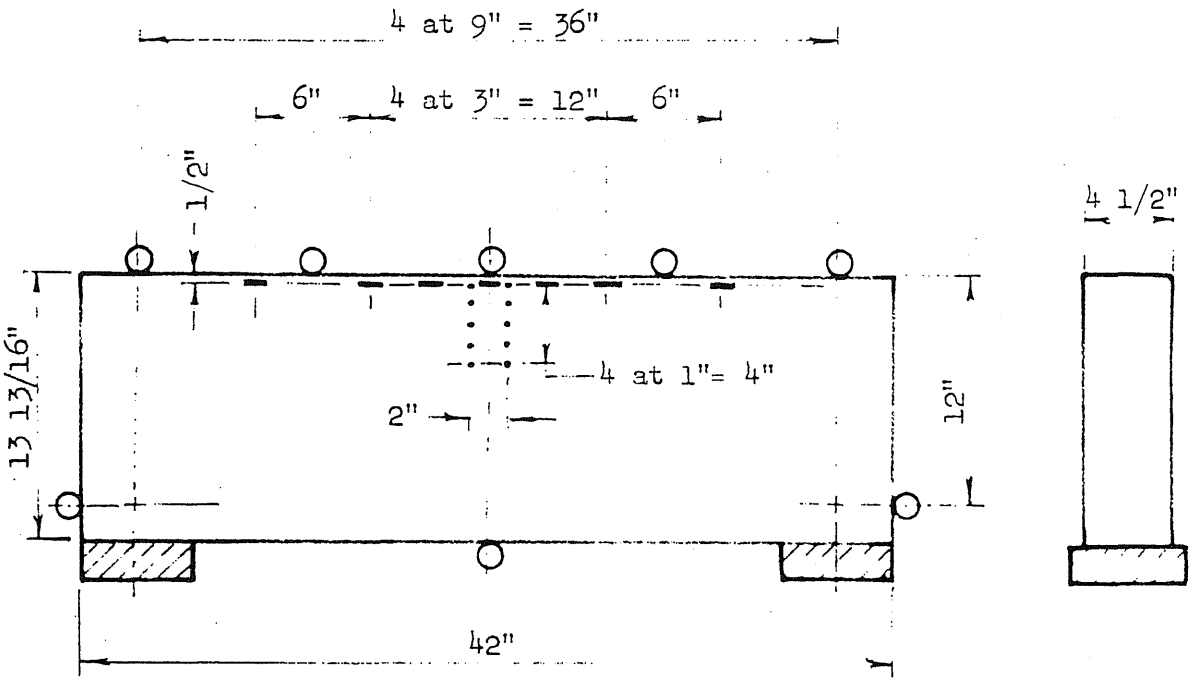

▬ SR-4 strain gage
O Deflection dial
• Whittemore gage point

FIG. 2(a) NOMINAL DIMENSIONS OF C-SERIES SPECIMENS AND LOCATION OF CONCRETE STRAIN GAGES AND DEFLECTION DIALS

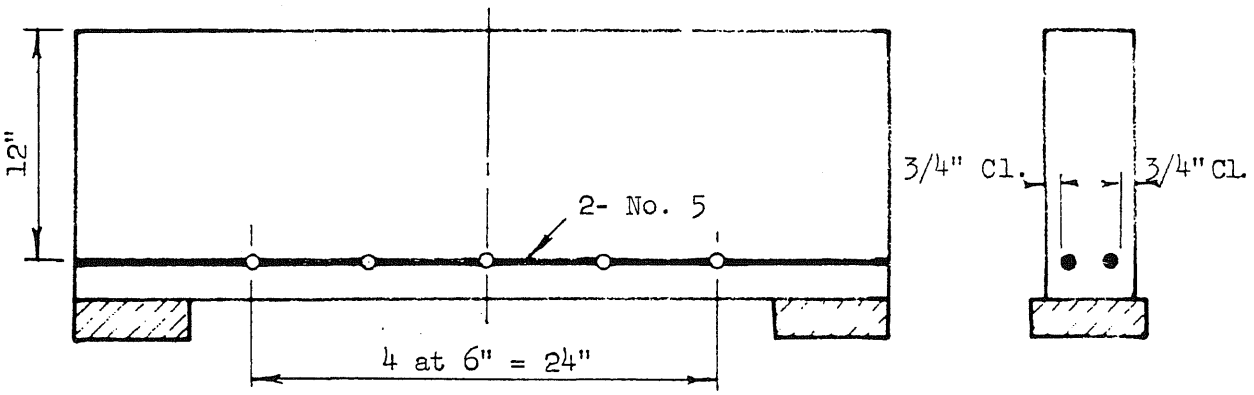

o SR-4 strain gage

Beam C-1

FIG. 2(b) PLACEMENT OF REINFORCEMENT AND LOCATION OF STEEL STRAIN GAGES: BEAM C-1

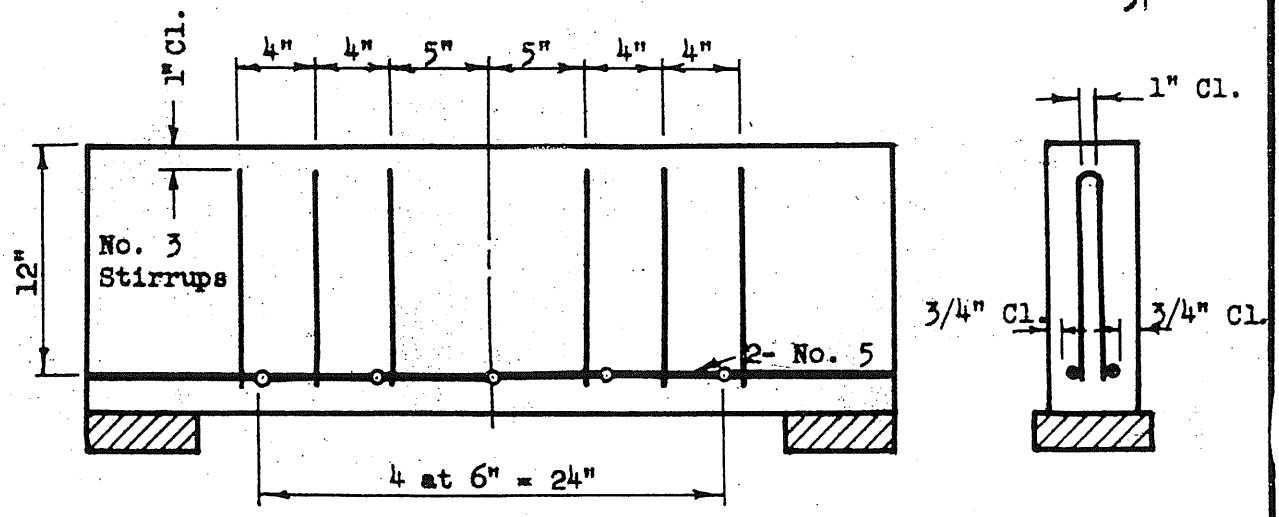

Beam C-2

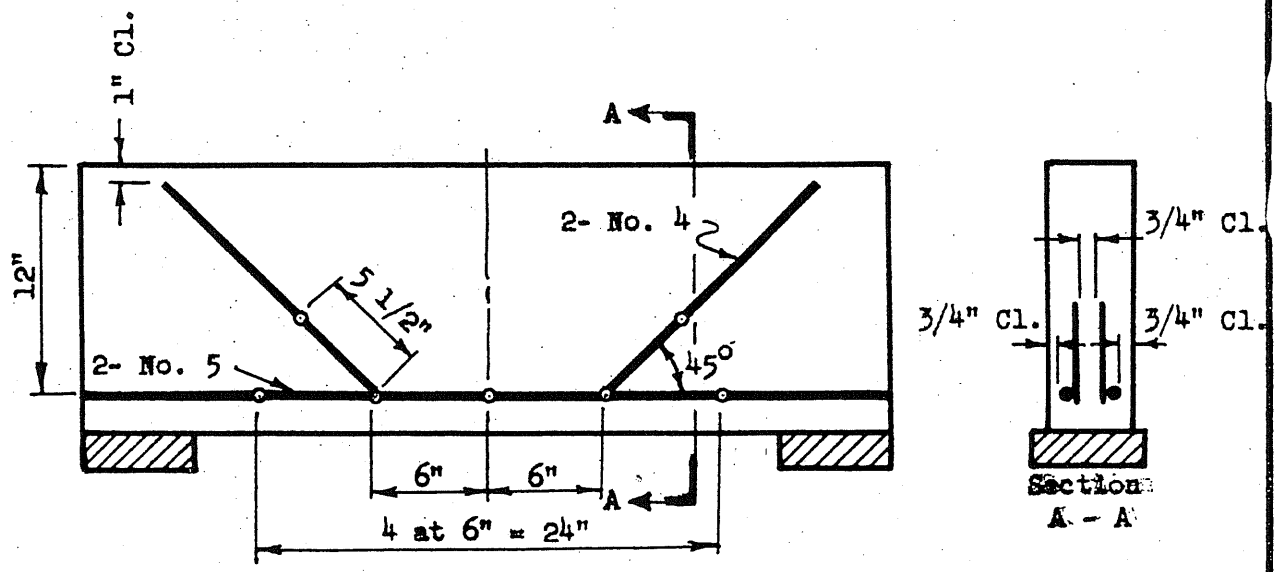

o SR-4 strain gage

Beam C-3

FIG. 3 PLACEMENT OF REINFORCEMENT AND LOCATION OF STEEL STRAIN GAGES: BEAMS C-2 AND C-3

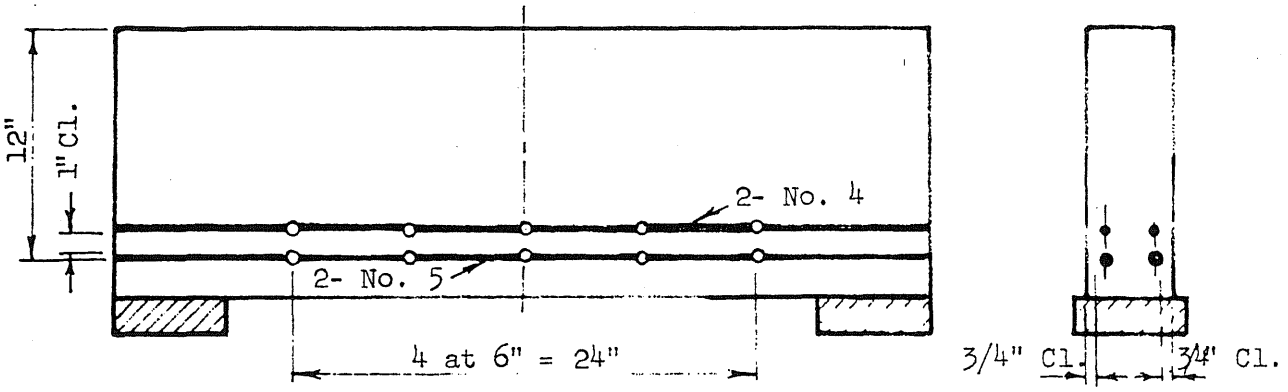

Beam C-4

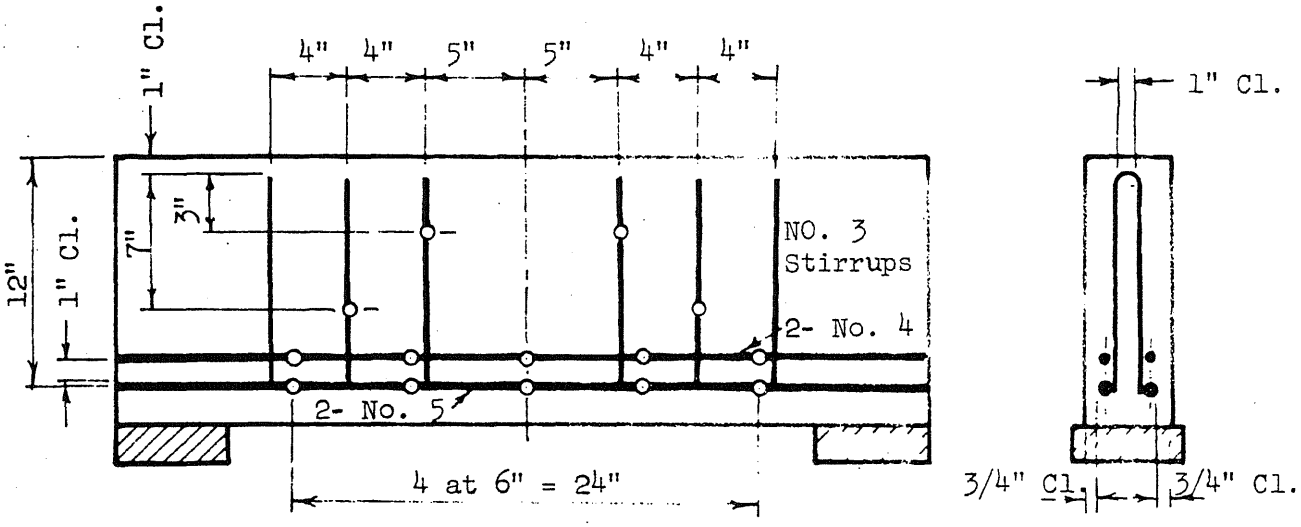

o SR-4 strain gage

Beam C-5

FIG. 4 PLACEMENT OF REINFORCEMENT AND LOCATION OF STEEL STRAIN GAGES: BEAMS C-4 AND C-5

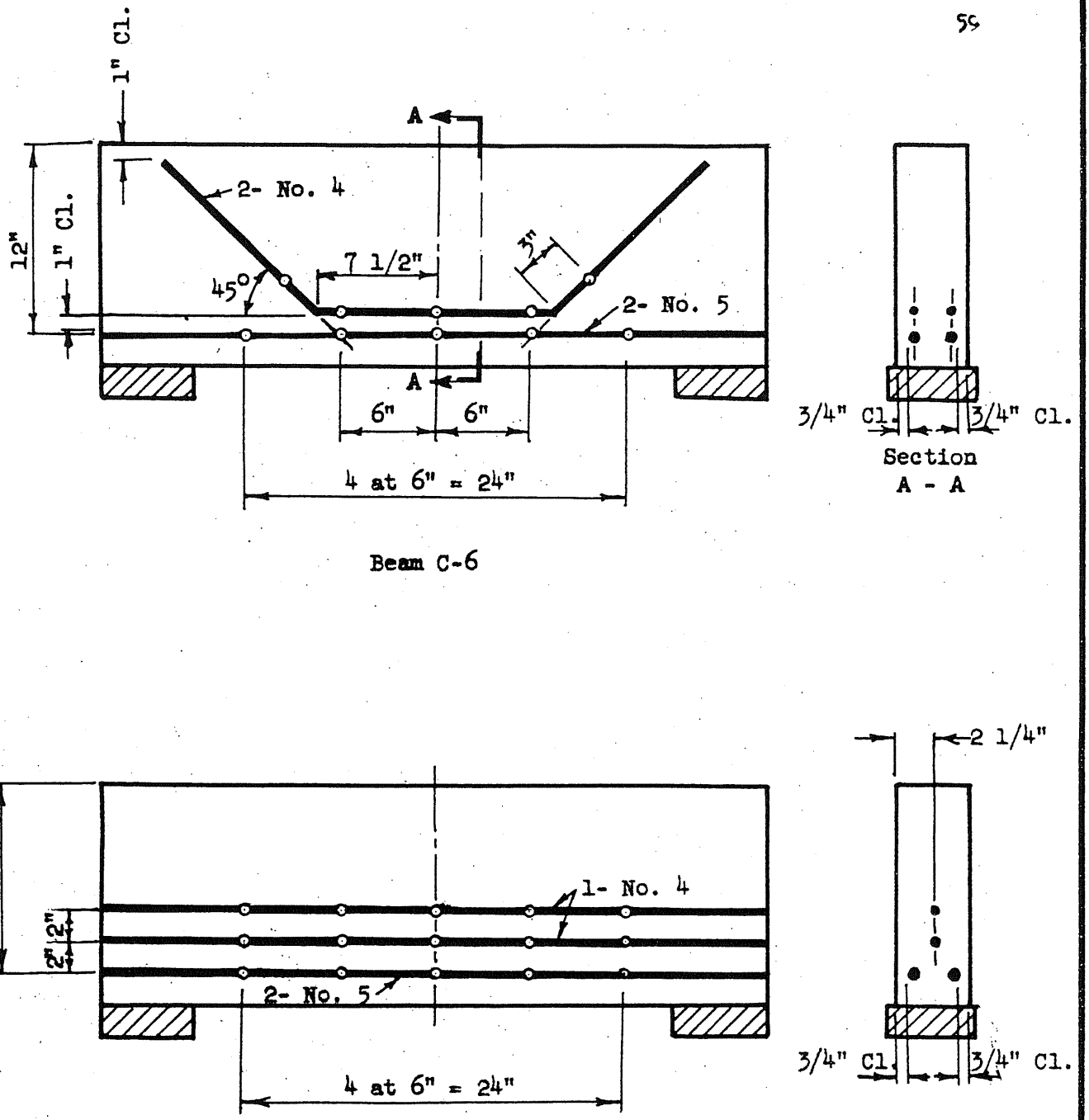

FIG. 5 PLACEMENT OF REINFORCEMENT AND LOCATION OF STEEL STRAIN GAGES: BEAMS C-6 AND C-7

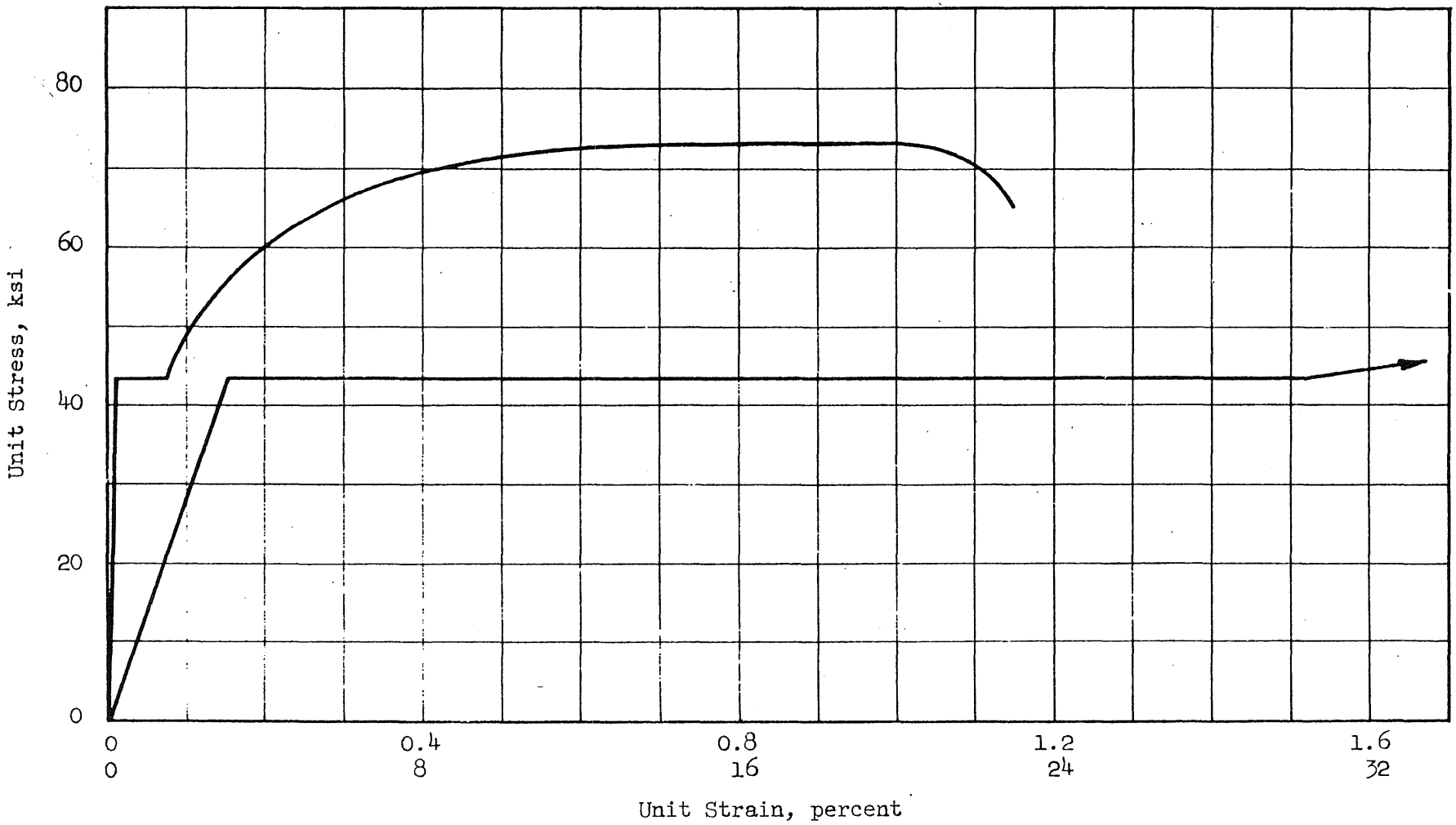

FIG. 6 TYPICAL STRESS-STRAIN CURVE FOR THE REINFORCING STEEL

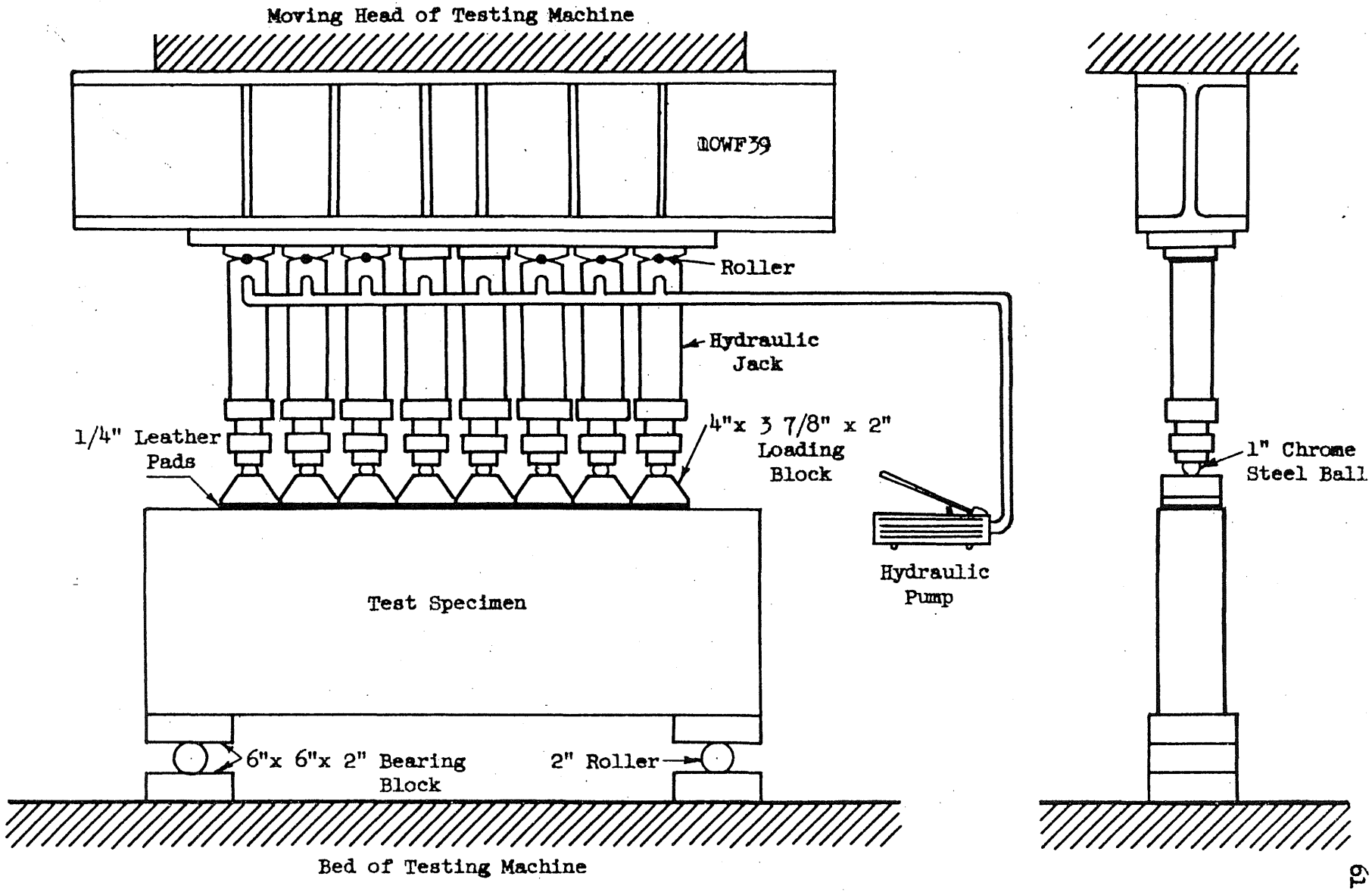

FIG. 7 TYPICAL TEST SET-UP

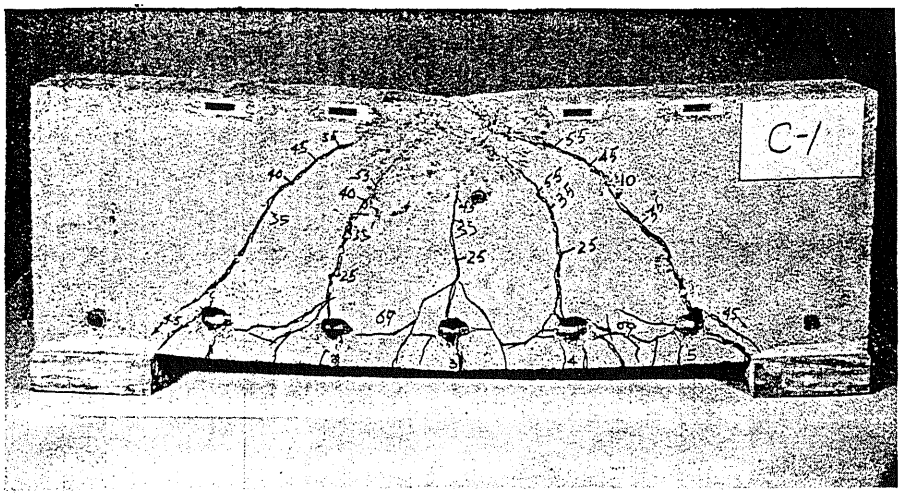

Beam C-1
W_u = 76.2^k

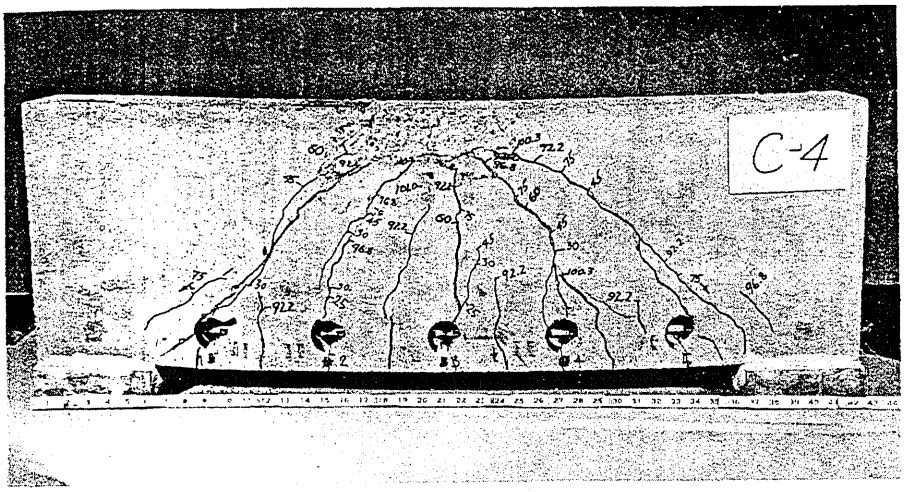

Beam C-4
W_u = 102.0^k

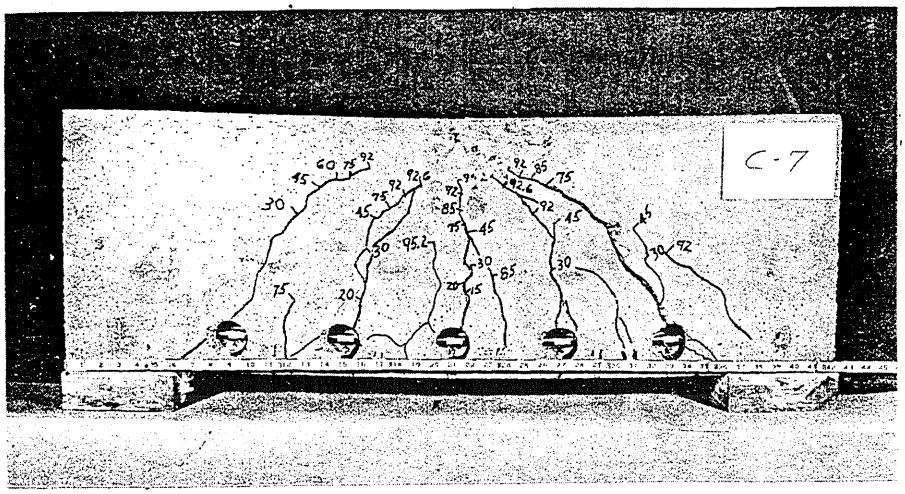

Beam C-7
W_u = 95.9^k

FIG. 8 BEAMS WITHOUT WEB REINFORCEMENT AFTER FAILURE

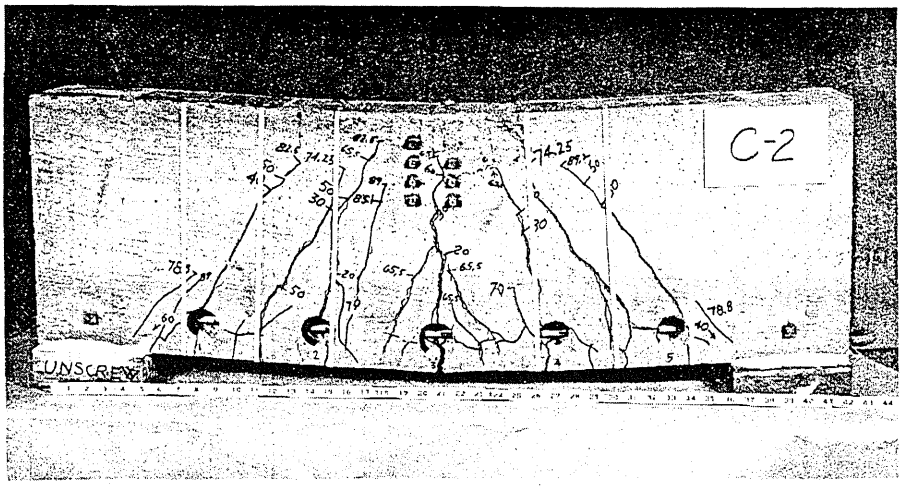

Beam C-2
W_u = 89.5^k

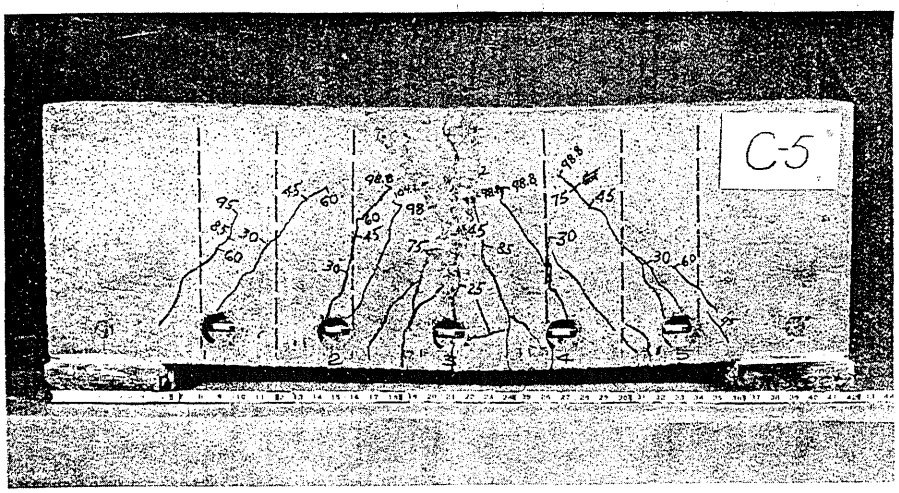

Beam C-5
W_u = 106.0^k

FIG. 9 BEAMS WITH VERTICAL STIRRUPS AFTER FAILURE

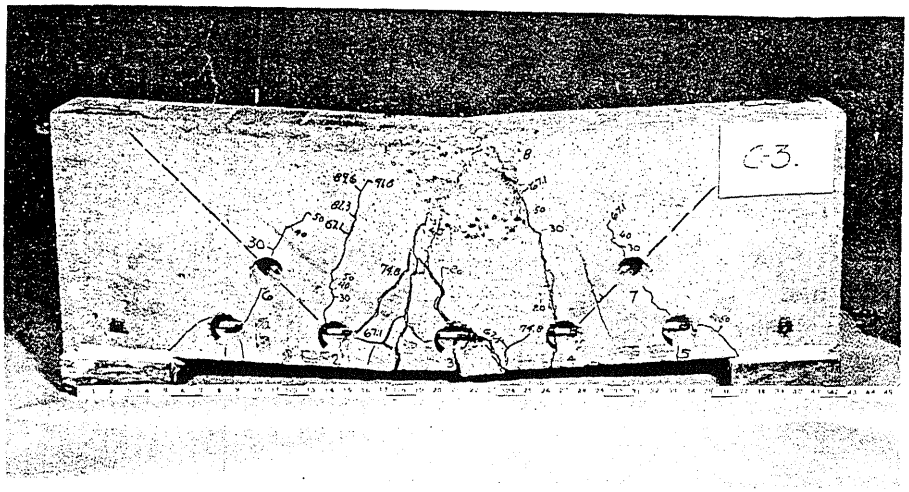

Beam C-3
W_u = 94.5^k

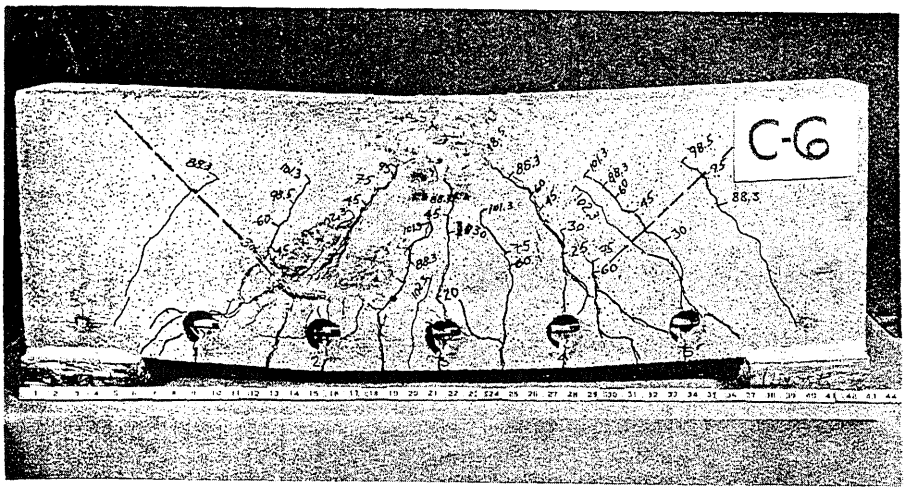

Beam C-6
W_u = 102.6^k

FIG. 10 BEAMS WITH INCLINED BARS AFTER FAILURE

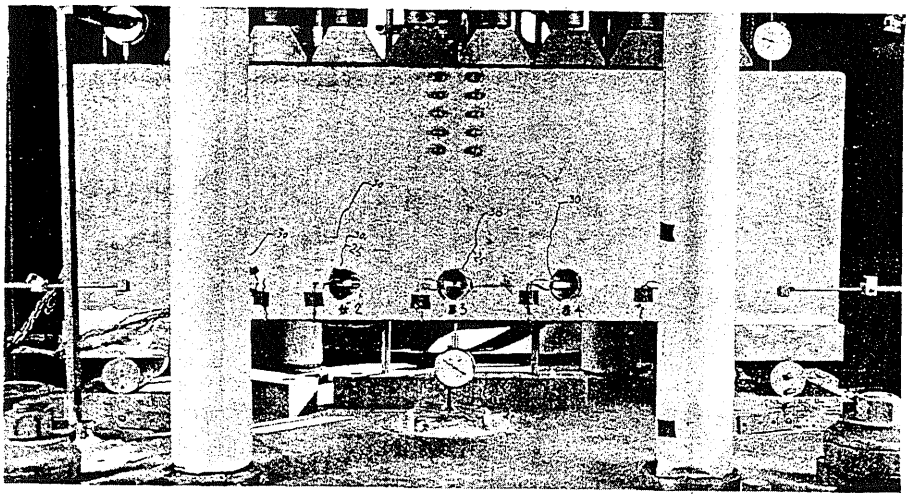

W = 30.0^{k}

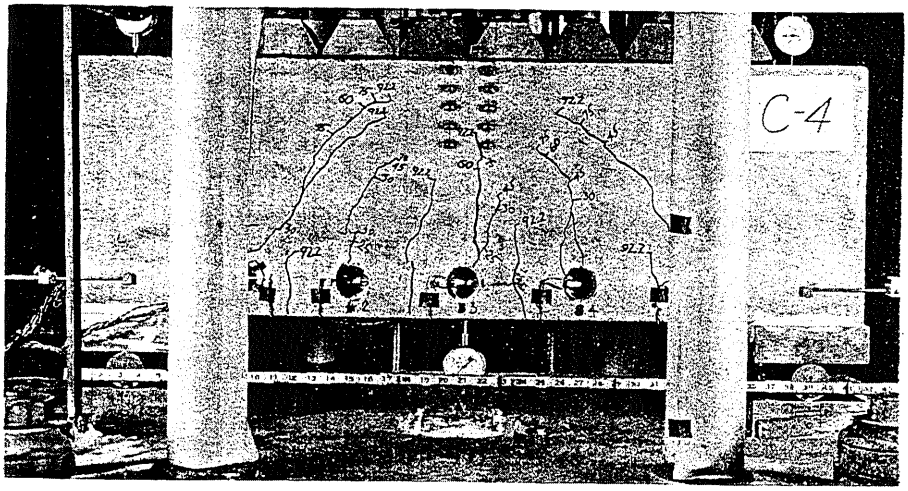

W = 92.2^{k}
(Yielding of tension steel)

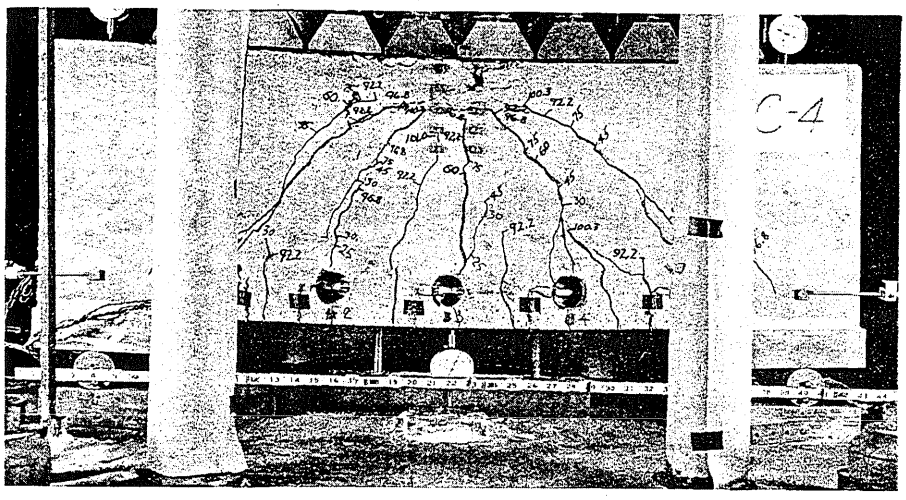

W_u = 102.0^{k}

FIG. 11 CRACK DEVELOPMENT: BEAM C-4

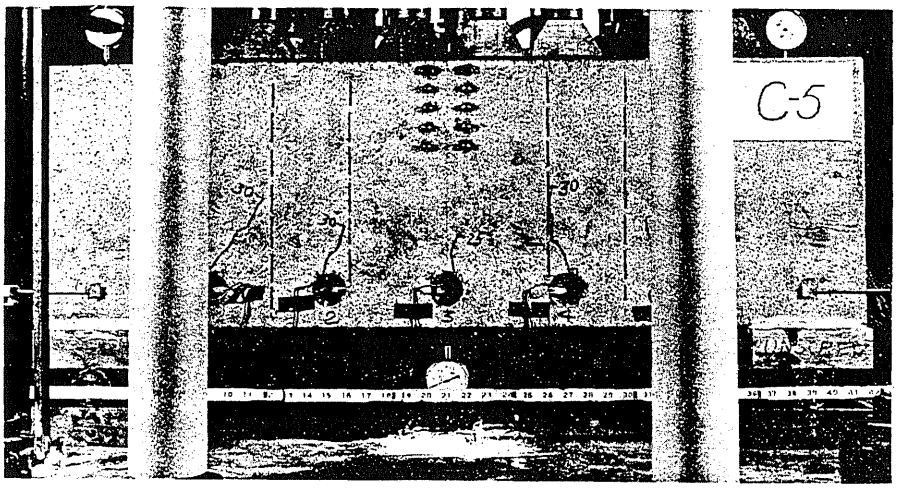

W = 30.0^{k}

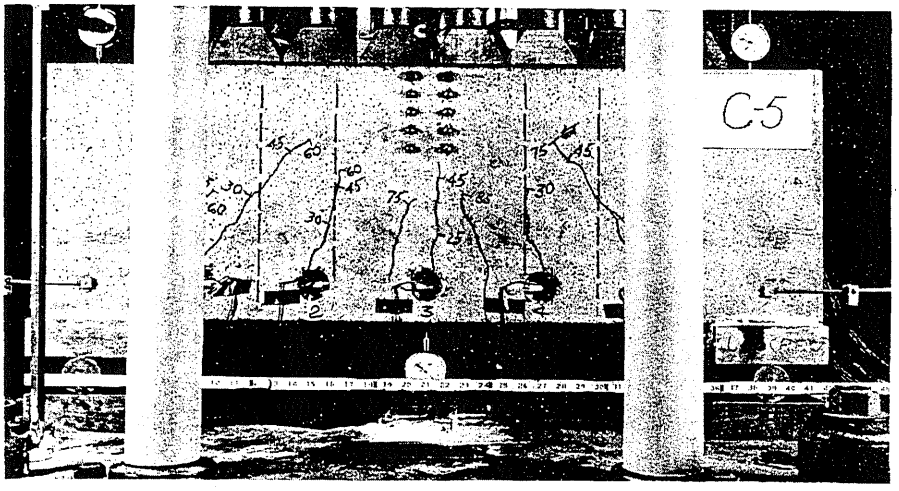

W = 85.0^{k}
(Yielding of tension steel)

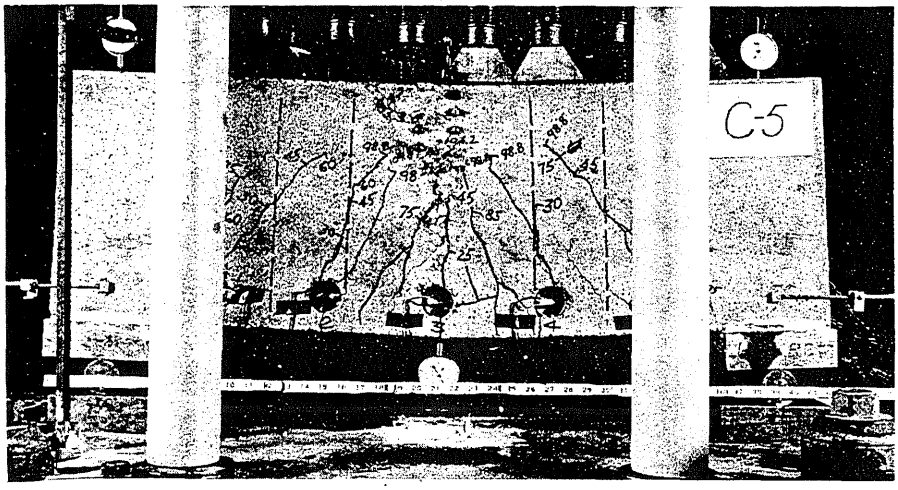

W_u = 106.0^{k}

FIG. 12 CRACK DEVELOPMENT: BEAM C-5

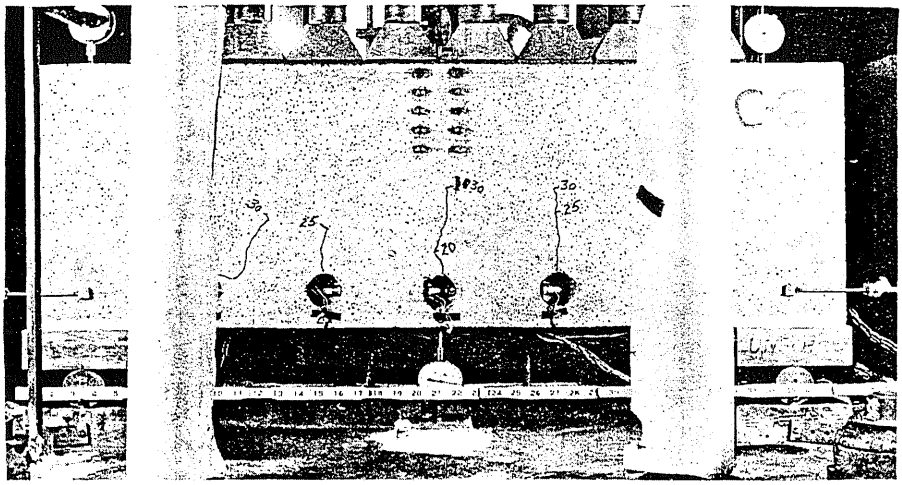

W = 30.0^{k}

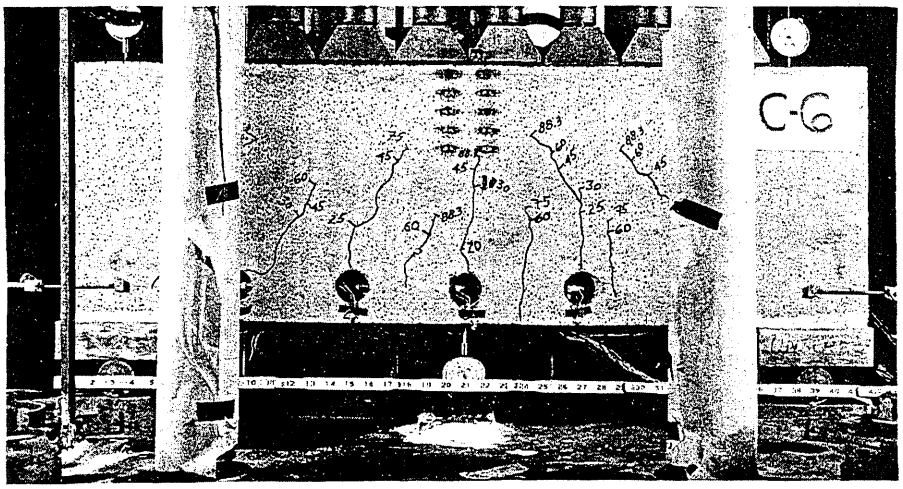

W = 88.3^{k}
(Yielding of tension steel)

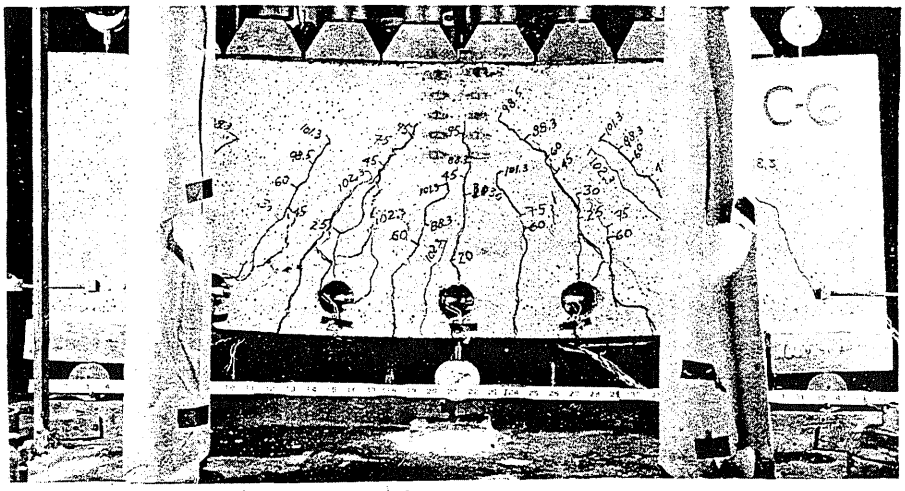

W_{u} = 102.6^{k}

FIG. 13 CRACK DEVELOPMENT: BEAM C-6

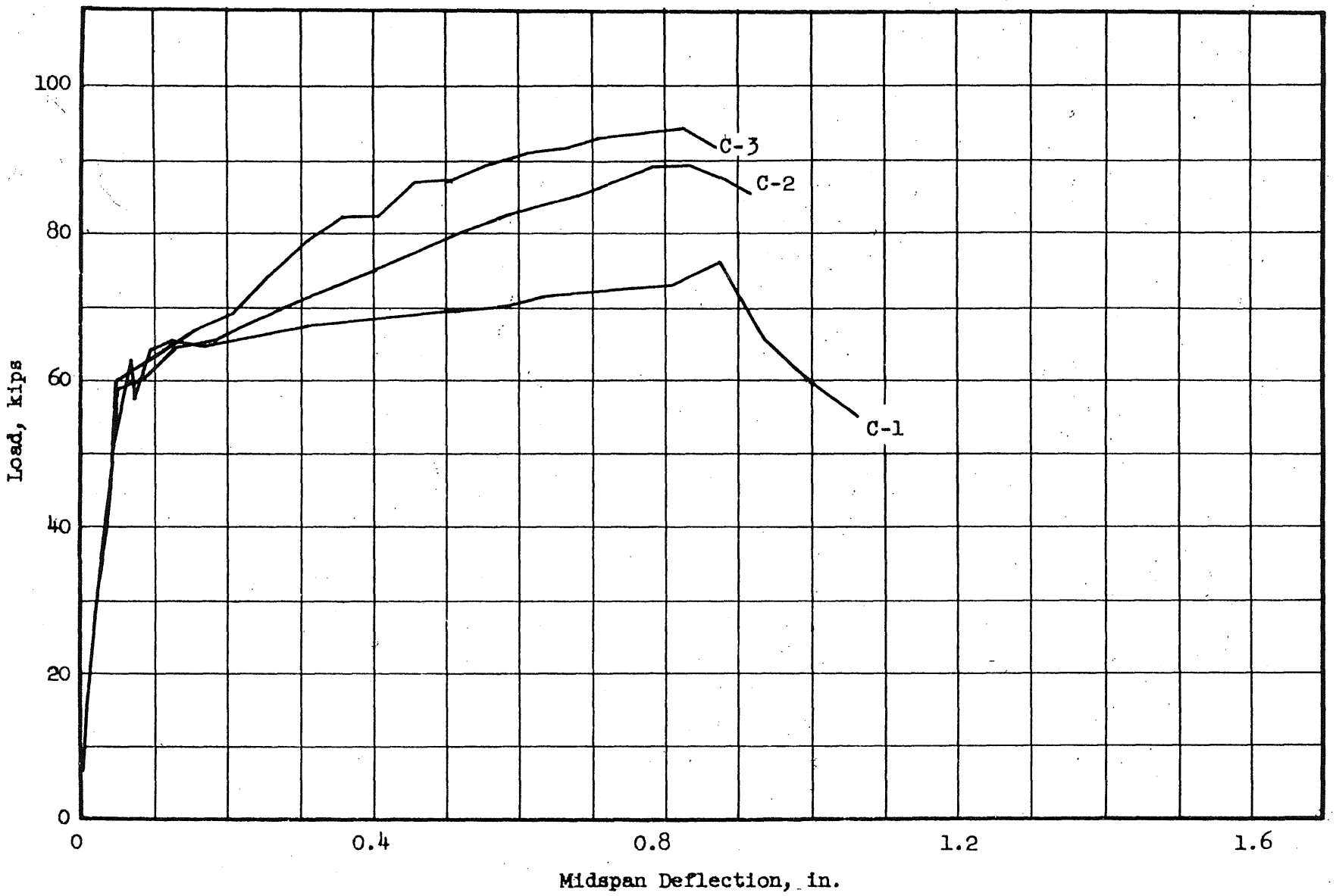

FIG. 14 LOAD-DEFLECTION CURVES FOR BEAMS WITH 1.15 PERCENT LONGITUDINAL STEEL

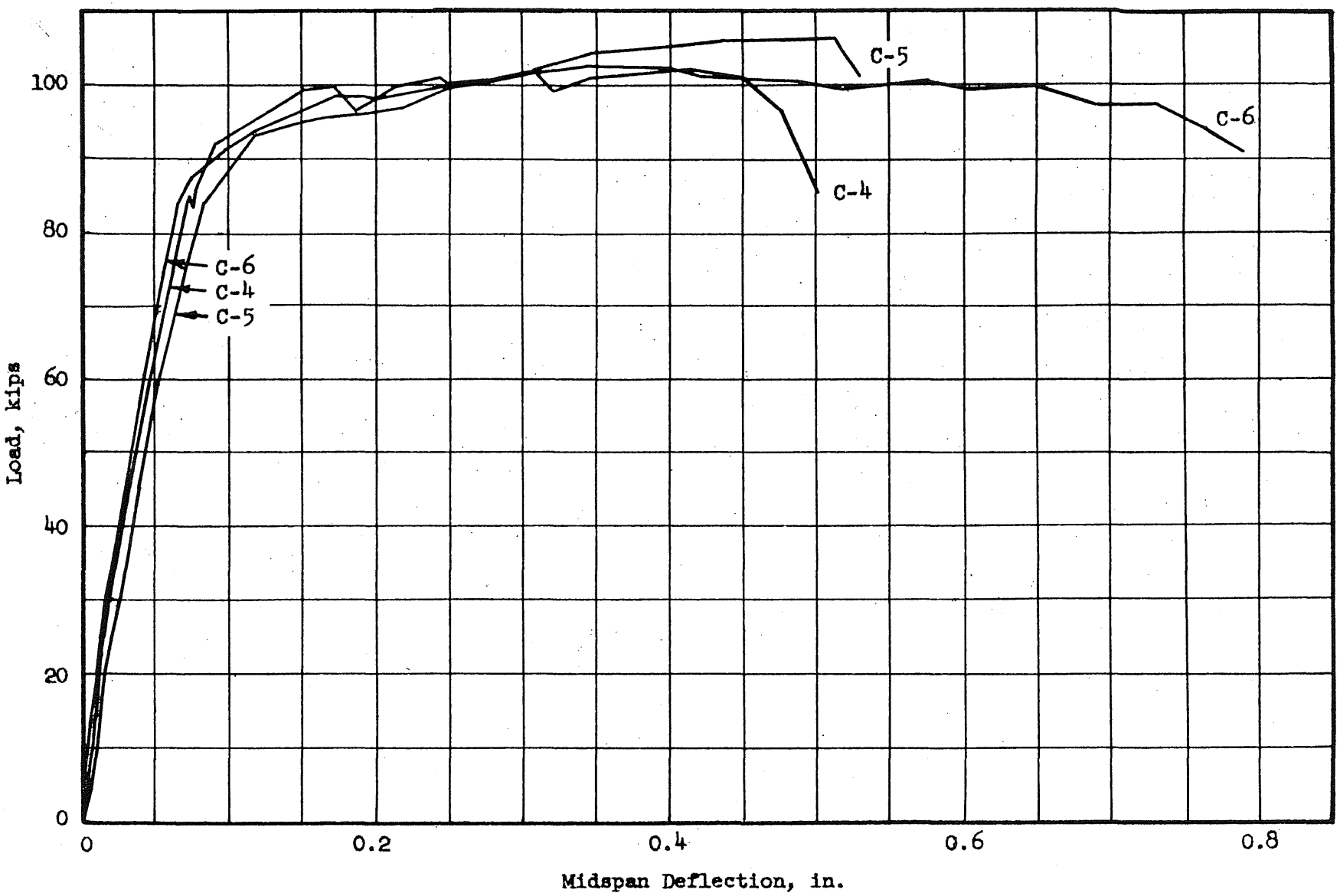

FIG. 15 LOAD-DEFLECTION CURVES FOR BEAMS WITH 1.99 PERCENT LONGITUDINAL STEEL

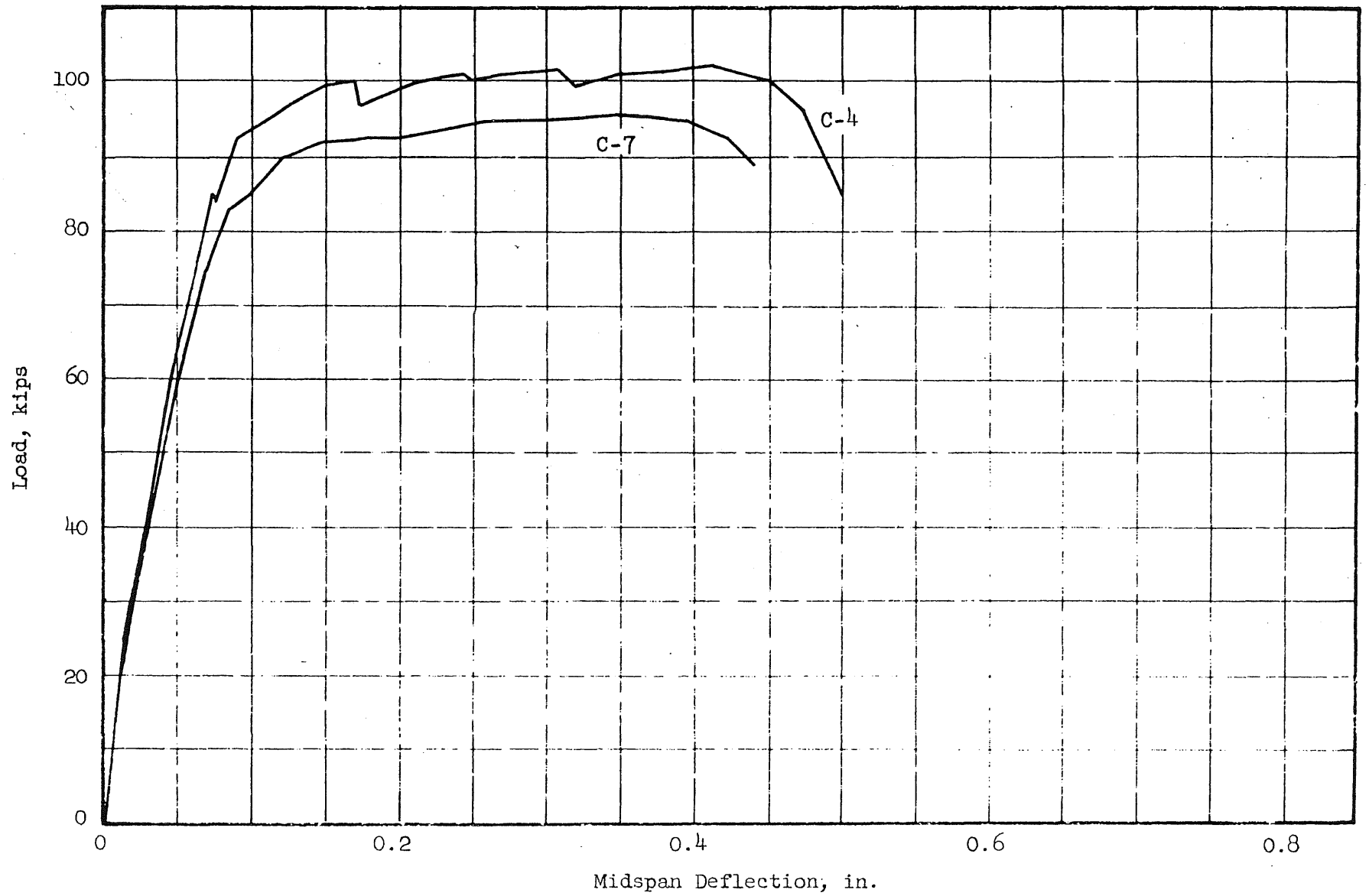

FIG. 16 LOAD-DEFLECTION CURVE FOR BEAM WITH 2.09 PERCENT LONGITUDINAL STEEL

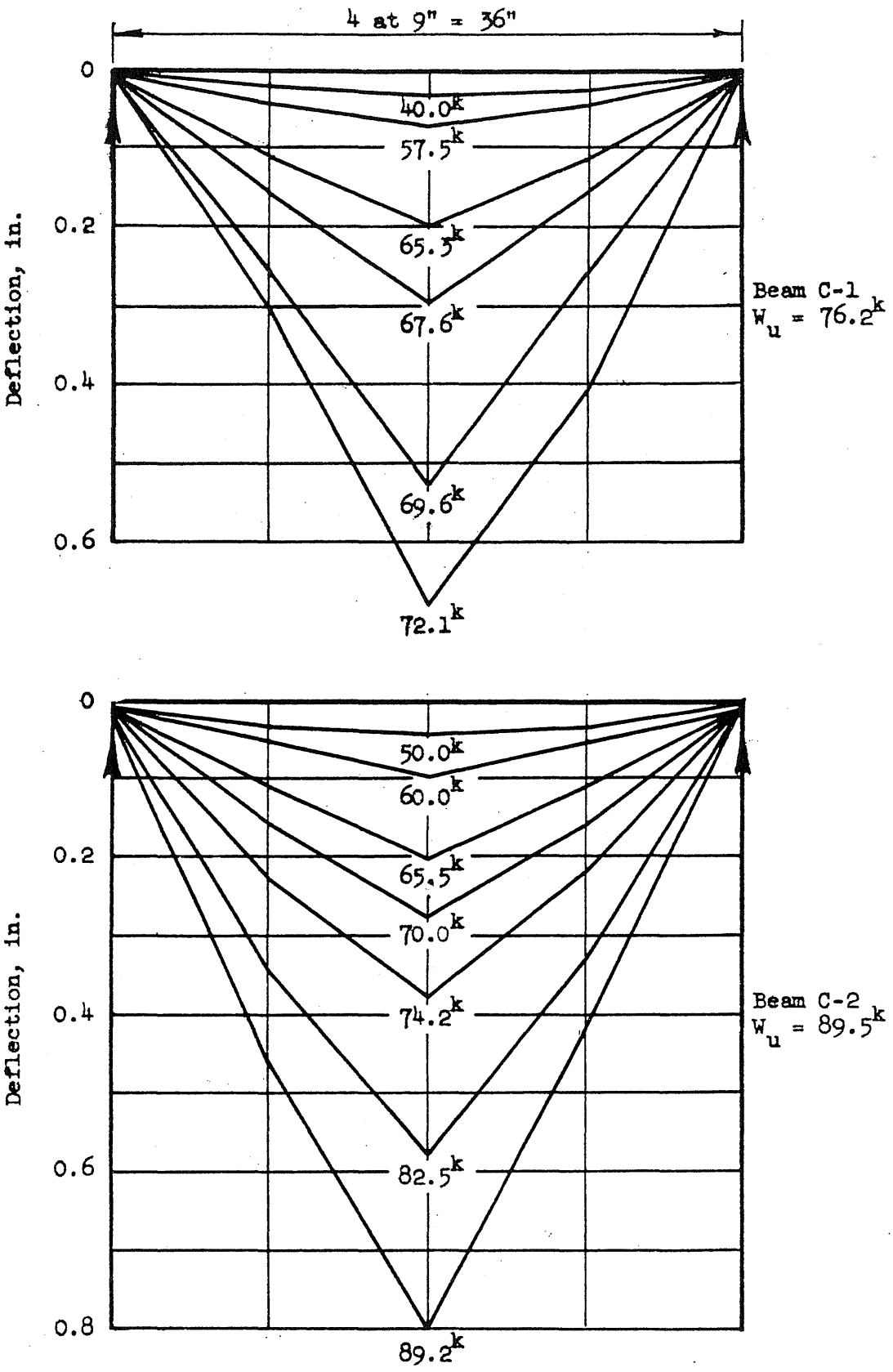

FIG. 17 DEFLECTED SHAPE OF BEAMS C-1 AND C-2

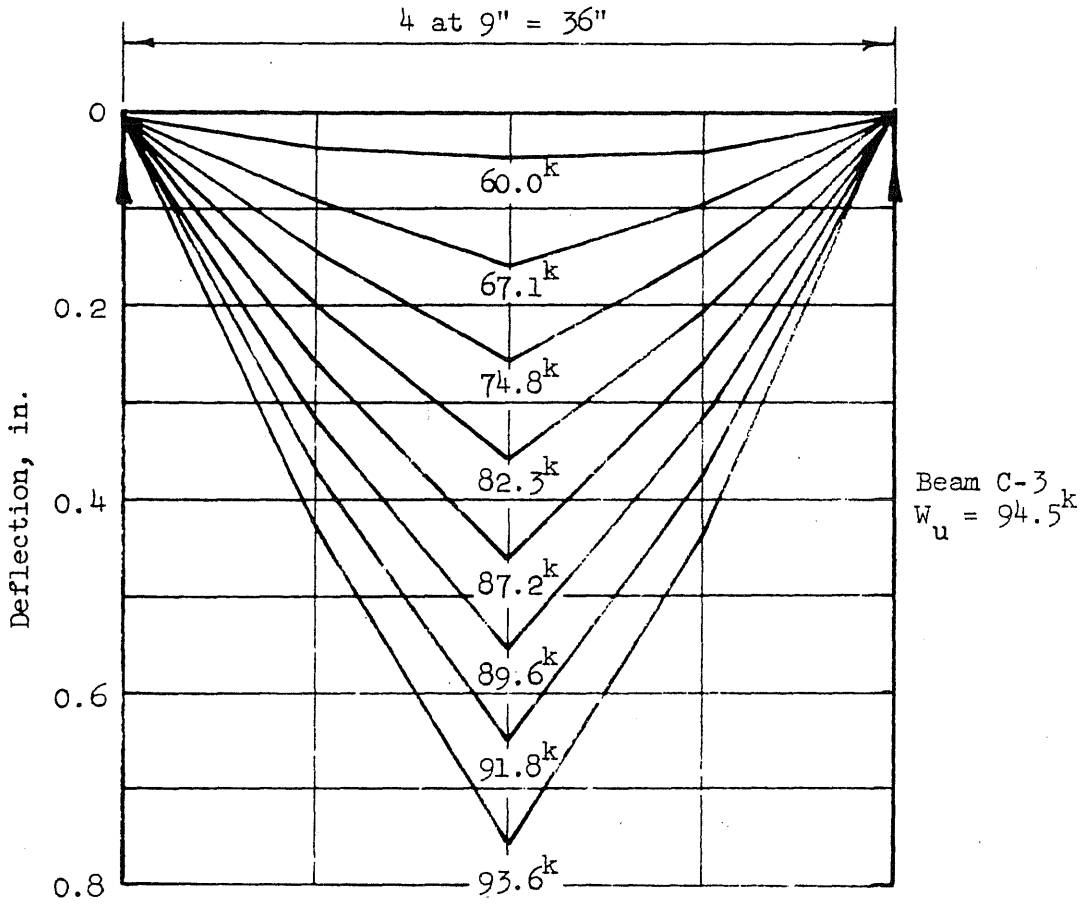

FIG. 18 DEFLECTED SHAPE OF BEAM C-3

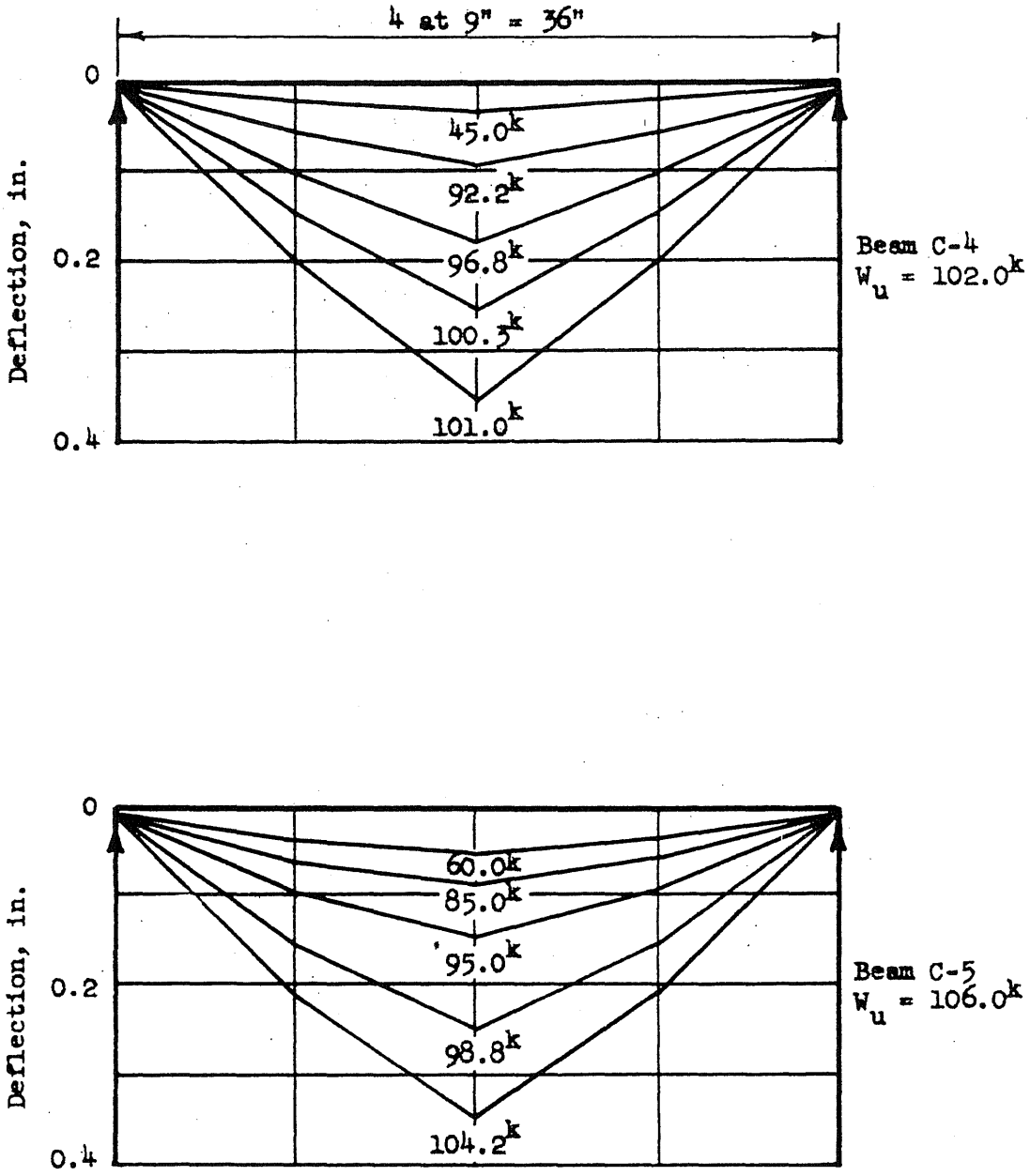

FIG. 19 DEFLECTED SHAPE OF BEAMS C-4 AND C-5

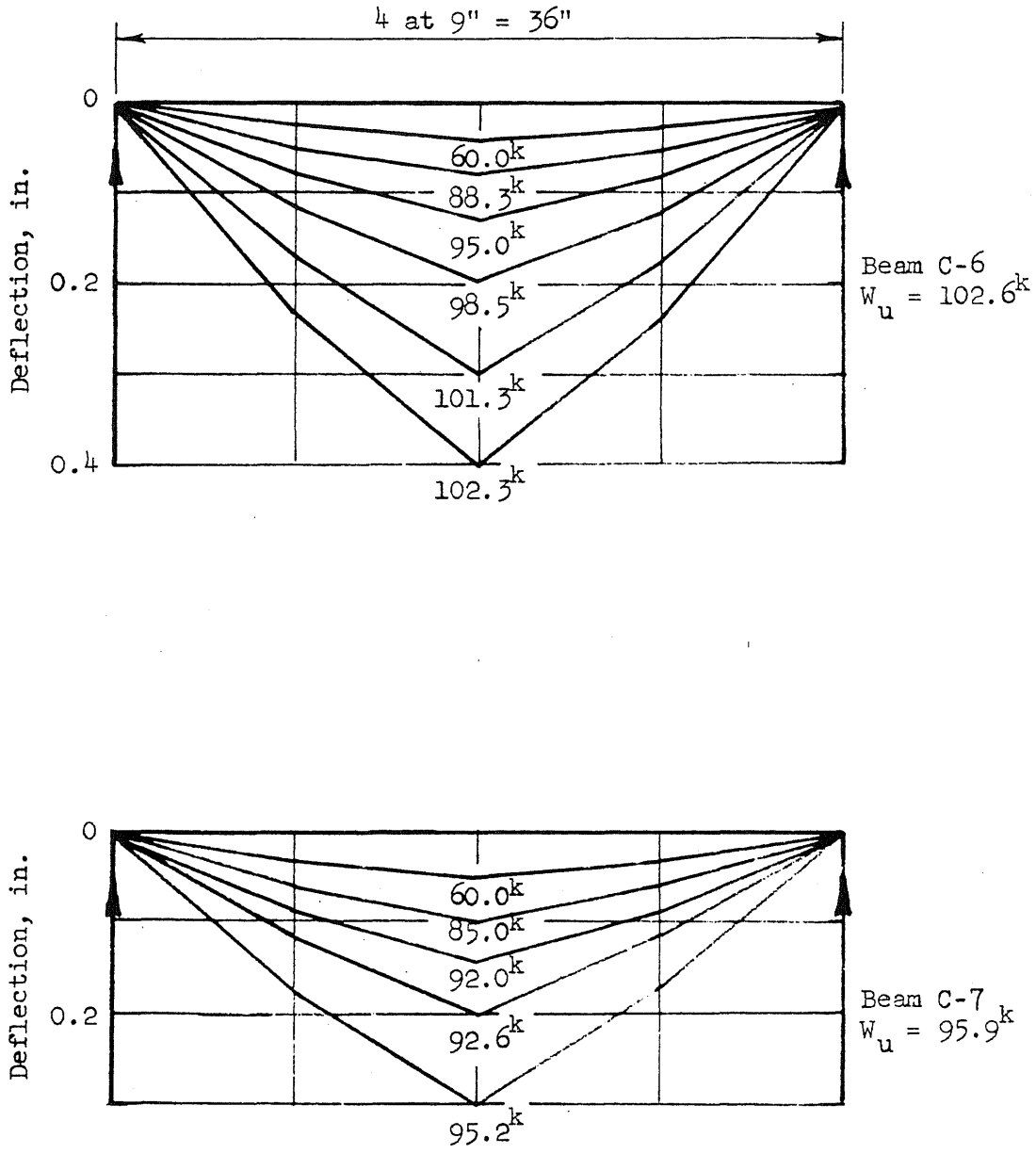

FIG. 20 DEFLECTED SHAPE OF BEAMS C-6 AND C-7

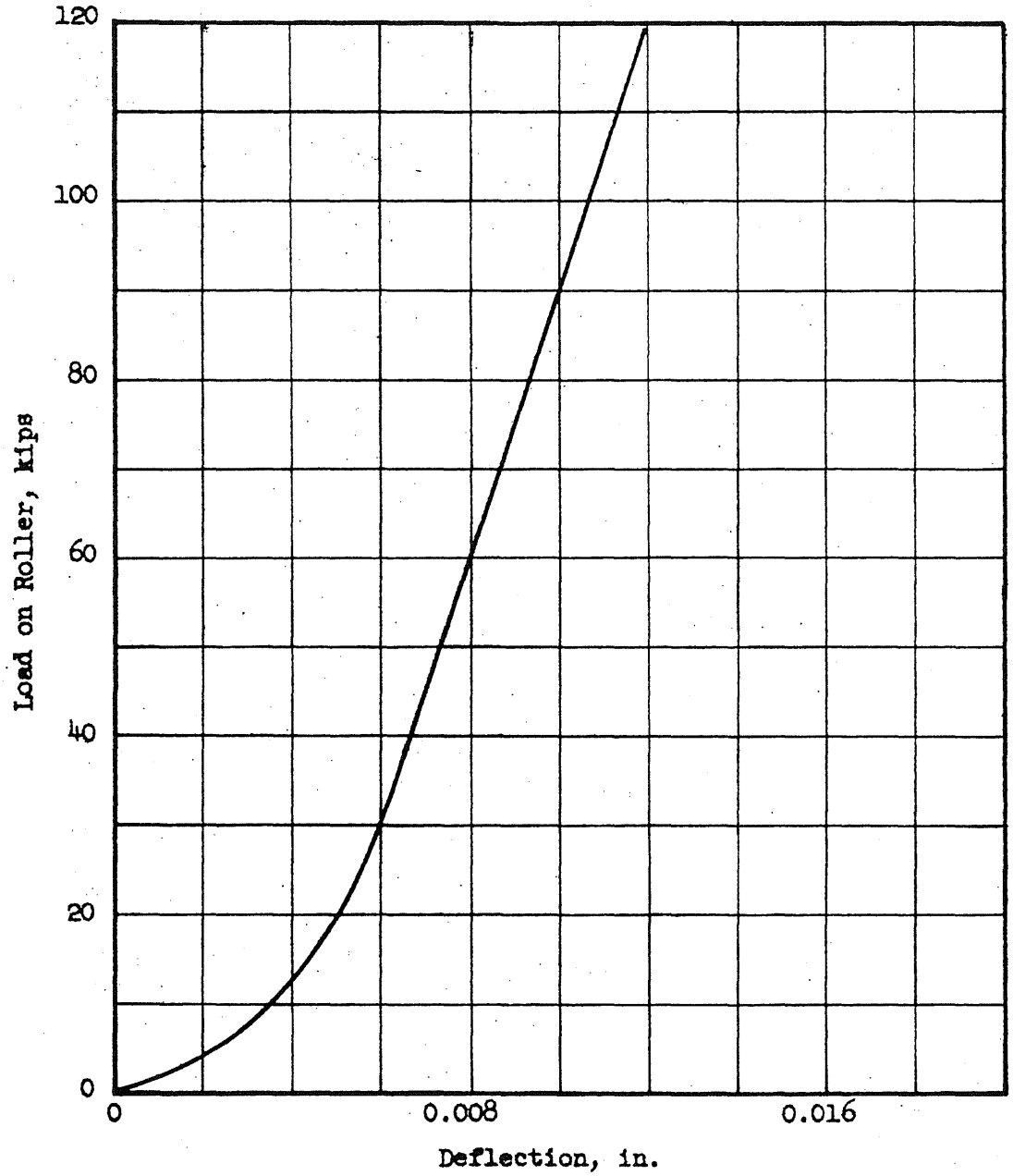

FIG. 21 LOAD-DEFLECTION CURVE FOR SUPPORTS

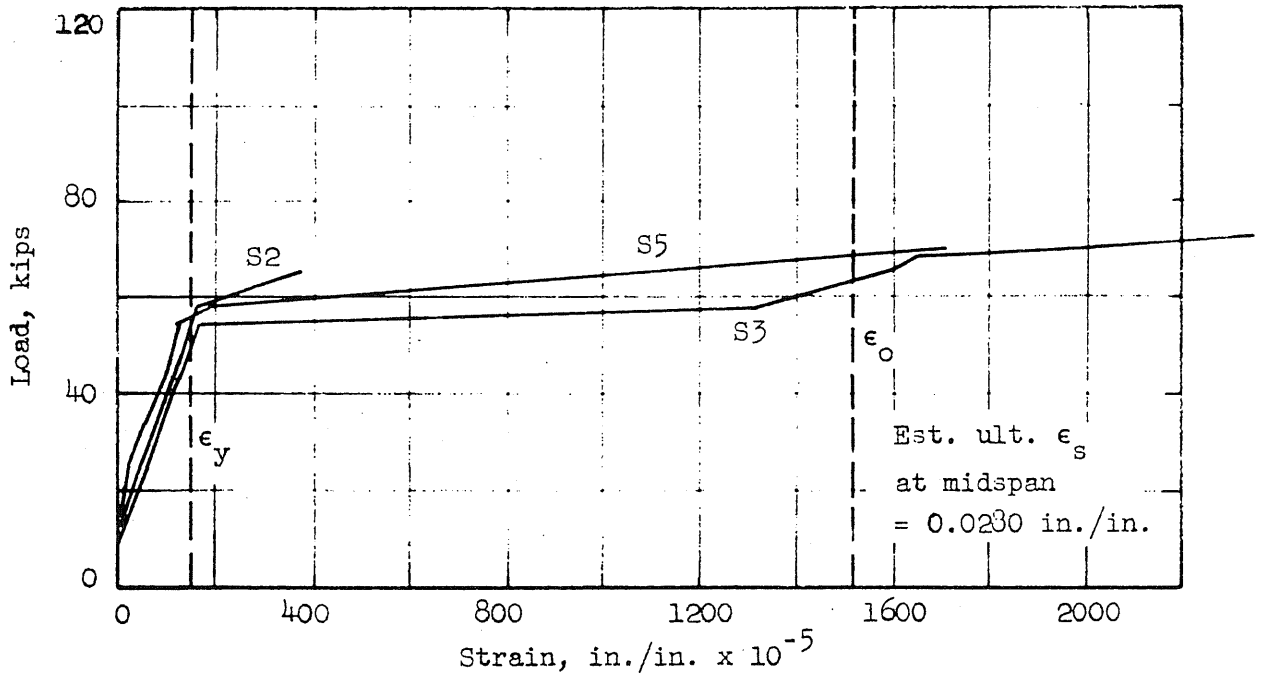

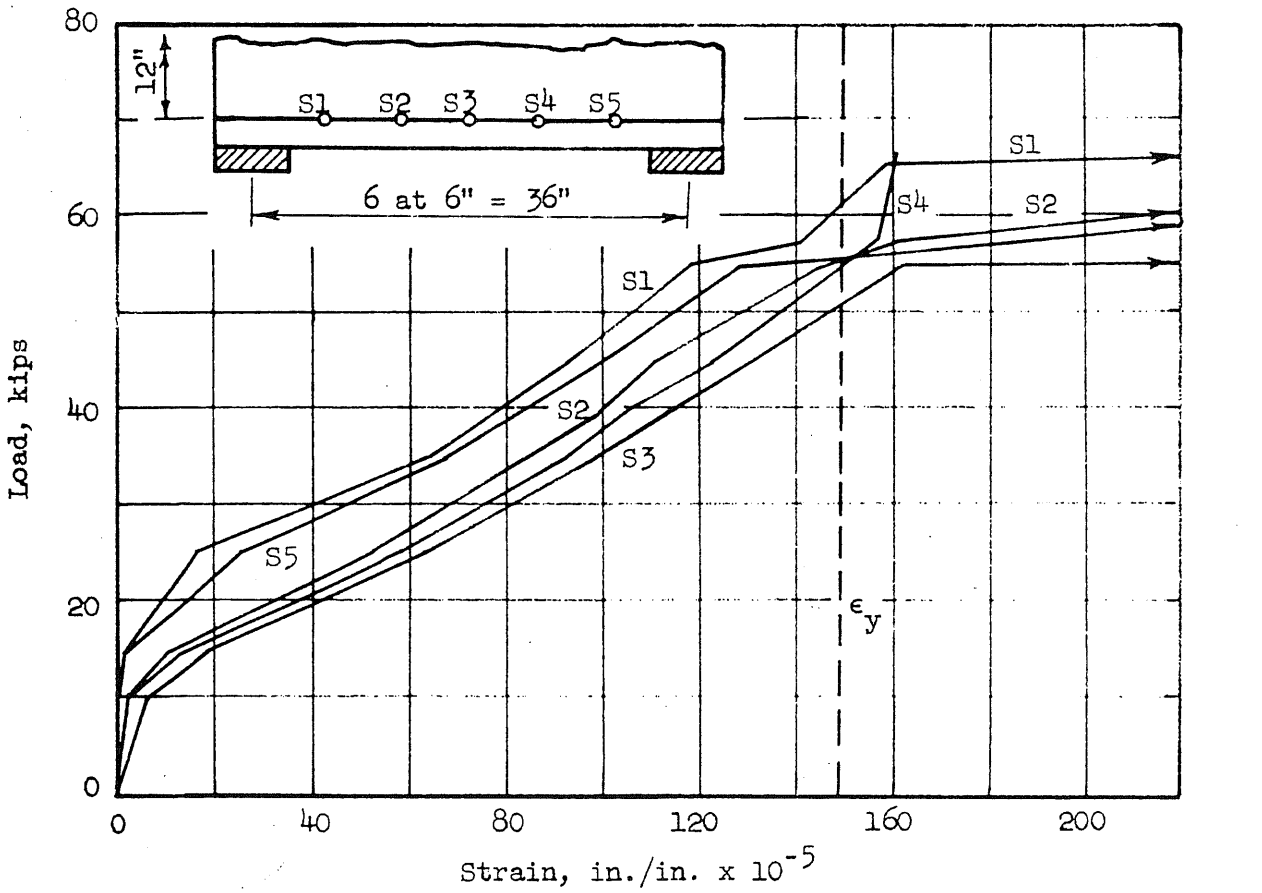

FIG. 22 LOAD-STEEL STRAIN CURVES FOR BEAM C-1

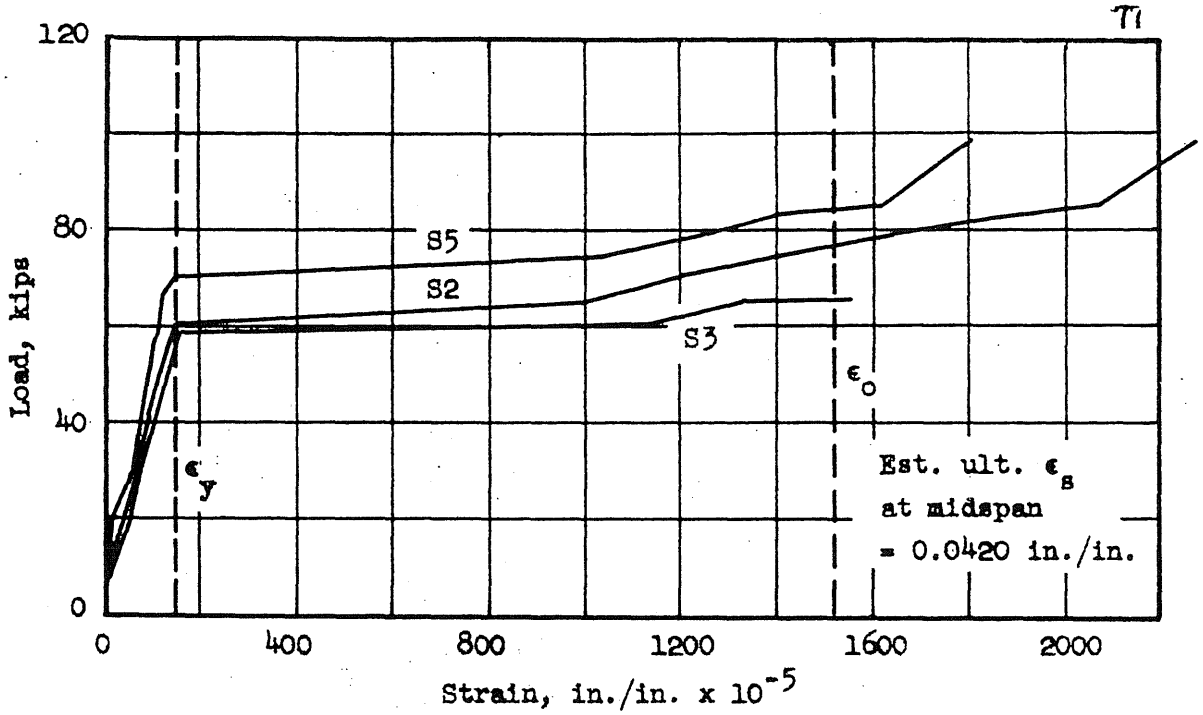

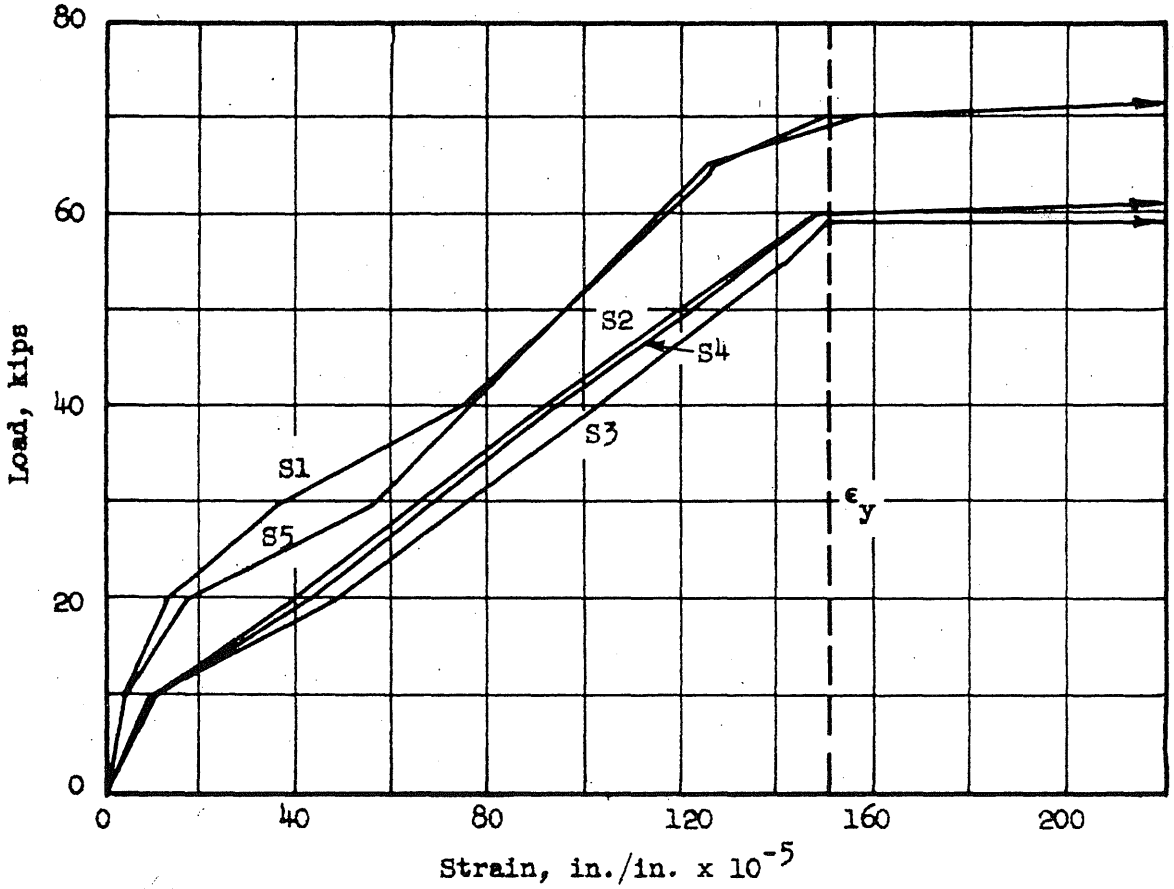

FIG. 23 LOAD-STEEL STRAIN CURVES FOR BEAM C-2

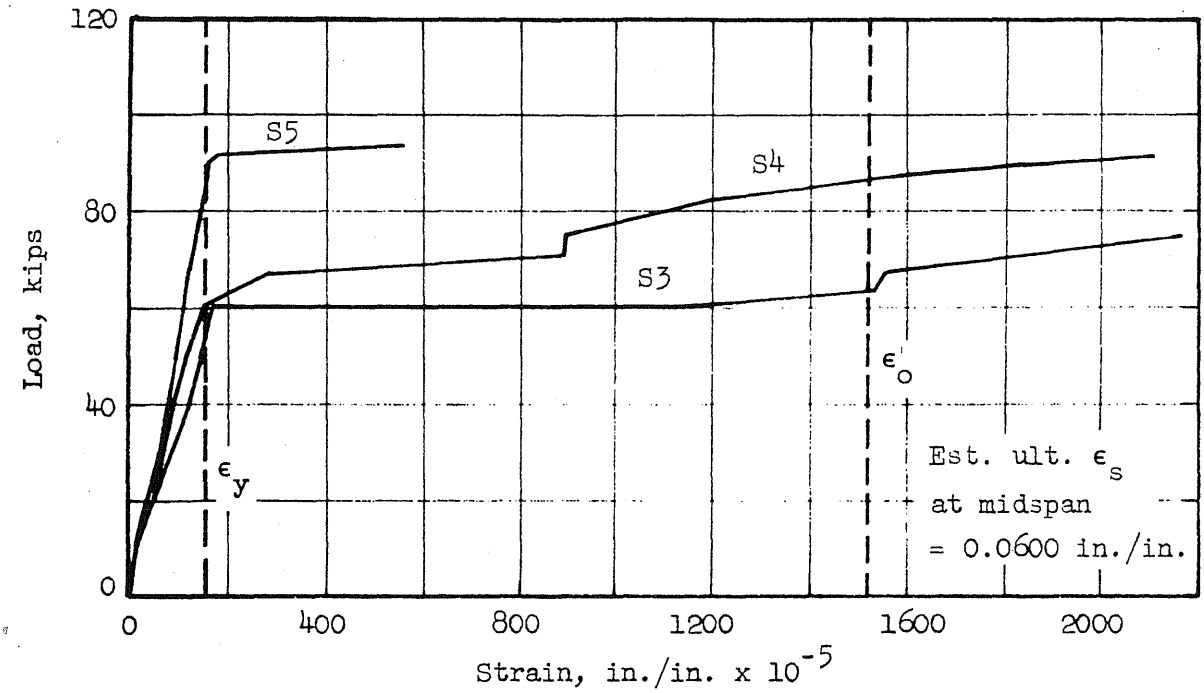

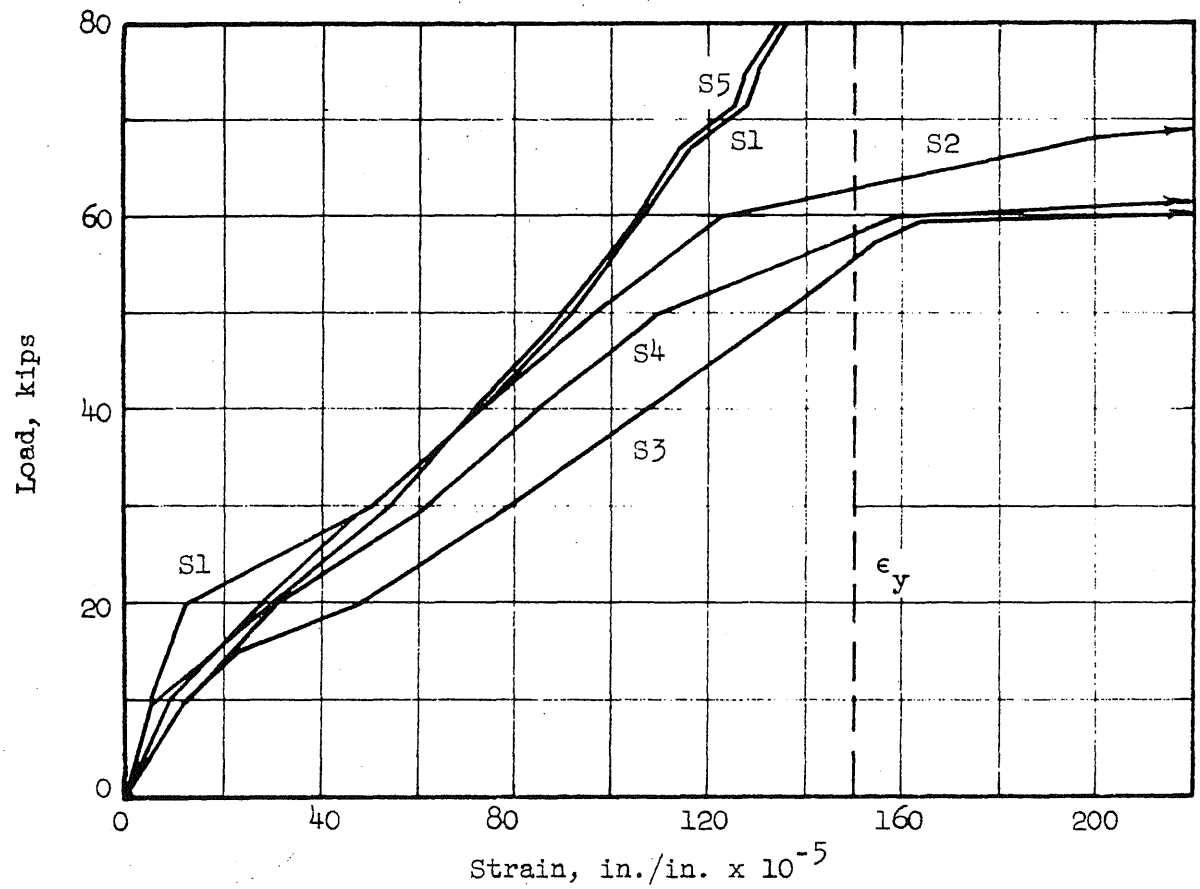

FIG. 24 LOAD-STEEL STRAIN CURVES FOR BEAM C-3

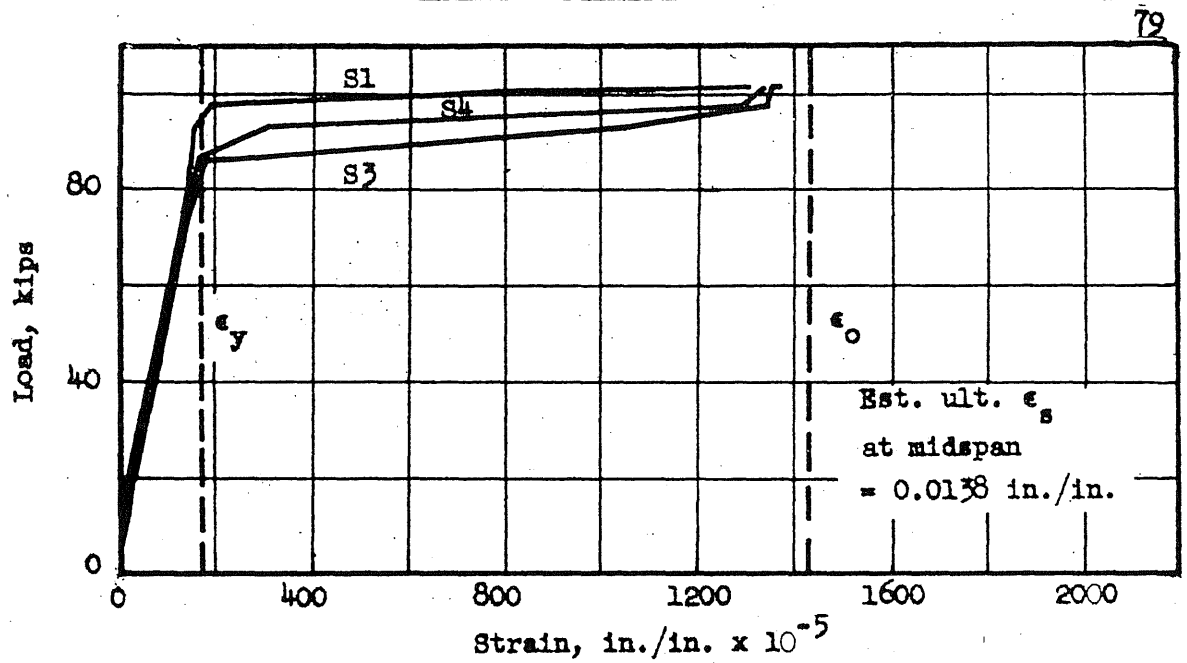

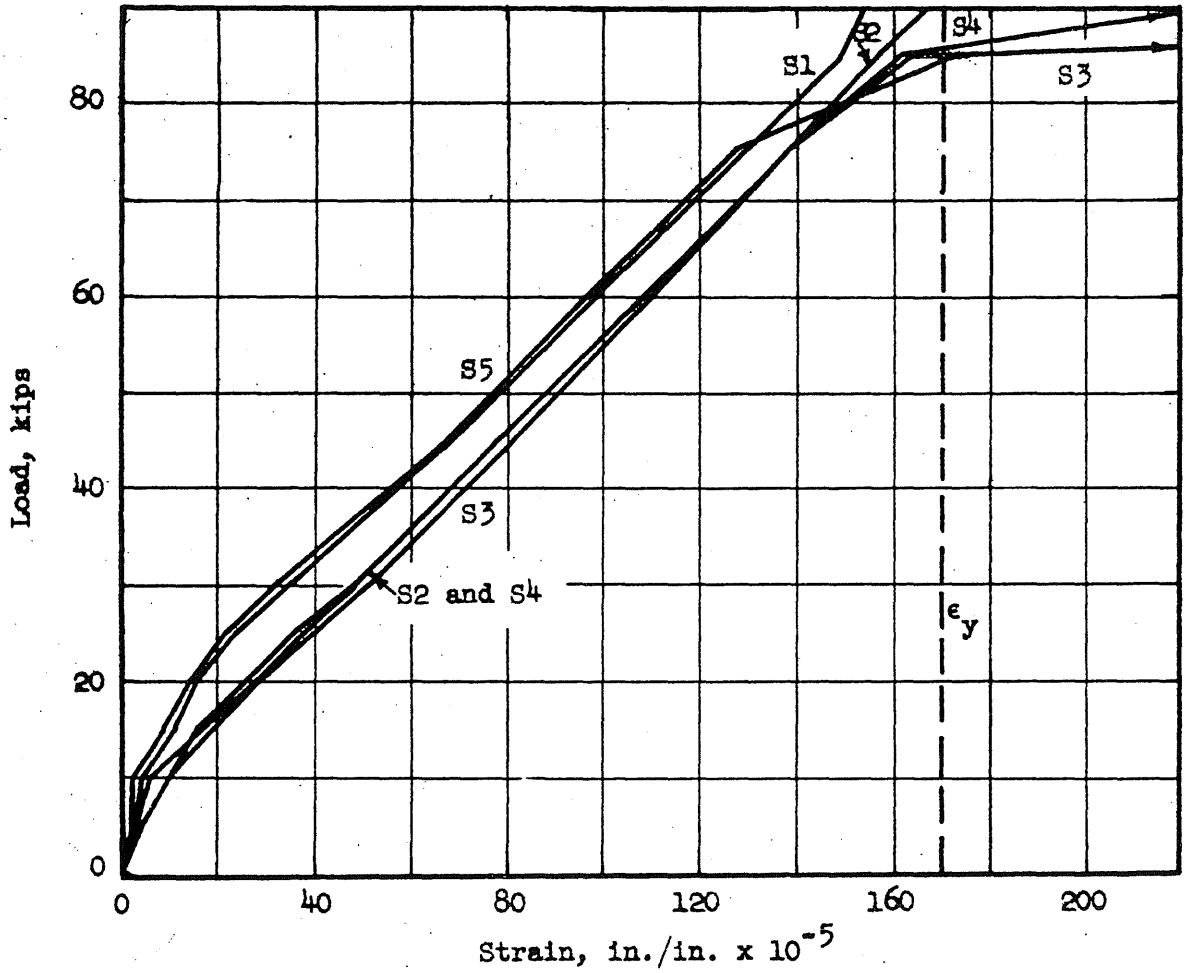

FIG. 25 LOAD-STEEL STRAIN CURVES FOR BEAM C-4

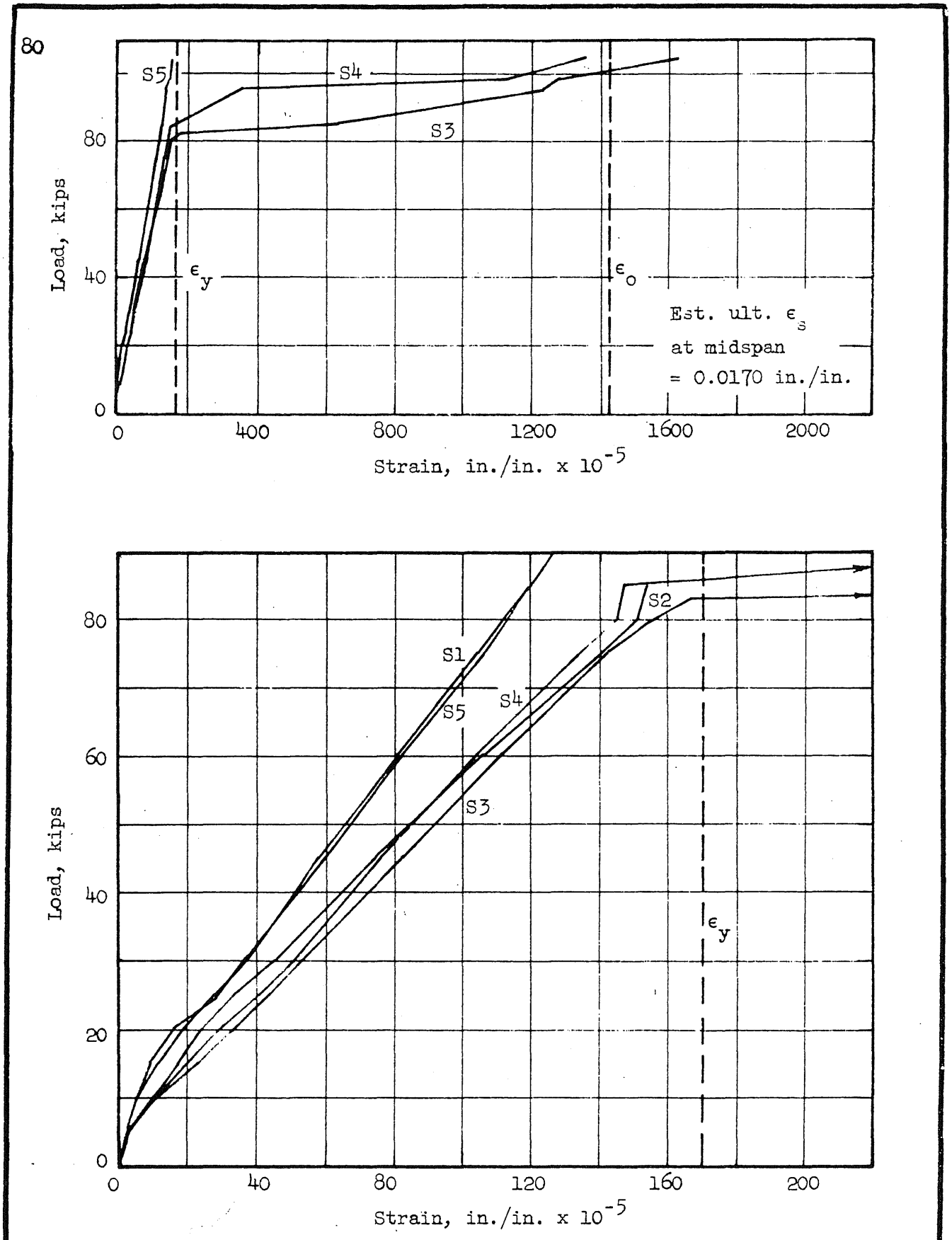

FIG. 26 LOAD-STEEL STRAIN CURVES FOR BEAM C-5

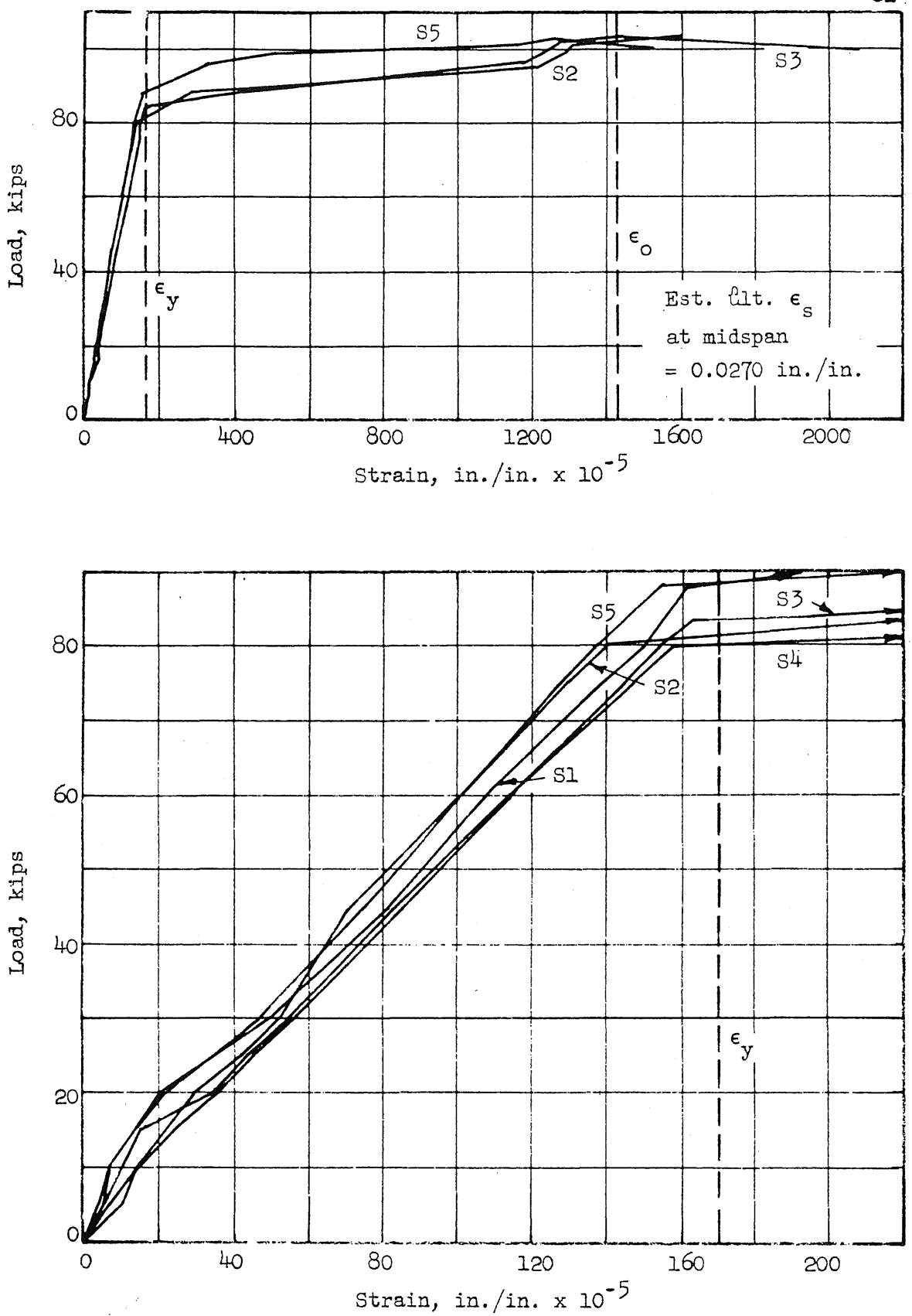

FIG. 27 LOAD-STEEL STRAIN CURVES FOR BEAM C-6

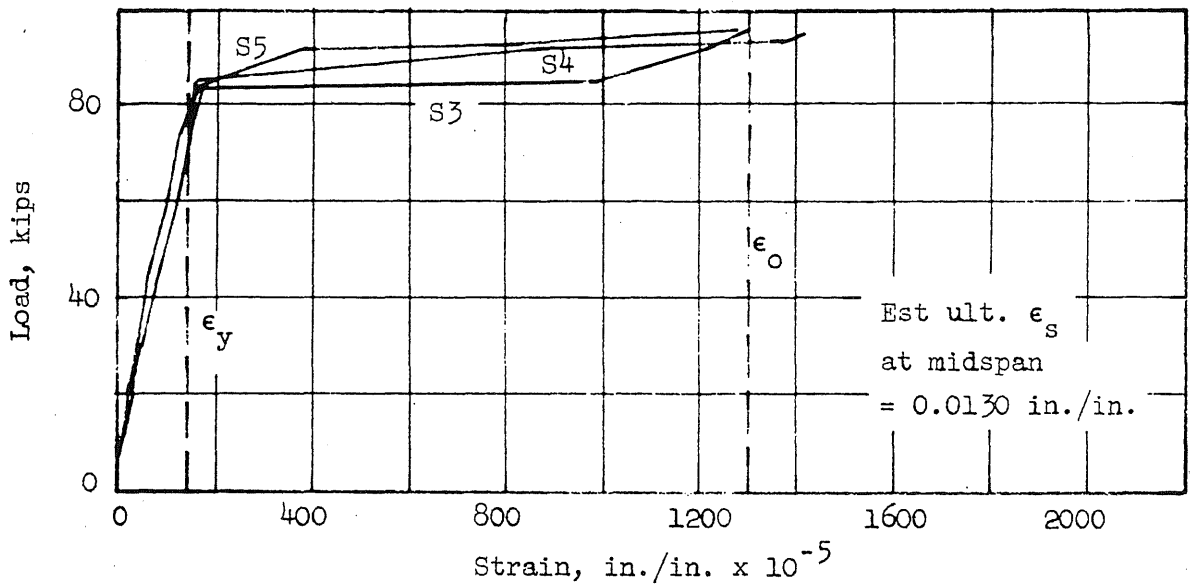

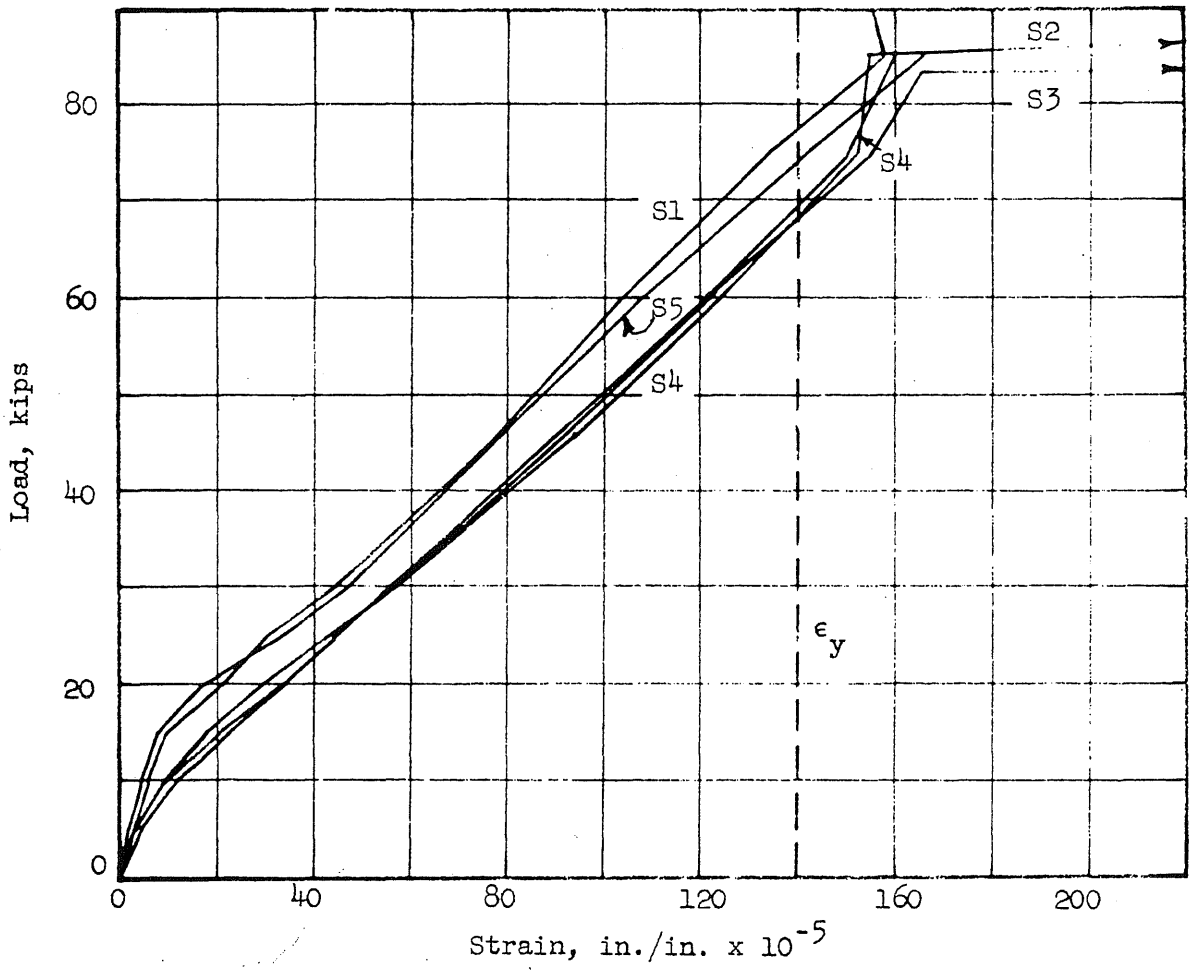

FIG. 28 LOAD-STEEL STRAIN CURVES FOR BEAM C-7

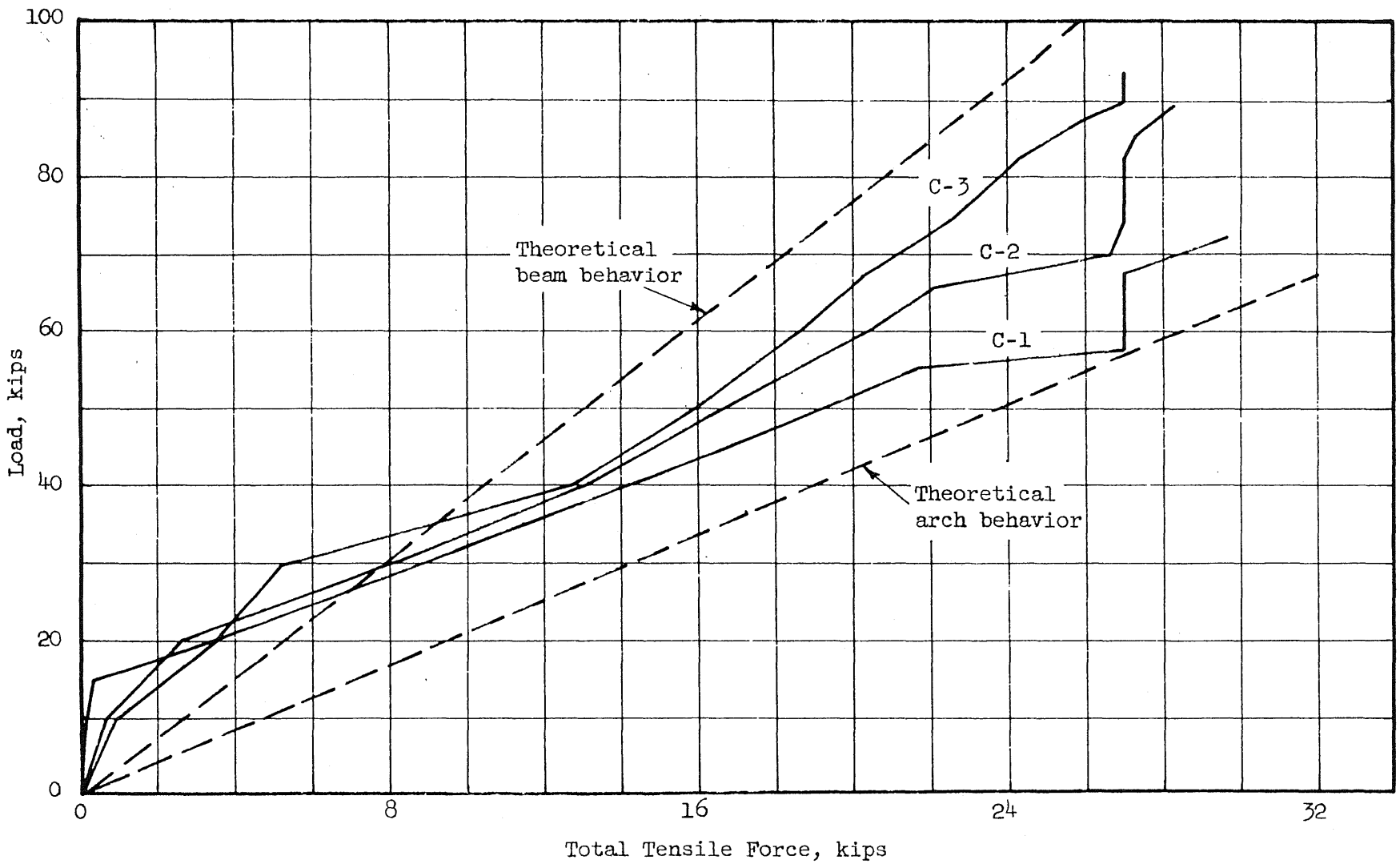

FIG. 29 LOAD vs. TOTAL TENSILE FORCE IN LONGITUDINAL STEEL AT SECTION 12 in. FROM MIDSPAN: BEAMS C-1, C-2, AND C-3

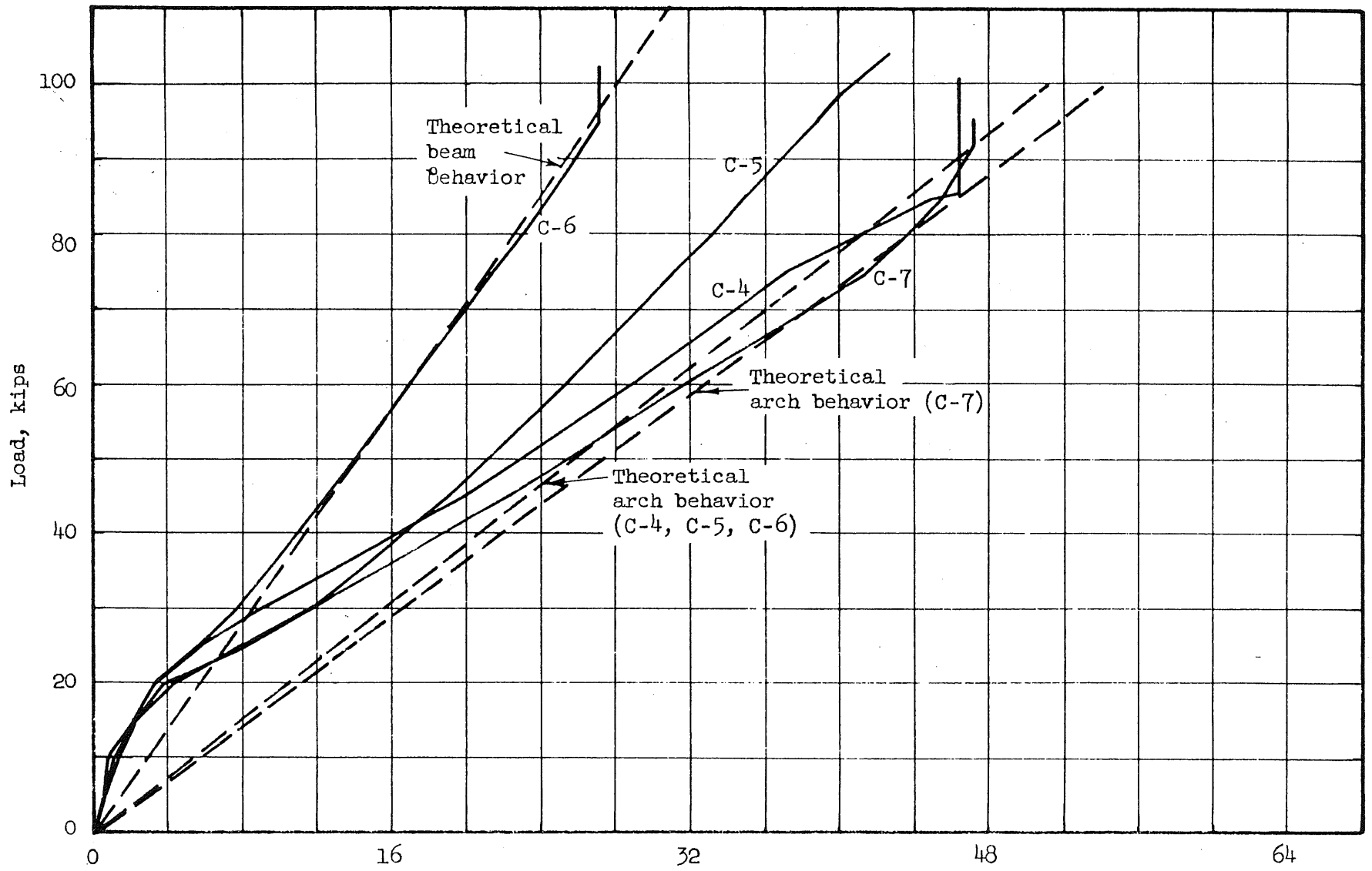

FIG. 30 LOAD vs. TOTAL TENSILE FORCE IN LONGITUDINAL STEEL AT SECTION 12 in. FROM MIDSPAN: BEAMS C-4, C-5, C-6, AND C-7

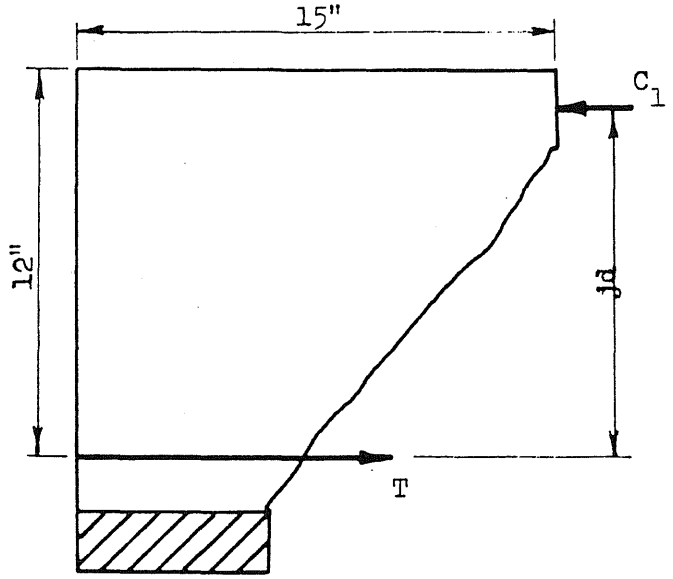

Beam C-1

$$T = \frac{M_1}{jd}$$

M_1 = external moment

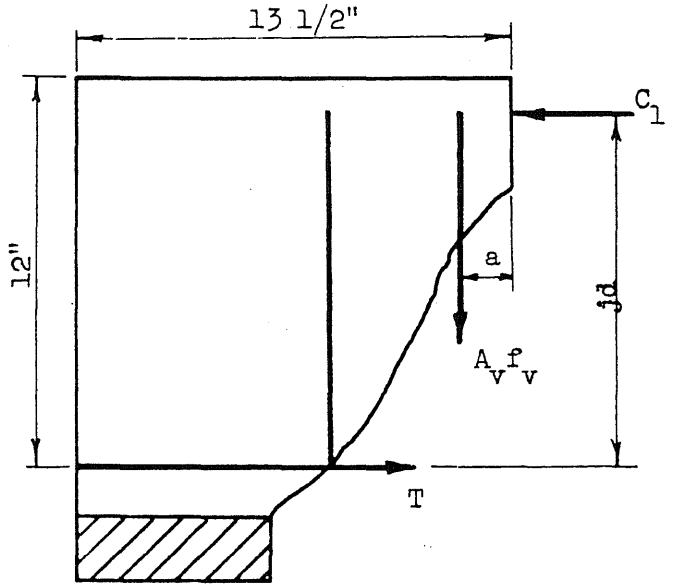

Beam C-2

$$T = \frac{M_2 - aA_v f_v}{jd}$$

M_2 = external moment

$M_2 < M_1$

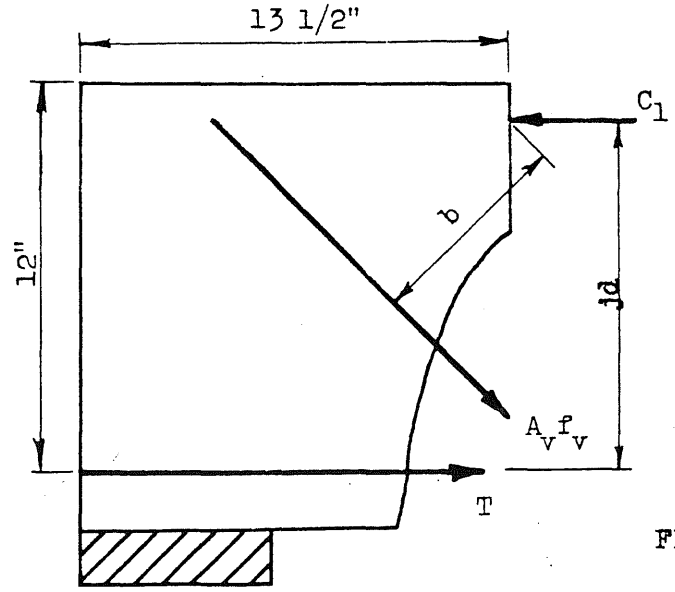

Beam C-3

$$T = \frac{M_2 - bA_v f_v}{jd}$$

$b > a$

FIG. 31 FREE-BODY DIAGRAMS OF CRACKED SPECIMENS

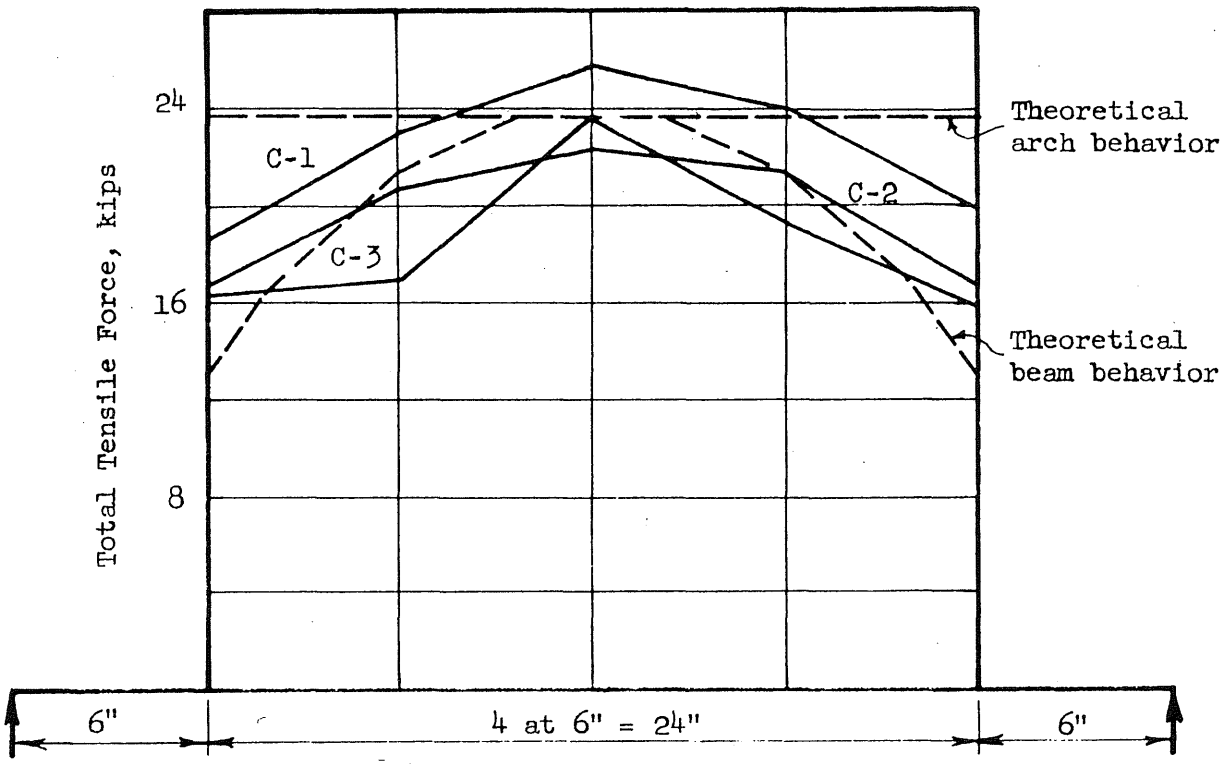

FIG. 32 DISTRIBUTION OF TOTAL TENSILE FORCE IN THE LONGITUDINAL REINFORCEMENT: BEAMS C-1, C-2, AND C-3

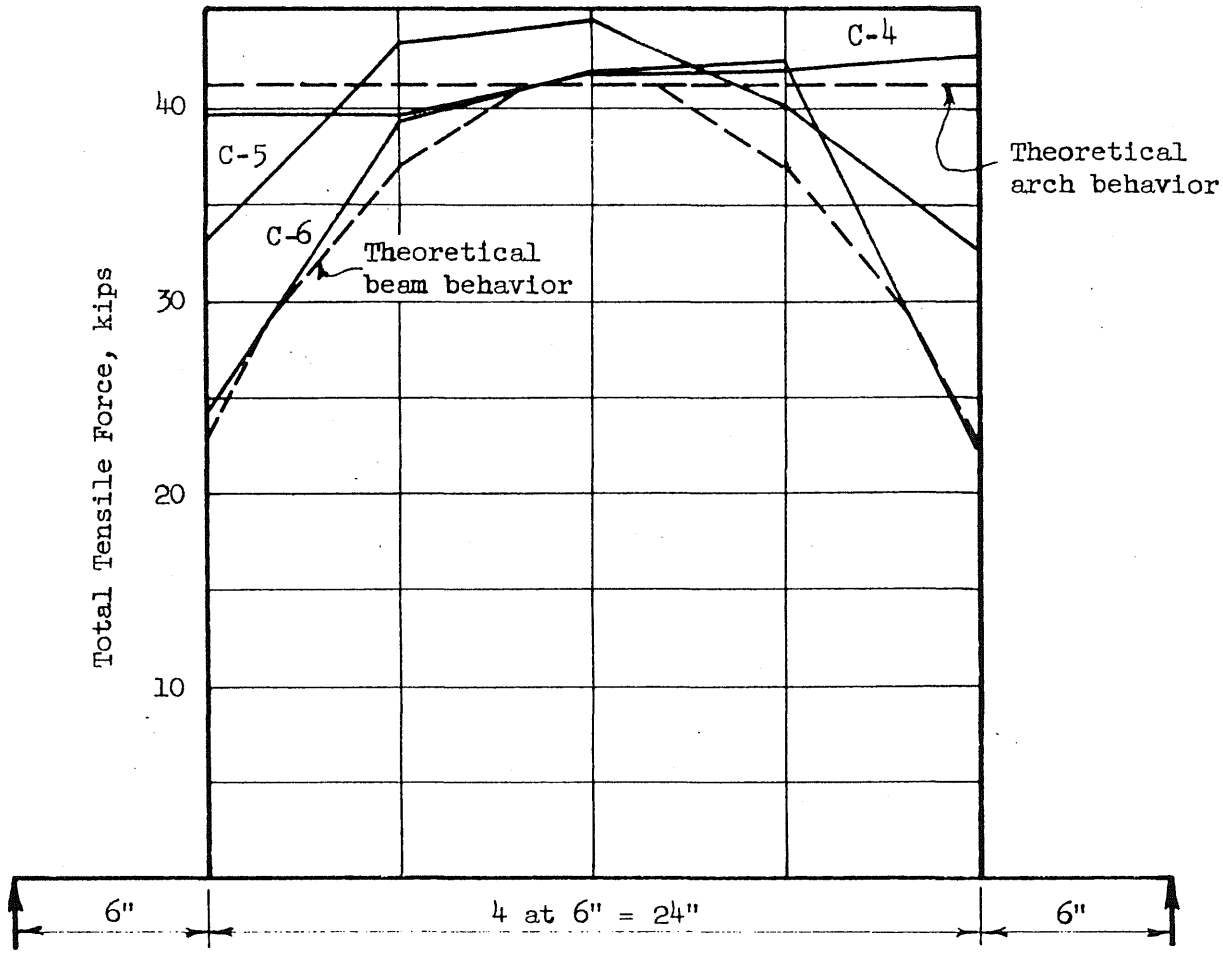

FIG. 33 DISTRIBUTION OF TOTAL TENSILE FORCE IN THE LONGITUDINAL REINFORCEMENT: BEAMS C-4, C-5, AND C-6

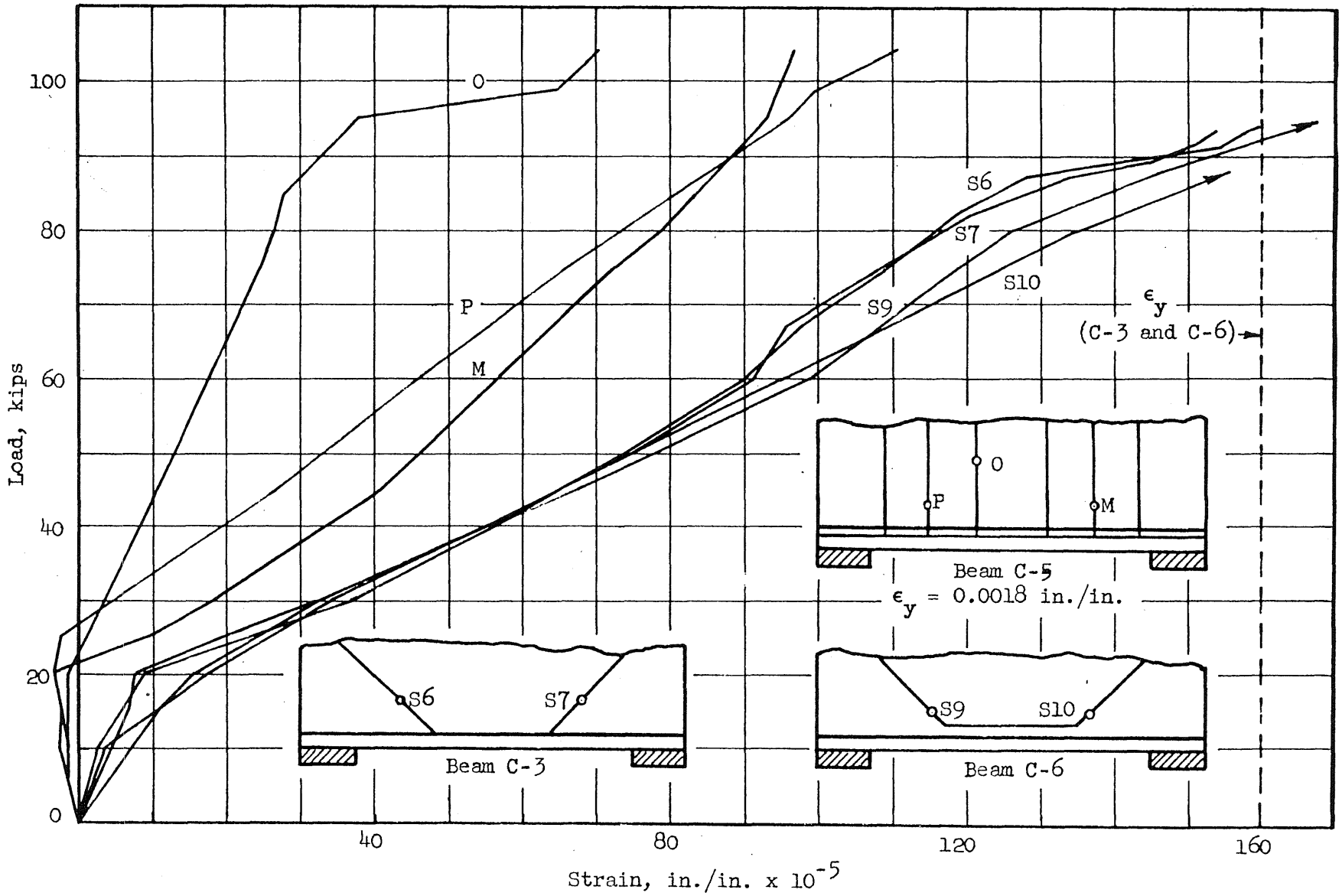

FIG. 34 LOAD-STEEL STRAIN CURVES FOR THE WEB REINFORCEMENT

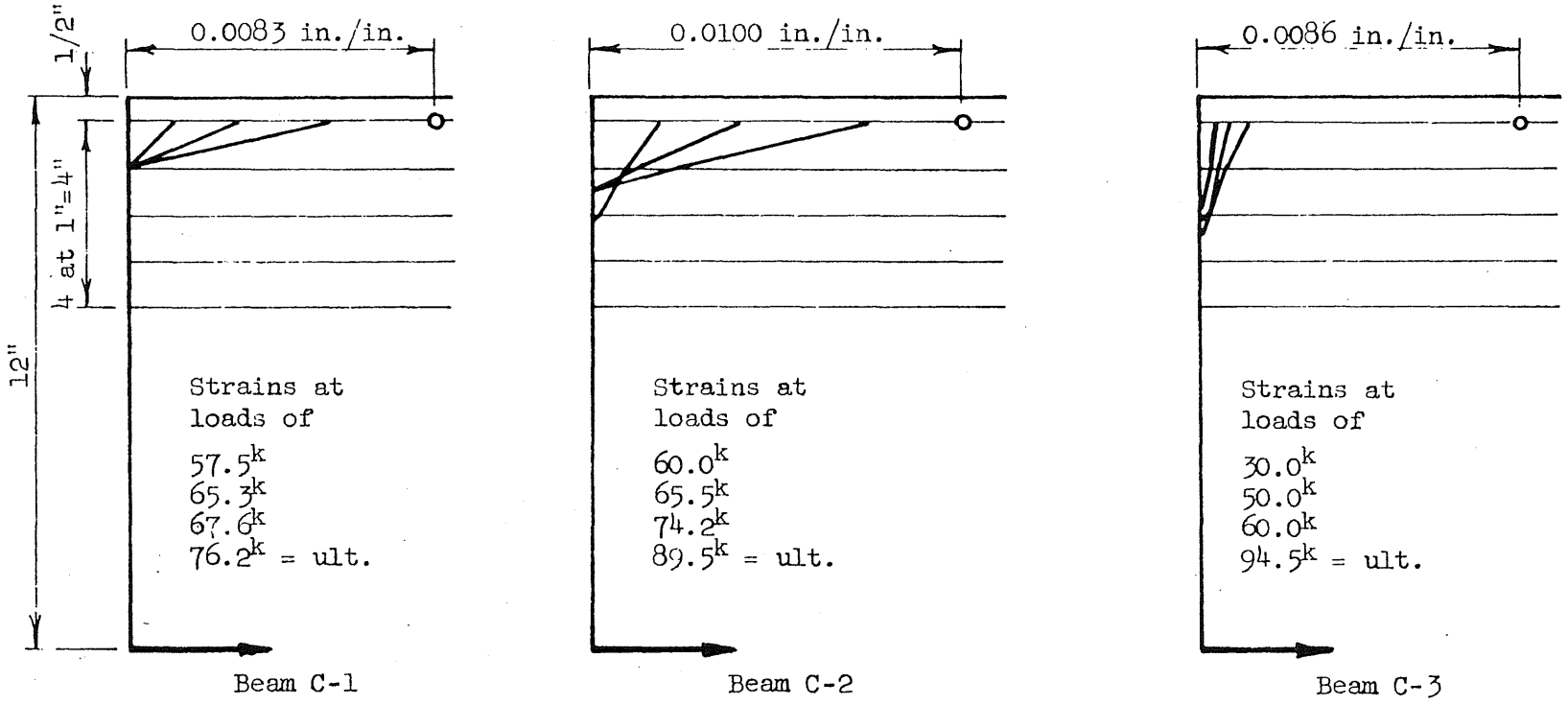

o Estimated ult. strain

FIG. 35 DISTRIBUTION OF CONCRETE STRAIN ALONG DEPTH OF BEAM AT MIDSPAN, BEAMS C-1, C-2 AND C-3

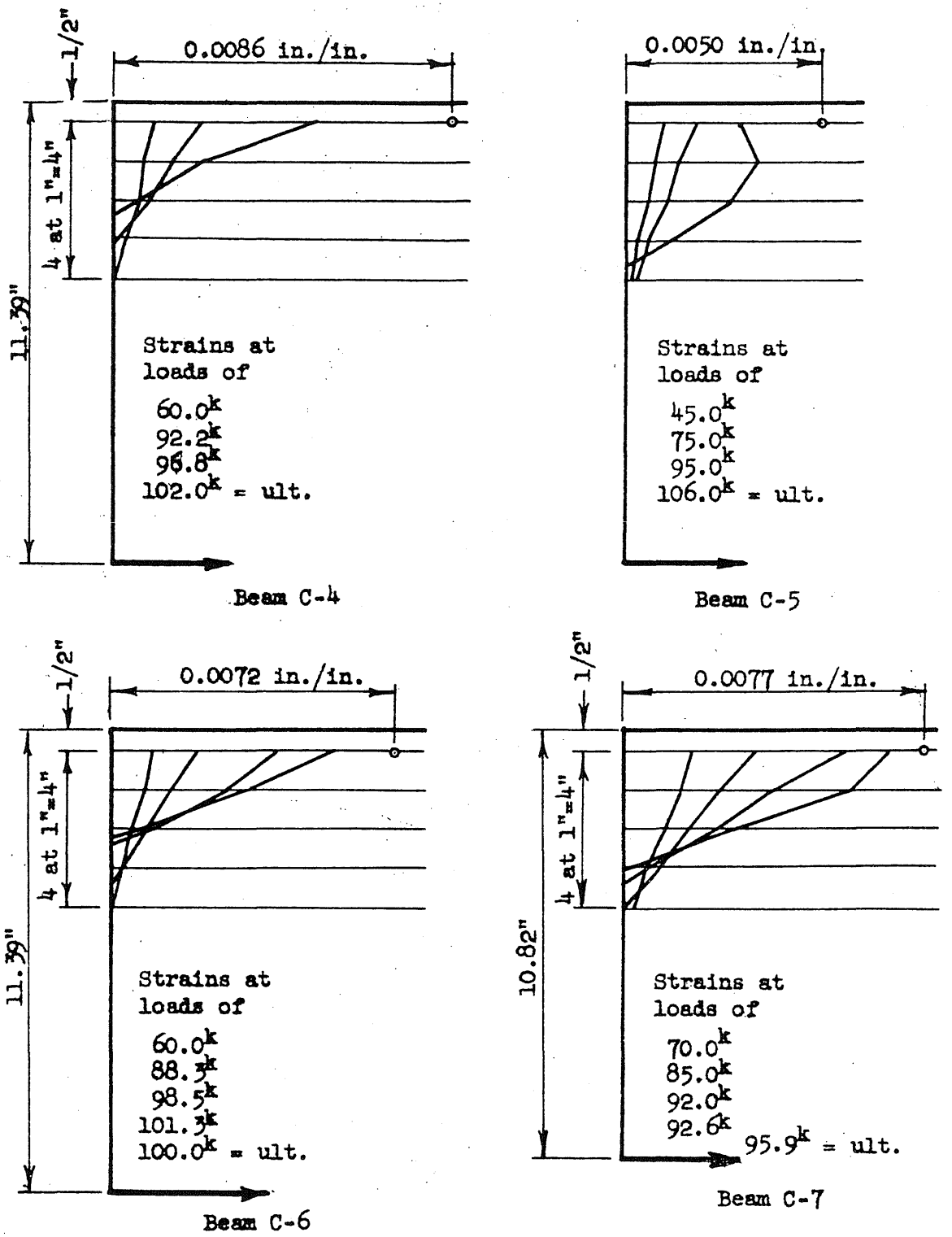

° Estimated ult. strain

FIG. 36 DISTRIBUTION OF CONCRETE STRAIN ALONG DEPTH OF BEAM AT MIDSPAN, BEAMS C-4, C-5, C-6 AND C-7

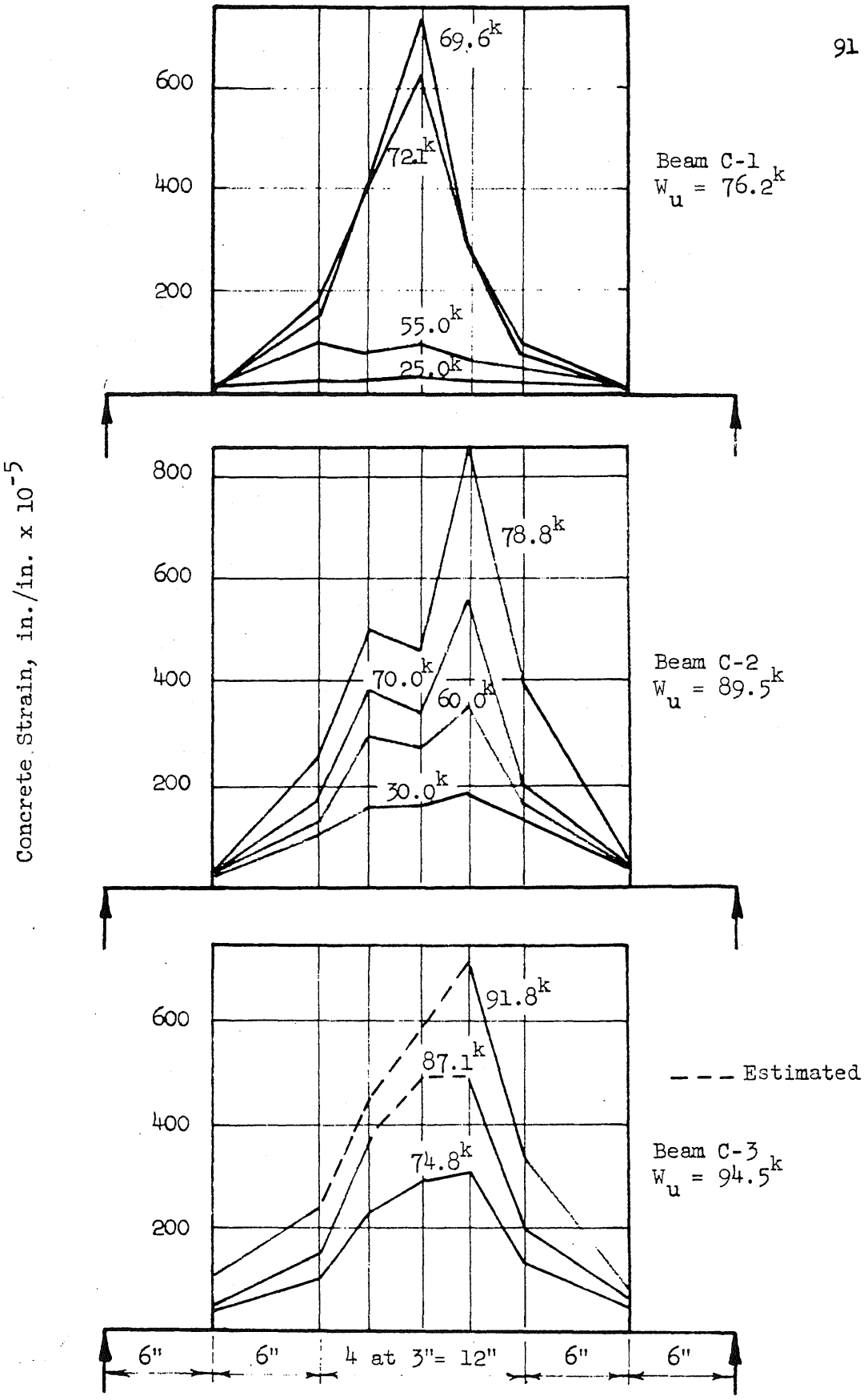

FIG. 37 DISTRIBUTION OF CONCRETE STRAIN ALONG TOP EDGE OF BEAM

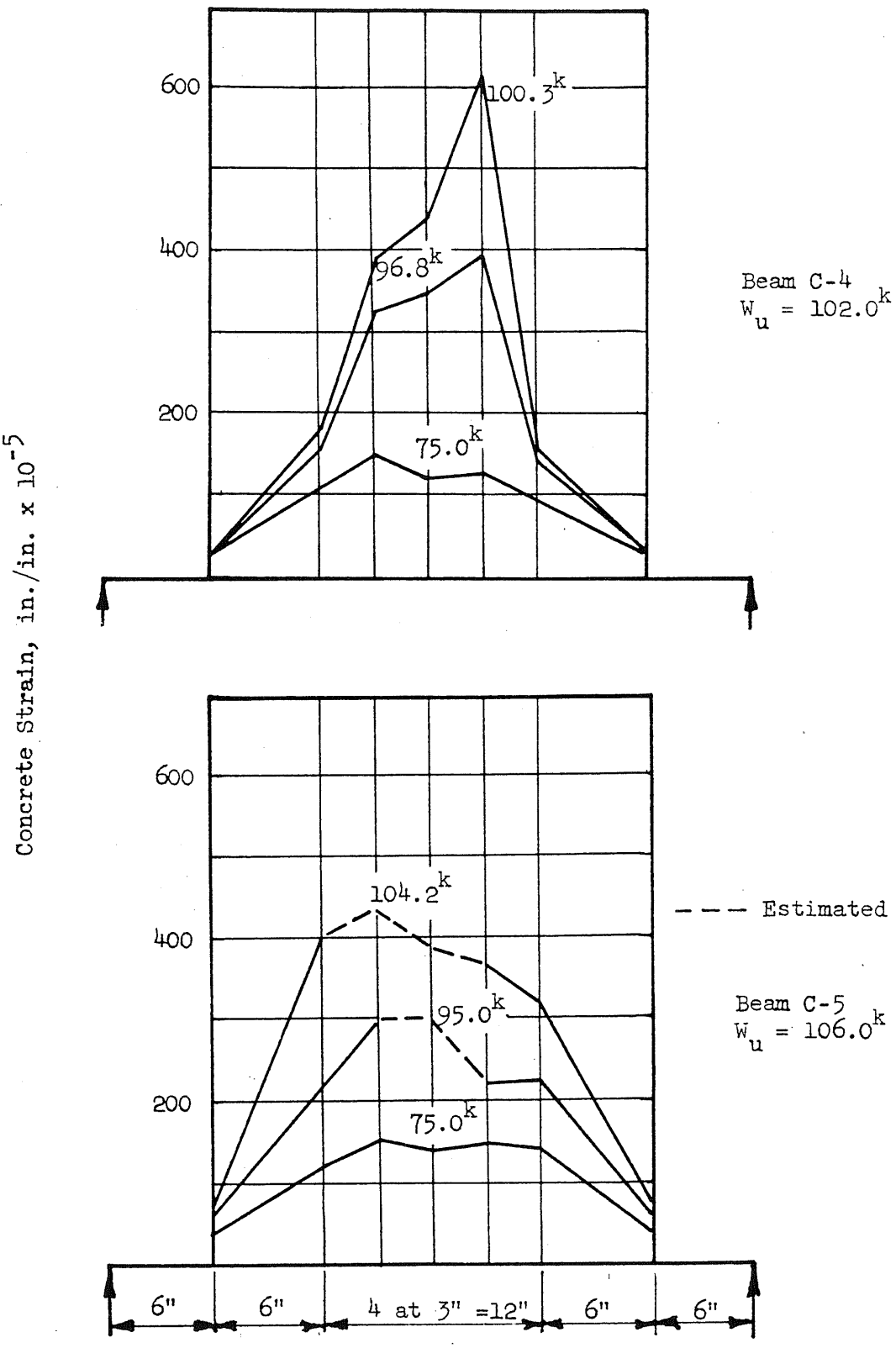

FIG. 38 DISTRIBUTION OF CONCRETE STRAIN ALONG TOP EDGE OF BEAM

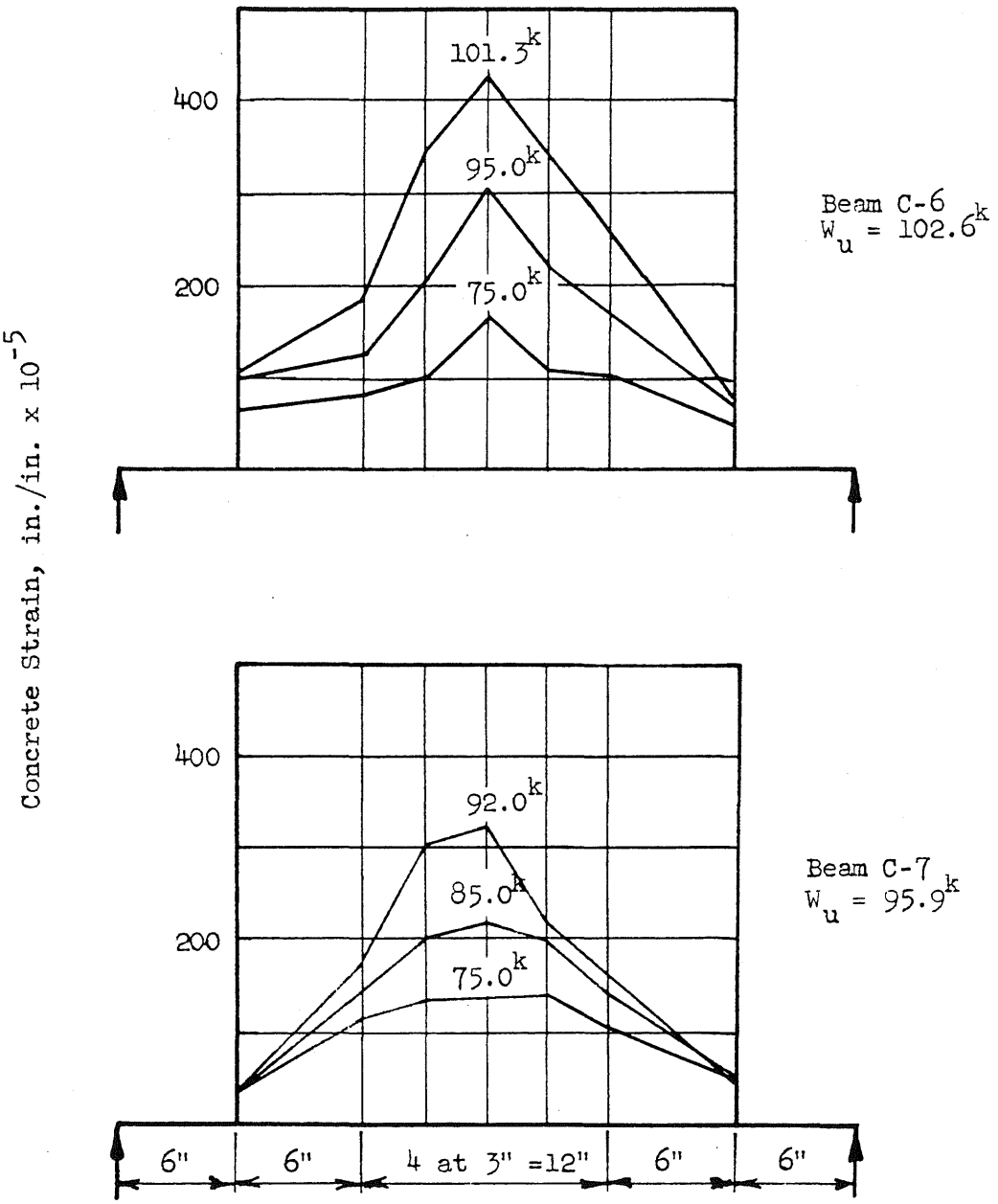

FIG. 39 DISTRIBUTION OF CONCRETE STRAIN ALONG TOP EDGE OF BEAM

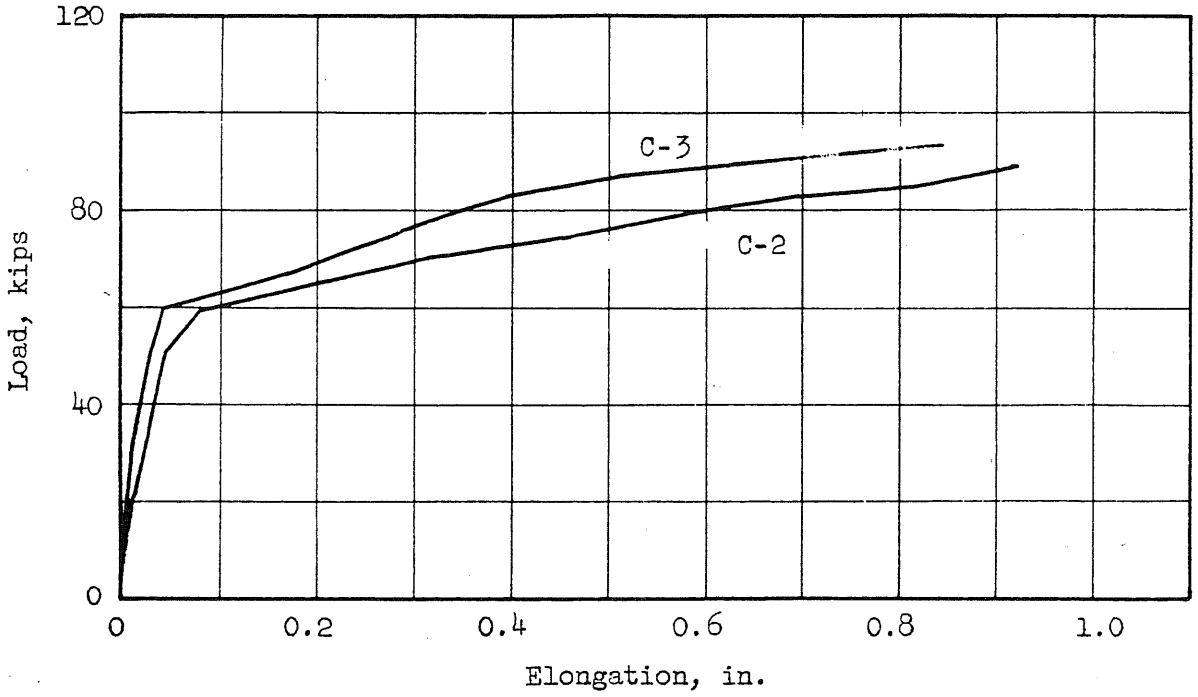

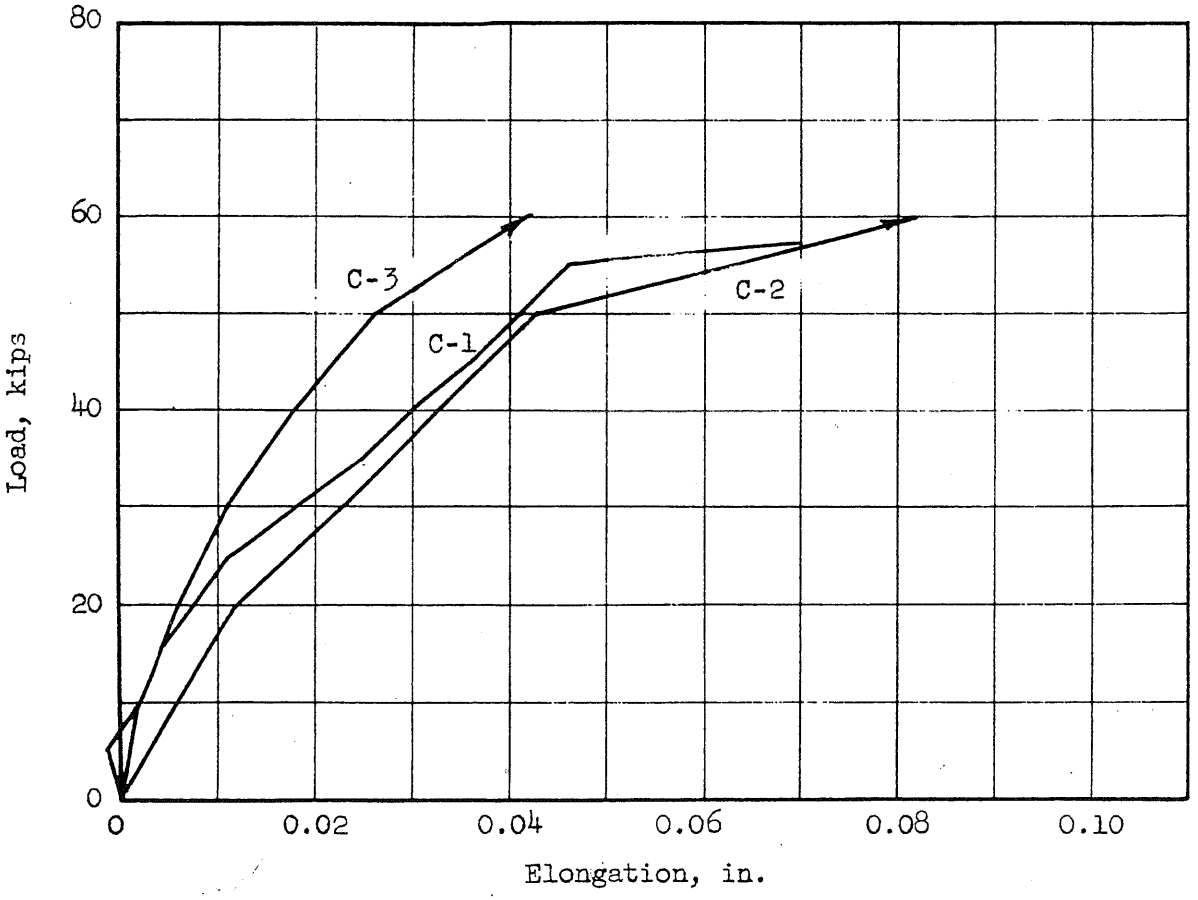

FIG. 40 ELONGATION OF TENSILE REINFORCEMENT: BEAMS C-1, C-2, AND C-3

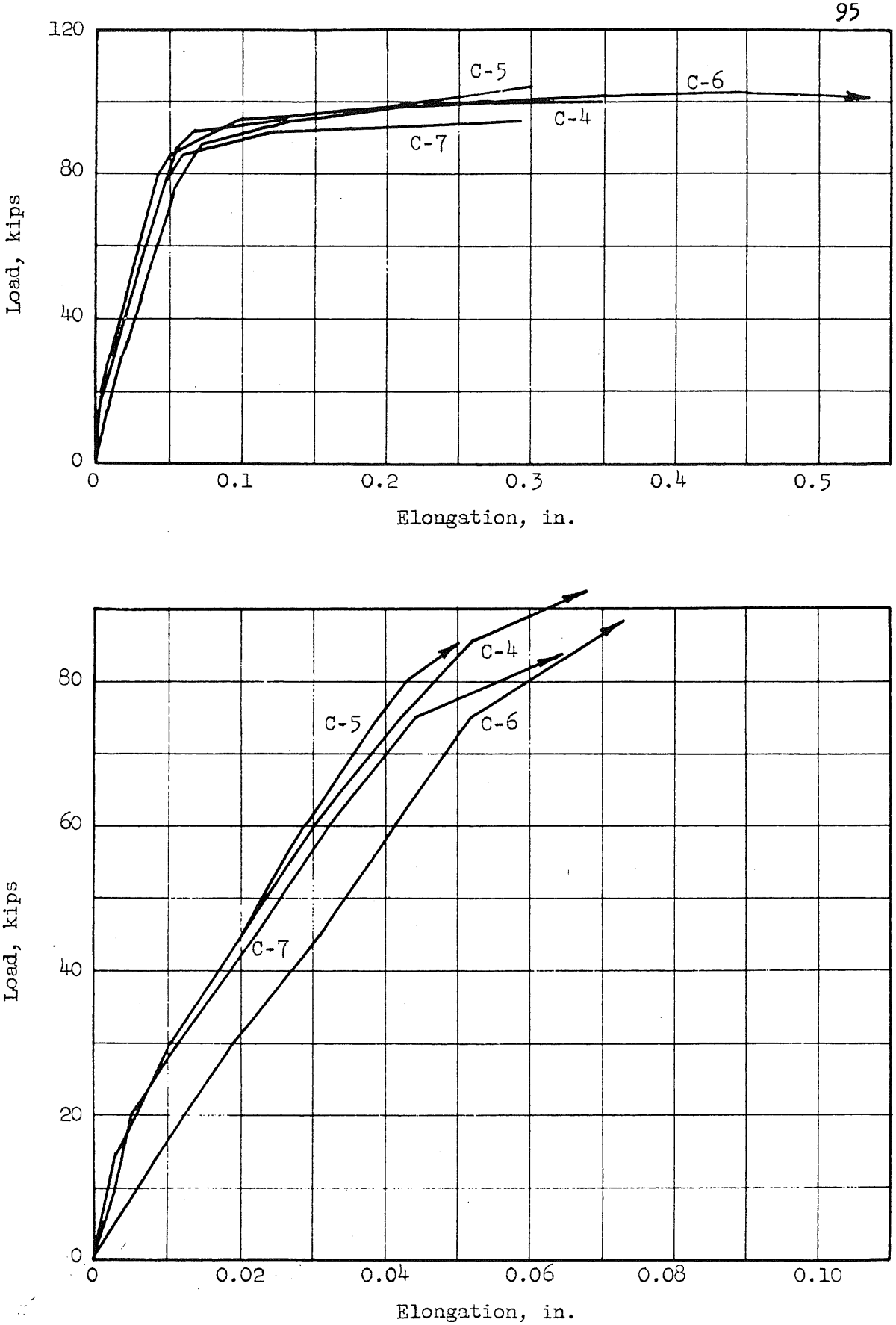

FIG. 41 ELONGATION OF TENSILE REINFORCEMENT: BEAMS C-4, C-5, C-6 AND C-7

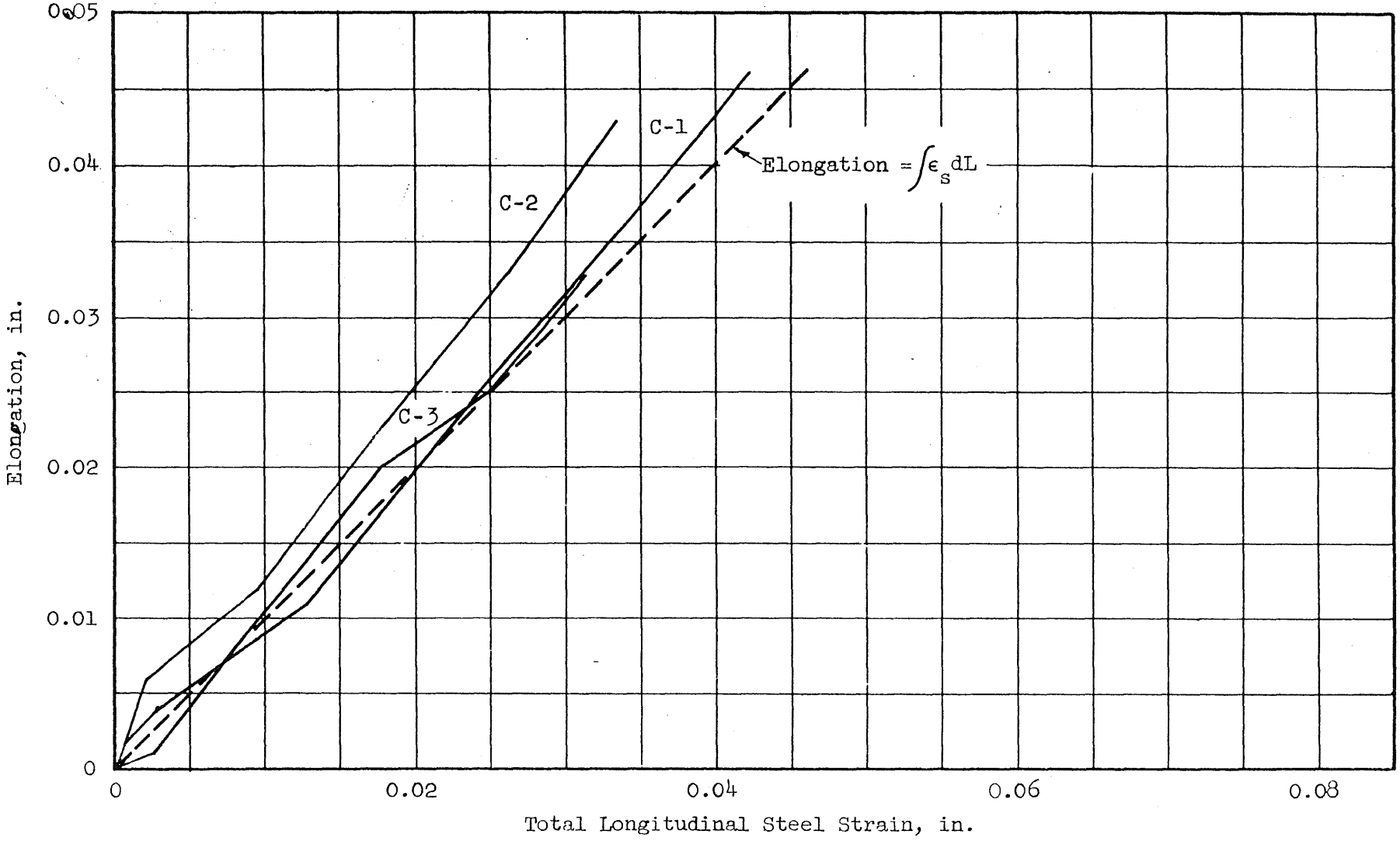

FIG. 42 TOTAL ELONGATION OF TENSILE REINFORCEMENT vs. SUM OF LONGITUDINAL STEEL STRAINS BELOW YIELD: BEAMS C-1, C-2, AND C-3

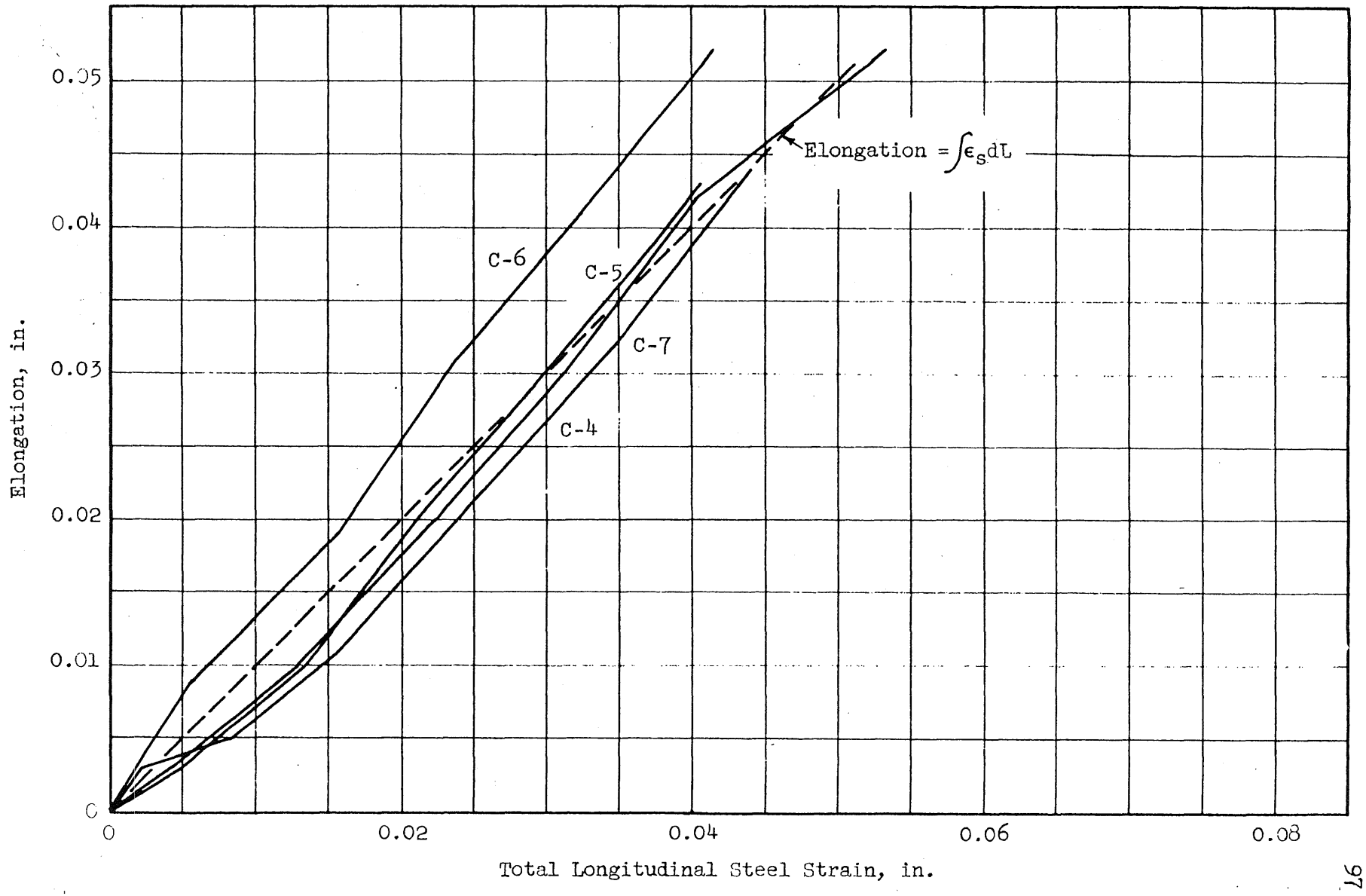

FIG. 43 TOTAL ELONGATION OF TENSILE REINFORCEMENT vs. SUM OF LONGITUDNIAL STEEL STRAINS BELOW YIELD: BEAMS C-4, C-5, C-6, AND C-7

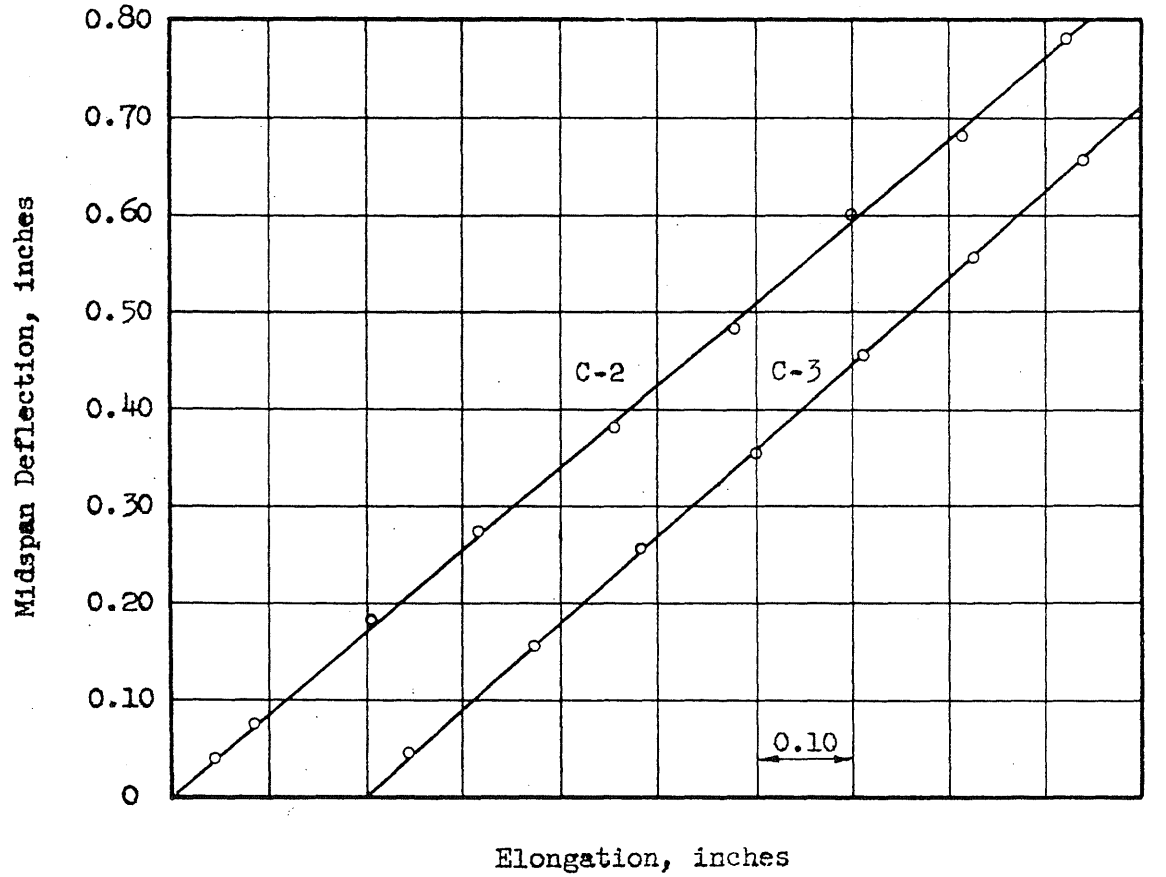

FIG. 44 MIDSPAN DEFLECTION VS. ELONGATION OF TENSILE REINFORCEMENT: BEAMS C-1, C-2, AND C-3

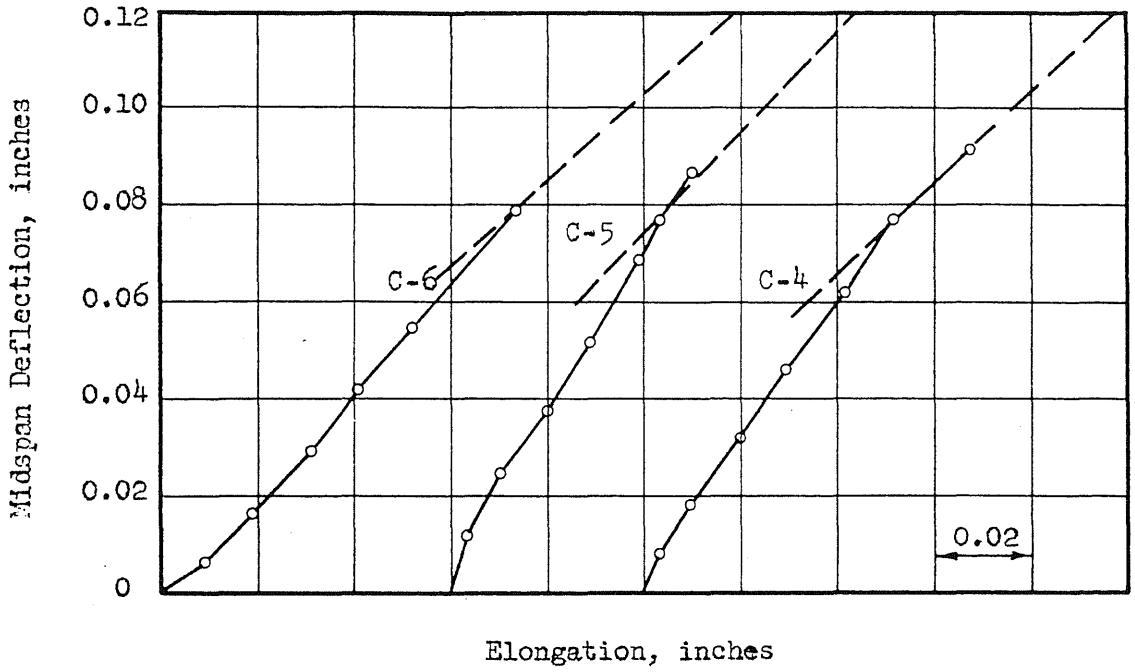

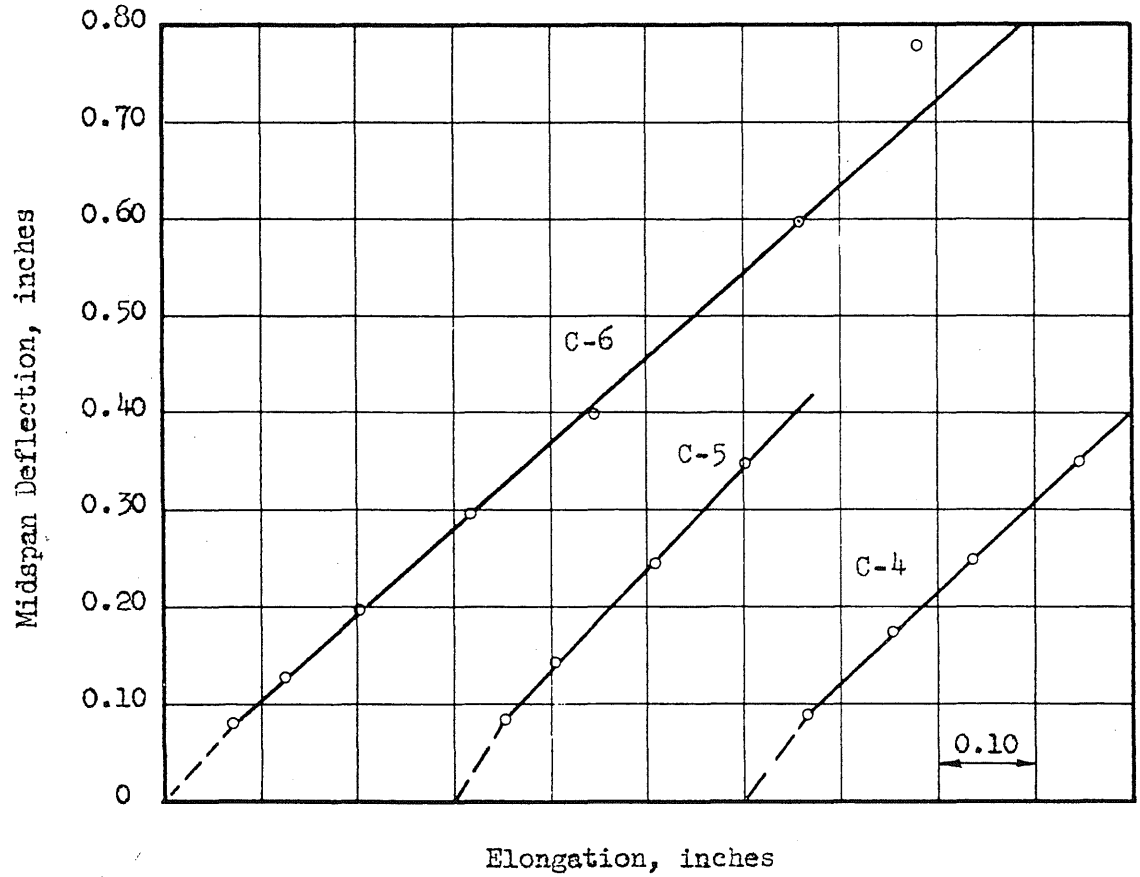

FIG. 45 MIDSPAN DEFLECTION VS. ELONGATION OF TENSILE REINFORCEMENT: BEAMS C-4, C-5, AND C-6

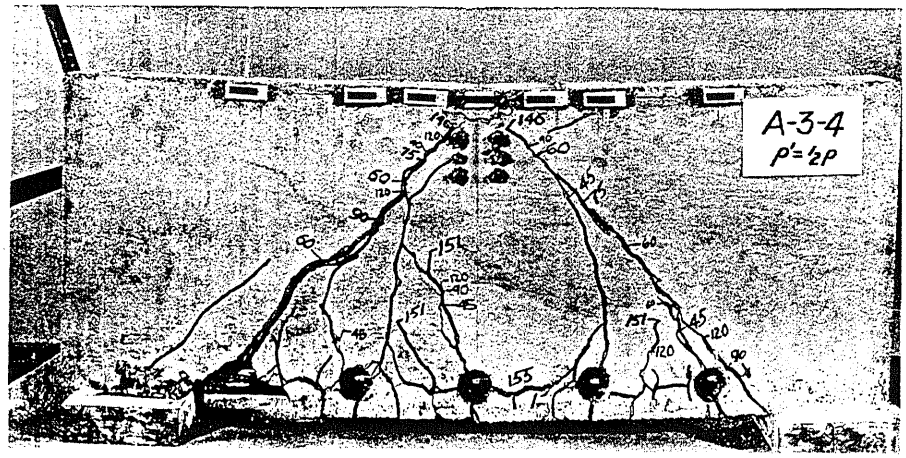

Beam A-3-4
W_u = 186.3^k
M_u = 745$^{in.-k}$

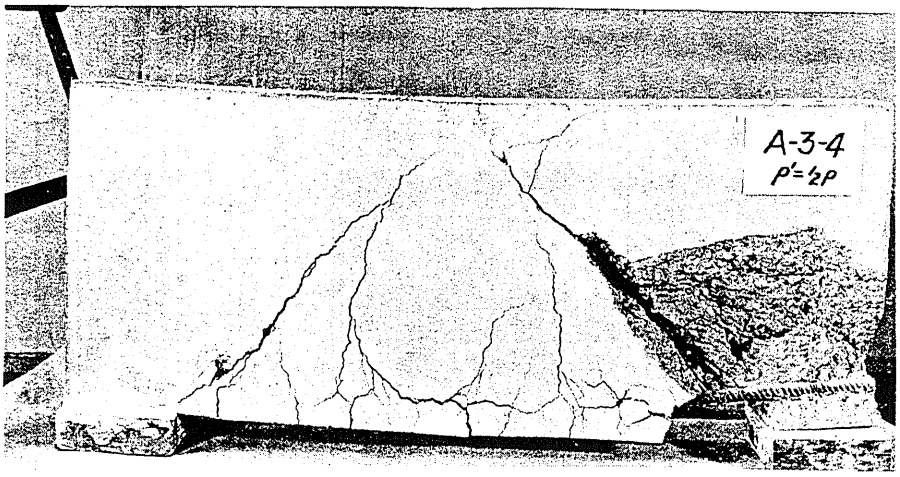

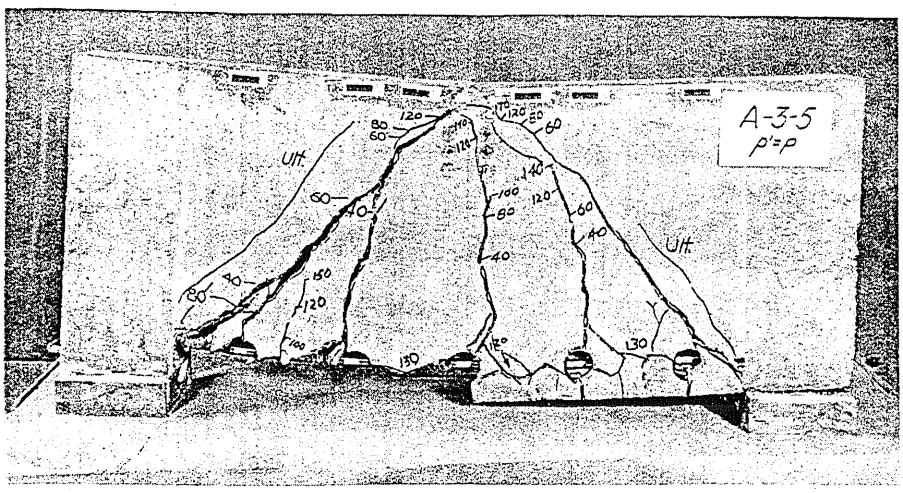

Beam A-3-5
W_u = 179.2^k
M_u = 896$^{in.-k}$

FIG. 46 BEAMS A-3-4 AND A-3-5 AFTER FAILURE

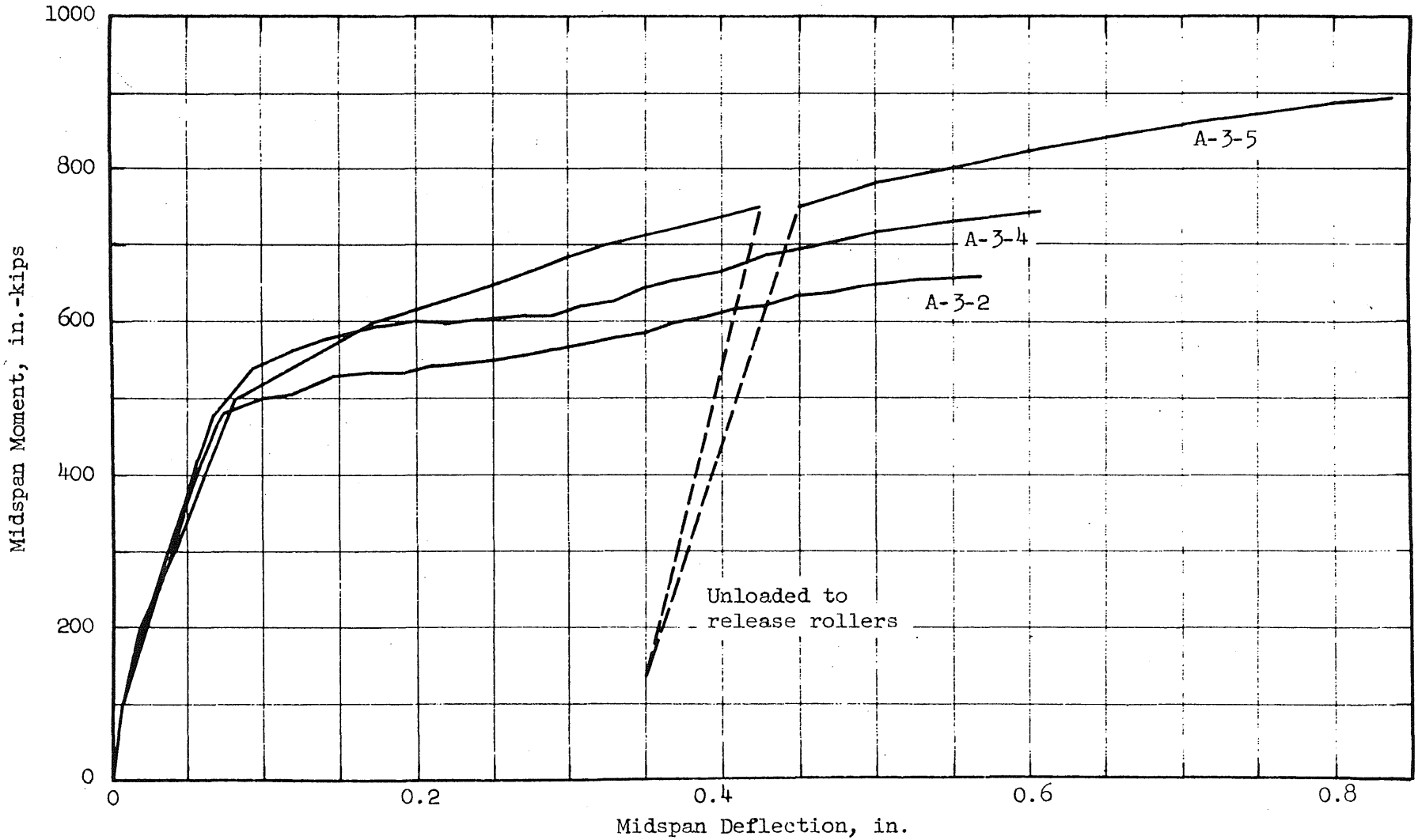

FIG. 47 MOMENT-DEFLECTION CURVES FOR A-SERIES BEAMS

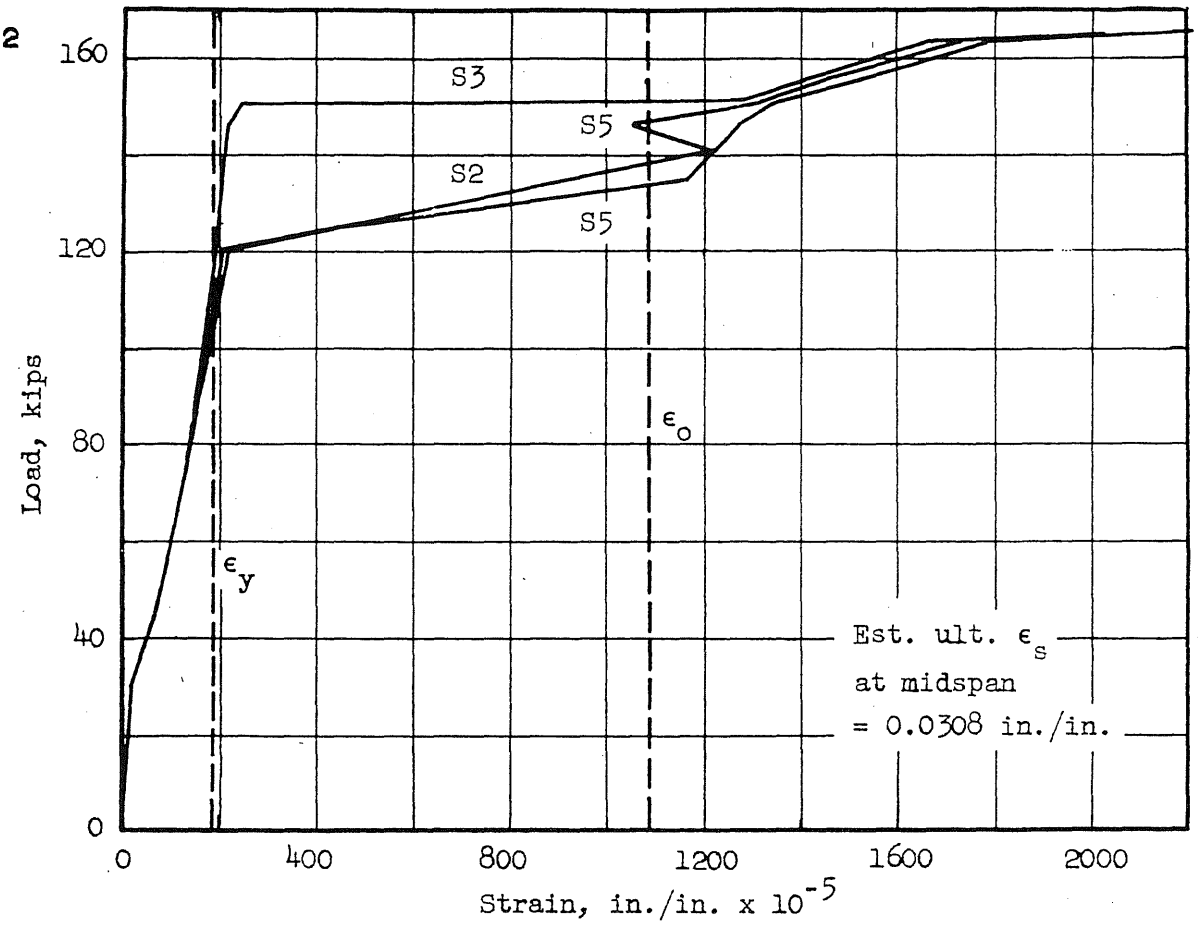

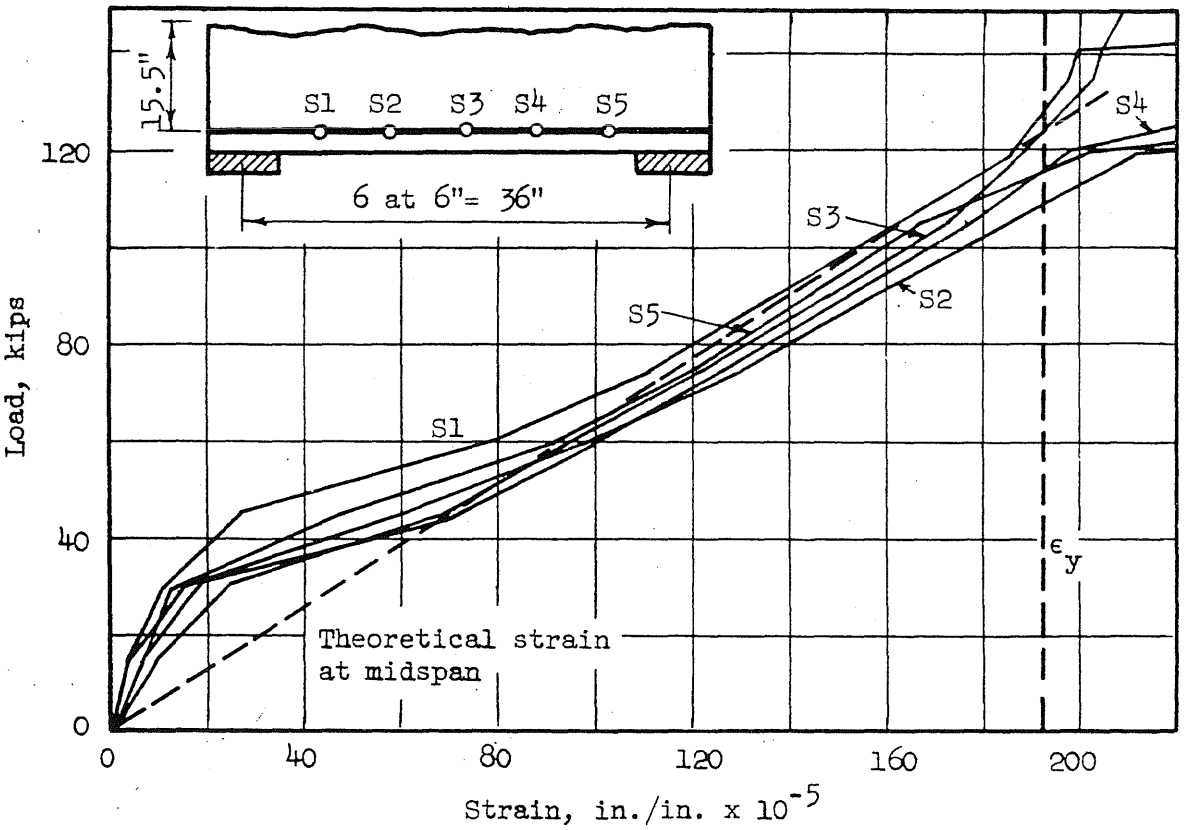

FIG. 48 LOAD-STEEL STRAIN CURVES FOR BEAM A-3-4

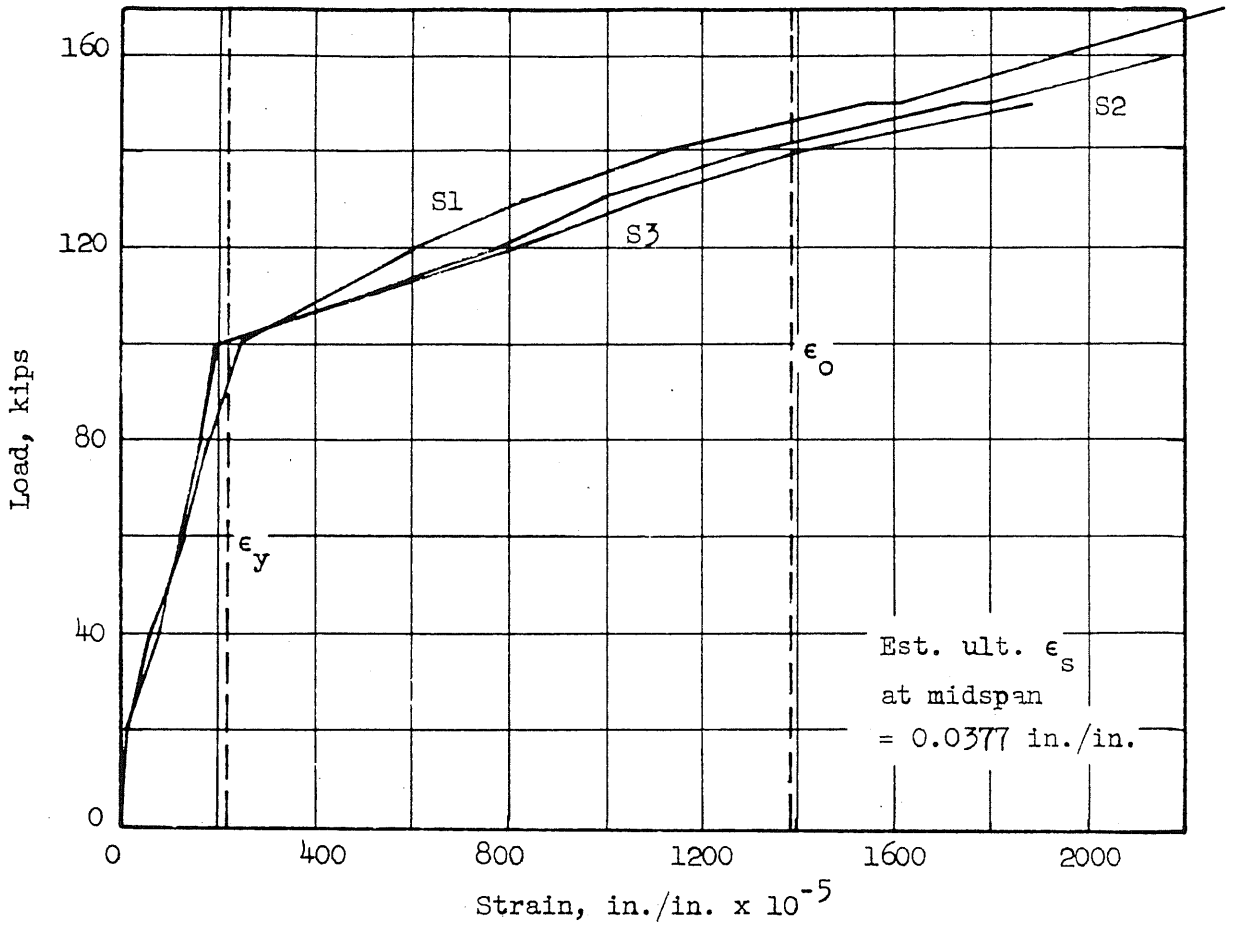

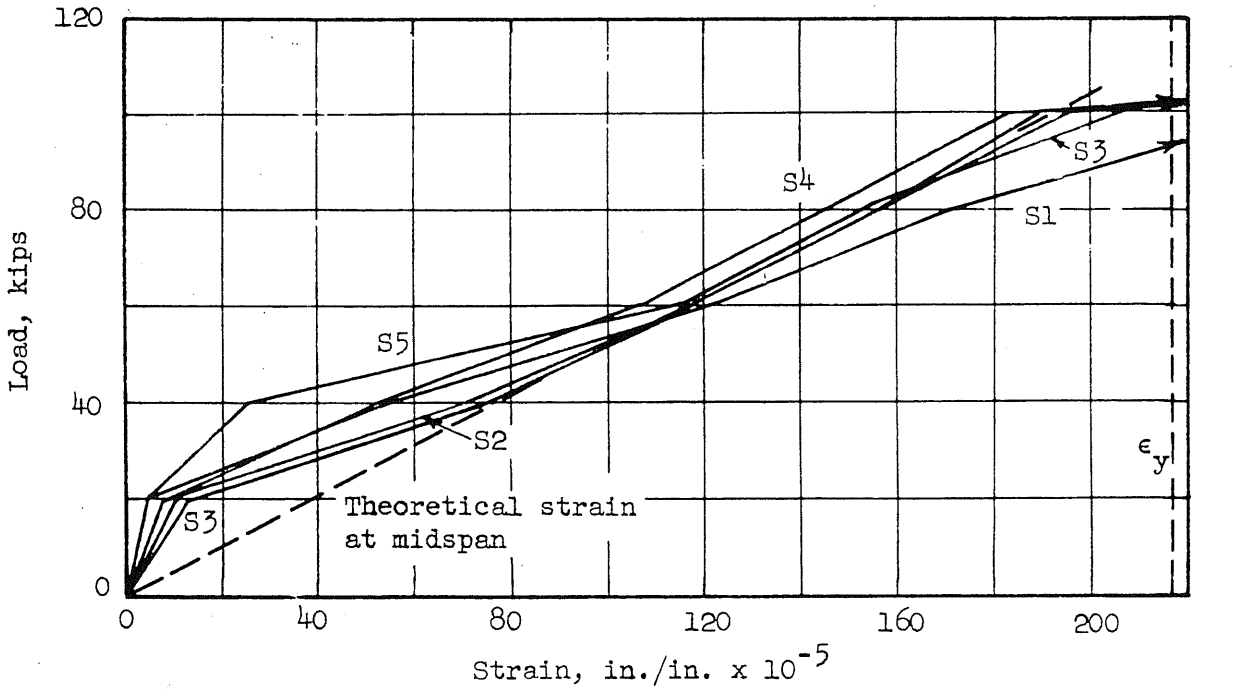

FIG. 49 LOAD-STEEL STRAIN CURVES FOR BEAM A-3-5

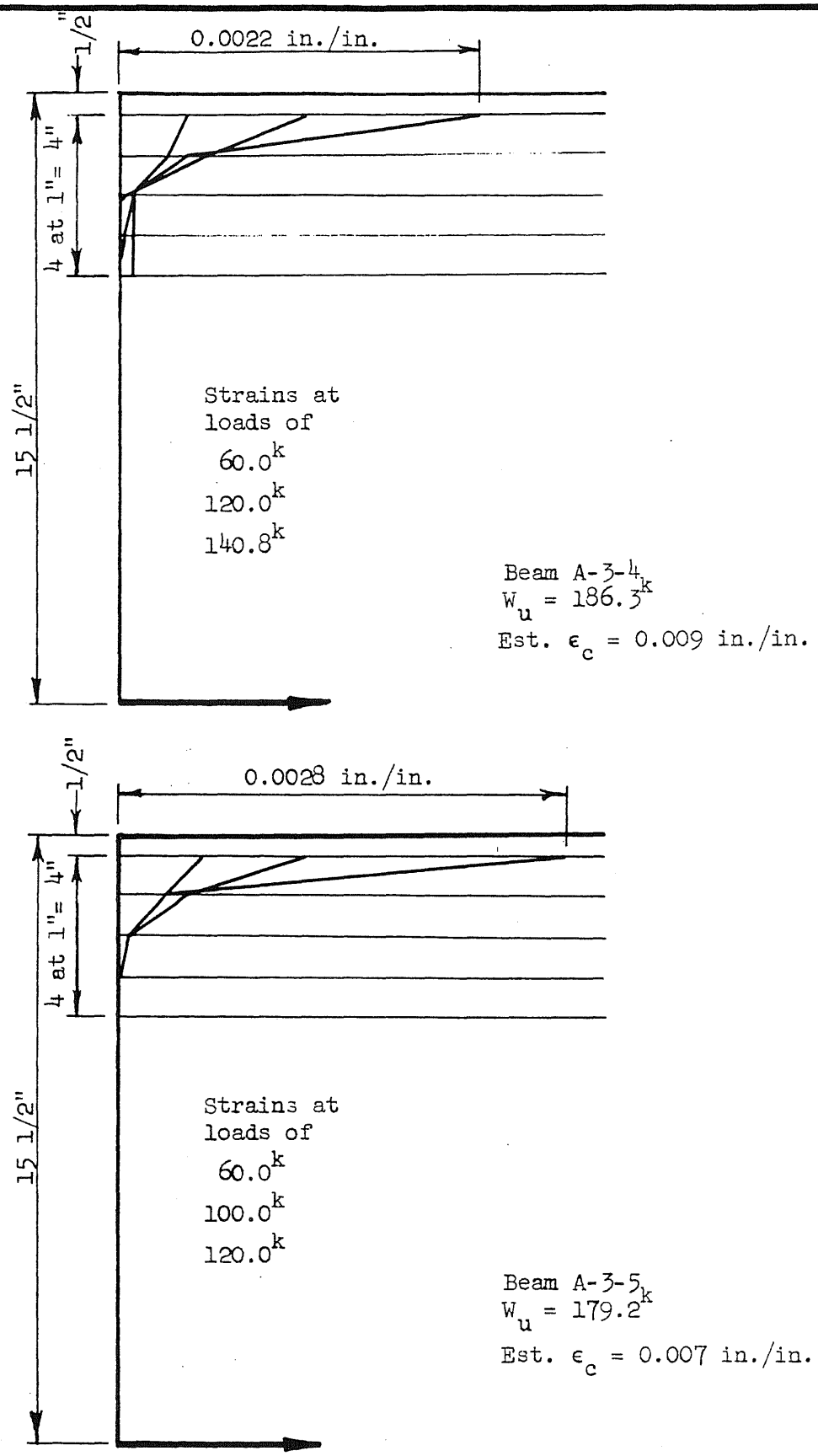

FIG. 30 DISTRIBUTION OF CONCRETE STRAIN ALONG DEPTH OF BEAM AT MIDSPAN, BEAMS A-3-4 AND A-3-5

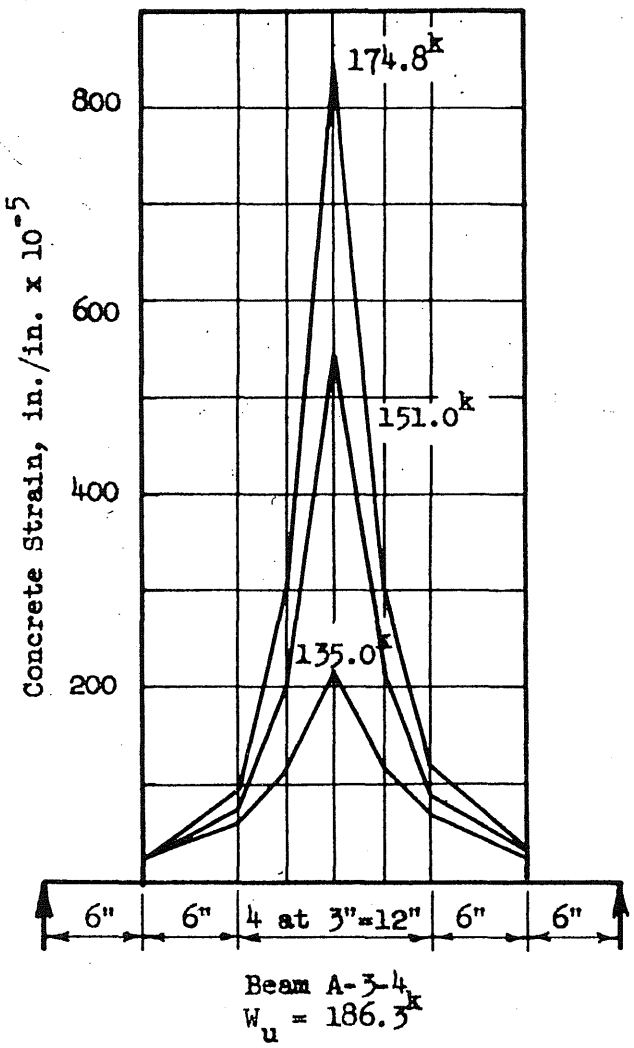

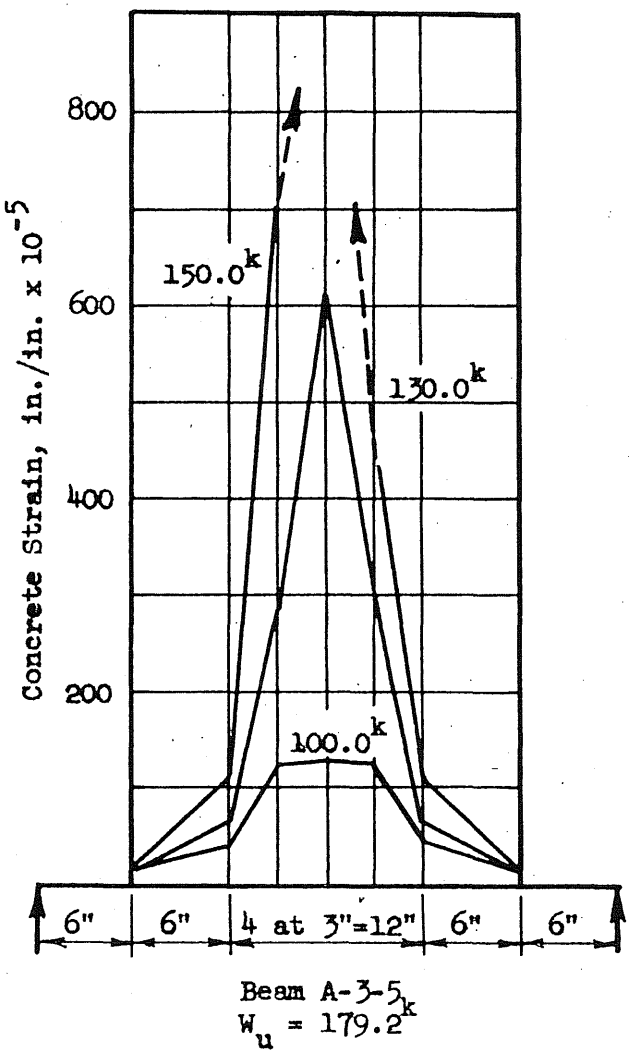

FIG. 51 DISTRIBUTION OF CONCRETE STRAIN ALONG TOP EDGE OF BEAMS A-3-4 AND A-3-5

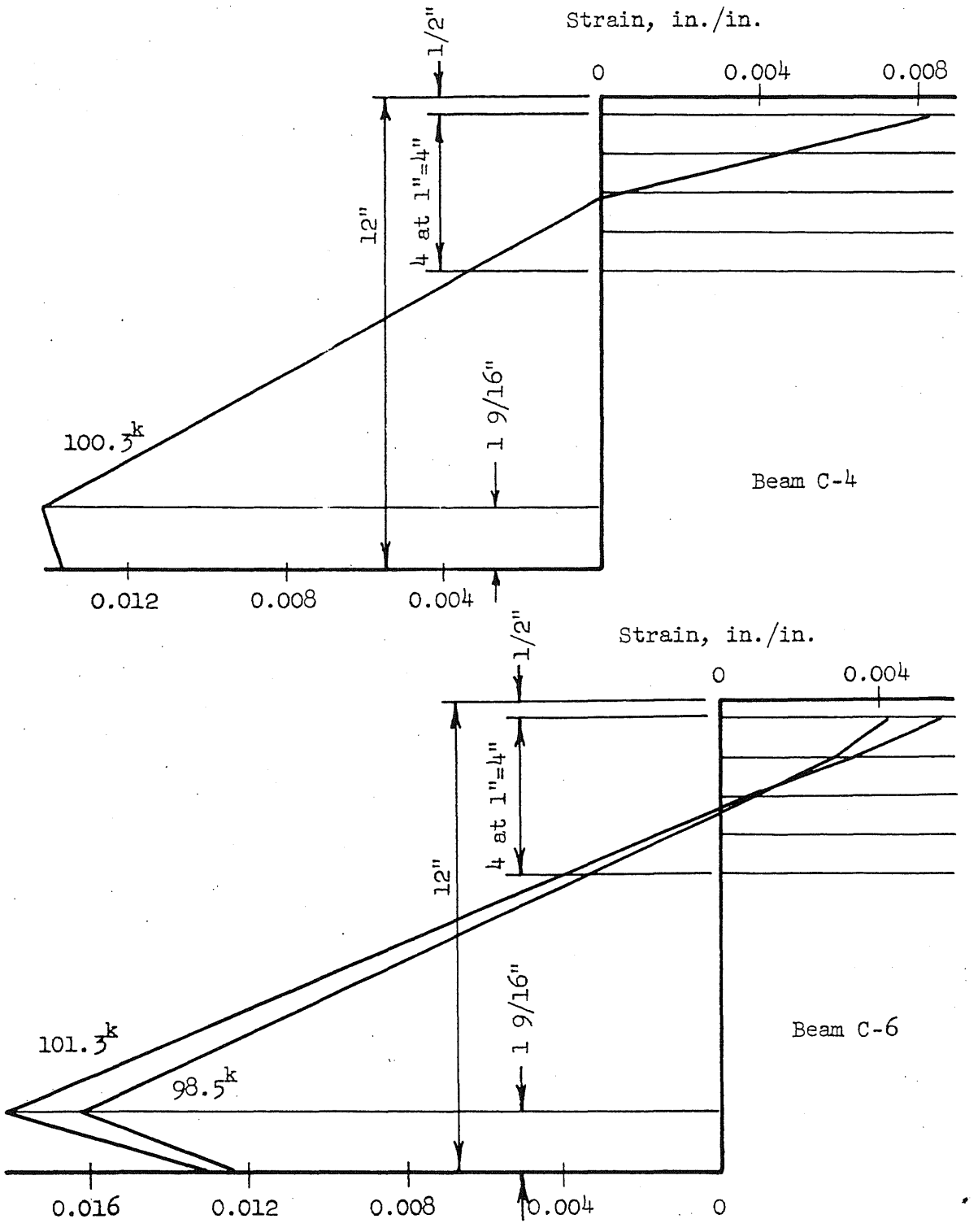

FIG. 52 DISTRIBUTION OF STRAIN ALONG ENTIRE DEPTH OF BEAM AT MIDSPAN: BEAMS C-4 AND C-6

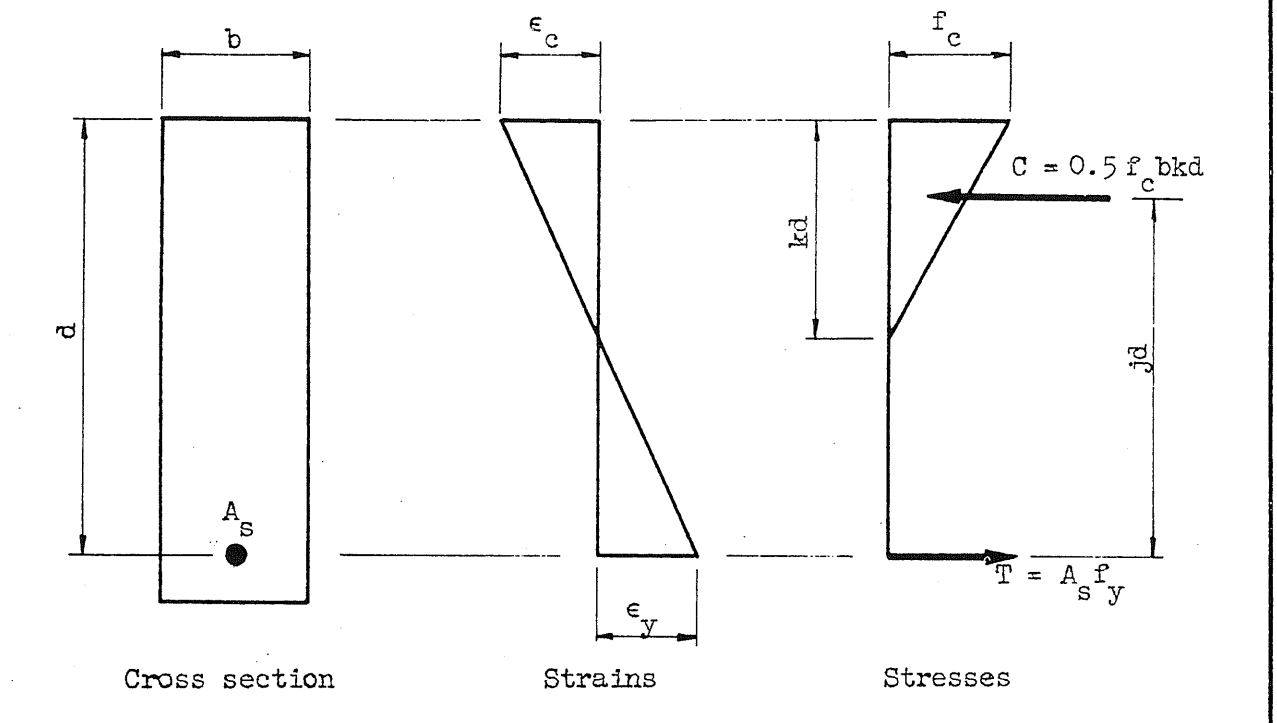

(a) Beams Reinforced in Tension Only

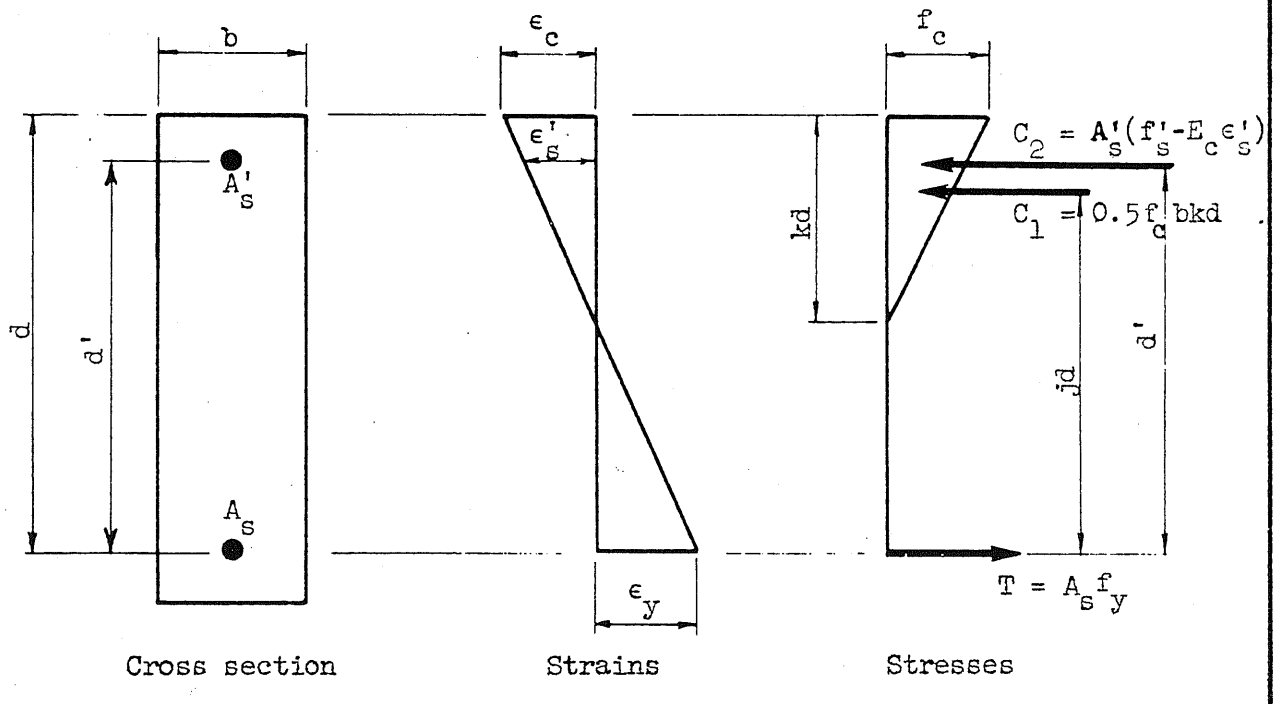

(b) Beams Reinforced in Tension and Compression

FIG. 53 STRAIN AND STRESS RELATIONSHIPS AT FLEXURAL YIELDING

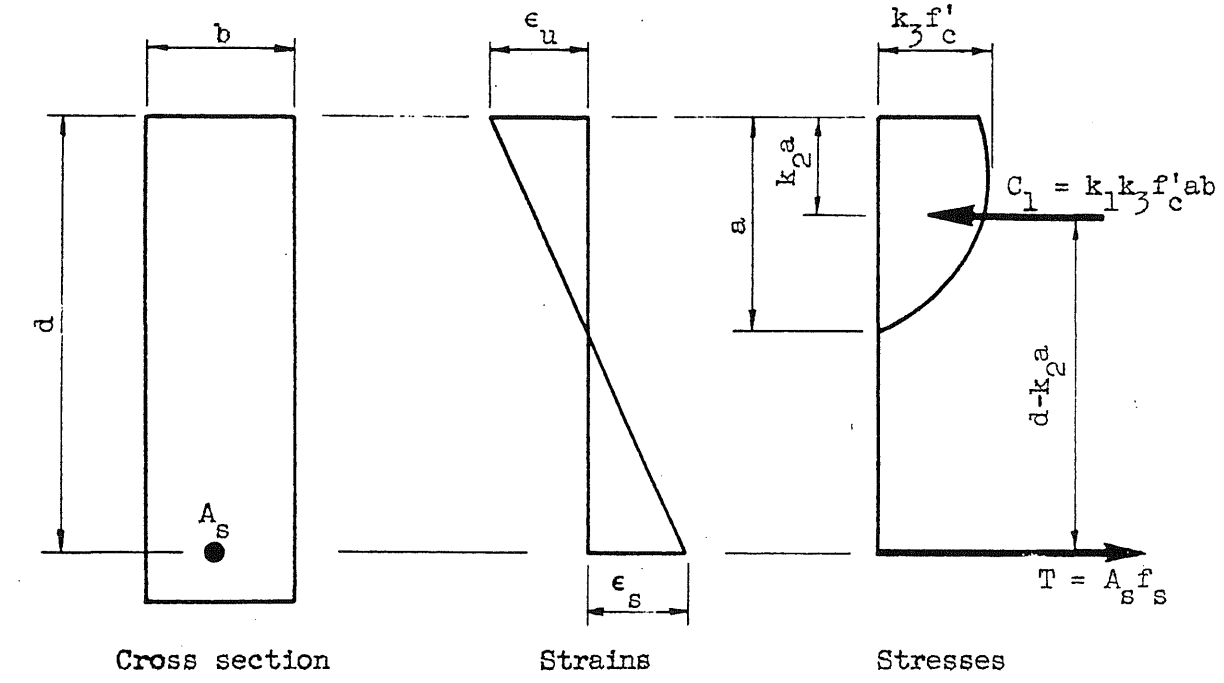

(a) Beams Reinforced in Tension Only

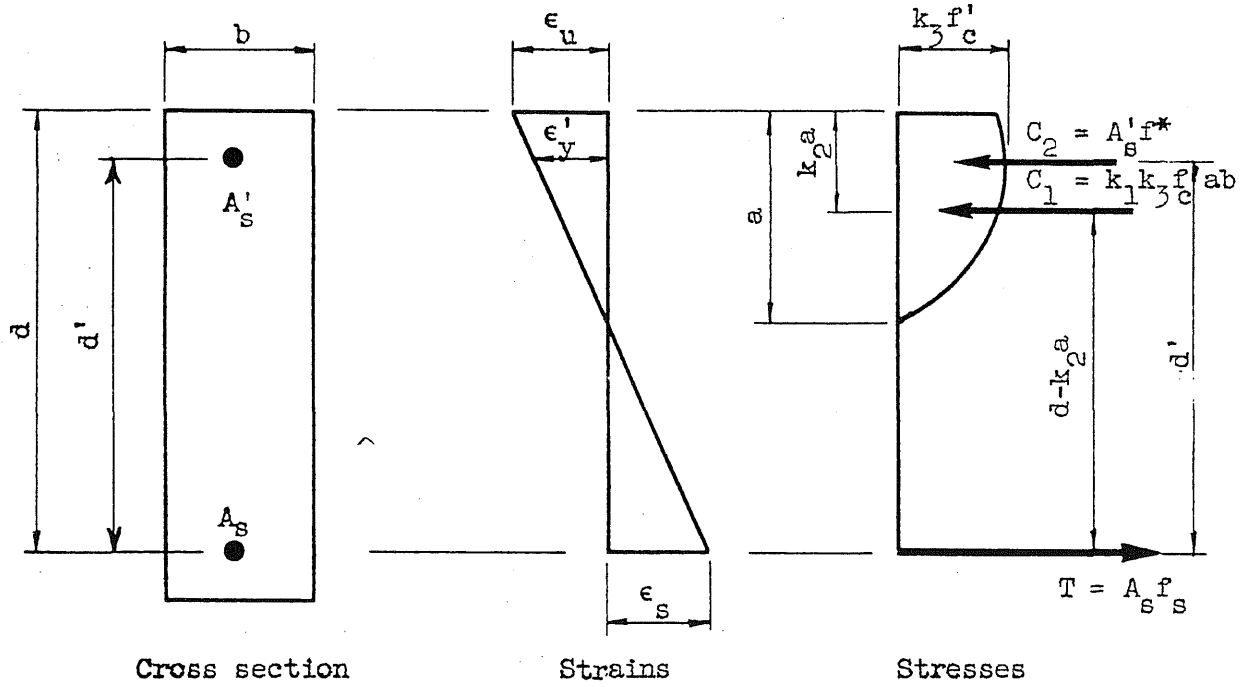

(b) Beams Reinforced in Tension and Compression

FIG. 54 STRAIN AND STRESS RELATIONSHIPS AT ULTIMATE FLEXURAL CAPACITY

DISTRIBUTION

No. Cys.

HEADQUARTERS USAF

1 Hq USAF (AFCOA), Wash 25, DC
1 Hq USAF (AFOCE), Wash 25, DC
1 Hq USAF (AFDRD), Wash 25, DC
1 Hq USAF (AFCIN), Wash 25, DC
1 USAF Dep IG for Insp (AFCDI-B-3), Norton AFB, Calif

MAJOR AIR COMMANDS

1 ARDC (RDR), Andrews AFB, Wash 25, DC
AFBMD, AF Unit Post Office, Los Angeles 45, Calif
1 ATTN: Dr. George Young
1 ATTN: Space Technology Lab
1 SAC (DINC), Offutt AFB, Nebr
1 TAC (TDA), Langley AFB, Va
1 AMC (MCW7), Wright-Patterson AFB, Ohio
1 ADC (Ops Anlys), Ent AFB, Colorado Springs, Colo
1 AUL, Maxwell AFB, Ala
1 USAFA, United States Air Force Academy, Colo

ARDC CENTERS

WADD, Wright-Patterson AFB, Ohio
1 (Director of Sys Mgt, Lt Col J. Stone)
1 (WCOSI)
1 (RDSIW)

KIRTLAND AFB

AFSWC, Kirtland AFB, N Mex
1 (SWNH)
3 (SWRS)
5 (SWOI)

OTHER AIR FORCE AGENCIES

1 USAF Project RAND, Via AF Liaison Office, (Nuclear Energy Division), The RAND Corporation, 1700 Main Street, Santa Monica, Calif
1 USAFIT, Wright-Patterson AFB, Ohio

DISTRIBUTION (Cont'd)

No. Cys.

ARMY ACTIVITIES

1 Chief of Research and Development, Department of the Army, ATTN: Special Weapons and Air Defense Division, Wash 25, DC

1 Director, Ballistic Research Laboratories, ATTN: Library, Aberdeen Proving Ground, Md

1 Commanding Officer, US Army Engineers, Research and Development Laboratories, Ft. Belvoir, Va

1 Director, Waterways Experiment Station, ATTN: W. J. Turnbull, Box 631, Vicksburg, Miss

1 Chief of Engineers, Department of the Army, ATTN: Protective Construction Branch, Wash 25, DC

NAVY ACTIVITIES

1 Commanding Officer, Naval Research Laboratory, Wash 25, DC

1 Chief, Bureau of Yards and Docks, ATTN: D-440, Wash 25, DC

1 Commanding Officer and Director, Naval Civil Engineering Laboratory, Port Hueneme, Calif

OTHER DOD ACTIVITIES

1 Director, Weapon Systems Evaluation Group, Office of Assistant Secretary of Defense, Room 2E1006, The Pentagon, Wash 25, DC

3 Chief, Defense Atomic Support Agency, ATTN: Blast and Shock Division, Wash 25, DC

1 Commander, Field Command, Defense Atomic Support Agency, ATTN: WET, Sandia Base, N Mex

1 ASTIA (TIPDR), Arlington Hall Sta, Arlington 12, Va

AEC ACTIVITIES

1 US Atomic Energy Commission, ATTN: Technical Reports Library (Mrs. J. O'Leary, for DMA), Wash 25, DC

1 President, Sandia Corporation, ATTN: T. B. Cook, Div 5111, Sandia Base, N Mex

1 Assistant Secretary of Defense, ATTN: H. Facci, Wash 25, DC

DISTRIBUTION (Cont'd)

No. Cys.

OTHER

1 American Machine and Foundry Company, ATTN: T. G. Morrison, 1104 South Wabash Ave., Chicago 5, Ill

1 Massachusetts Institute of Technology, Dept of Civil and Sanitary Engineering, ATTN: Prof. R. J. Hansen, 77 Massachusetts Ave., Cambridge 99, Mass

1 University of Massachusetts, Dept of Civil Engineering, ATTN: Prof. Merit P. White, Amherst, Mass

1 Holmes and Narver, Inc., ATTN: Sherwood B. Smith, 824 S. Figueroa St., Los Angeles 14, Calif

1 E. H. Plesset Associates, Inc., ATTN: Marc Peter, Jr., 6399 Wilshire Blvd., Los Angeles 48, Calif